



University of  
Massachusetts  
Amherst

## IMPROVING THE SHEAR BEHAVIOR OF CROSS LAMINATED TIMBER (CLT) PANELS BY OPTIMIZATION OF LAMINATES PLY-ORIENTATION USING EASTERN HEMLOCK

Item Type	Dissertation (Open Access)
Authors	Bahmanzad, Alireza
DOI	<a href="https://doi.org/10.7275/236f-rp42">10.7275/236f-rp42</a>
Download date	2026-05-18 02:53:48
Link to Item	<a href="https://hdl.handle.net/20.500.14394/17927">https://hdl.handle.net/20.500.14394/17927</a>

**IMPROVING THE SHEAR BEHAVIOR OF CROSS LAMINATED TIMBER  
(CLT) PANELS BY OPTIMIZATION OF LAMINATES PLY-ORIENTATION  
USING EASTERN HEMLOCK**

A Dissertation Presented

by

ALIREZA BAHMANZAD

Submitted to the Graduate School of the  
University of Massachusetts Amherst in partial fulfillment  
of the requirements for the degree of

DOCTOR OF PHILOSOPHY

September 2019

Environmental Conservation

© Copyright by Alireza Bahmanzad 2019

All Rights Reserved

IMPROVING THE SHEAR BEHAVIOR OF CROSS LAMINATED TIMBER (CLT)  
PANELS BY OPTIMIZATION OF LAMINATES PLY-ORIENTATION USING  
EASTERN HEMLOCK

A Dissertation Presented

By

ALIREZA BAHMANZAD

Approved as to style and content by:

\_\_\_\_\_, Chair  
Peggi L. Clouston

\_\_\_\_\_, Member  
Alexander C. Schreyer

\_\_\_\_\_, Outside Member  
Sanjay R. Arwade

\_\_\_\_\_  
Curt Griffin, Department Head,  
Environmental Conservation

## DEDICATION

To my loving wife and kind parents.

## ABSTRACT

IMPROVING THE SHEAR BEHAVIOR OF CROSS LAMINATED TIMBER (CLT) PANELS  
BY OPTIMIZATION OF LAMINATES PLY-ORIENTATION USING EASTERN HEMLOCK

SEPTEMBER 2019

ALIREZA BAHMANZAD, B.SC., UNIVERSITY OF NAJAFABAD

M.SC., UNIVERSITY OF NAJAFABAD

PH.D., UNIVERSITY OF MASSACHUSETTS AMHERST

Directed by: Professor Peggi L. Clouston

Cross-laminated timber (CLT), is a new generation of engineered wood product initially established in Europe, is utilized in residential and non-residential applications in several countries. CLT is new to the north of the United States, but Europeans have used CLT more than 25 years as an eco-friendly construction product in many construction sectors. Also many spectacular low, mid and even high-rise building constructed around the world using CLT products. CLT panels can be used in wall, roof and floor system. Using CLT specifically in a floor system is a growing trend that has proven structural benefits greater than traditional light frame wood joisted floors.

One of the problems associated with the CLT floors is that considerable shear deformation may occur in a plane perpendicular to the grain direction due to low rolling shear stiffness especially in the low span-to-depth ratio floor panels. This vulnerability is more problematic for CLT using locally low-valued eastern species. To address this

challenge, this dissertation investigates the mechanical properties improvement of CLT floor system by optimizing the orientation and configuration of lamstocks in CLT panel.

For this purpose, firstly, a regular CLT panel with three and five layers for variety orientation was analyzed using classical lamination theory to determine the effective engineering constant of laminates. Then, the two-plate shear test was performed according to ASTM D-2718 for determination of shear properties of lumbers for fiber orientations of  $0^\circ$ ,  $30^\circ$ ,  $45^\circ$ ,  $60^\circ$ , and  $90^\circ$  with respect to the load direction. Next, sixteen three layers of angled CLT specimens with the mid-layer orientation of  $30^\circ$ ,  $45^\circ$ ,  $60^\circ$ , and  $90^\circ$  and twelve four layers asymmetric panel with the fiber orientation of  $30^\circ$ , and  $45^\circ$  were fabricated from Eastern Hemlock species. To measure the deformation and shear strength of the panels, the three-point bending test was used according to ASTM D198. To determine the shear stress distribution, estimate the deformation of panels, and investigate the coupling effect of the asymmetric panels under the three-point bending test, further numerical Finite Element (FE) analysis in the elastic range was conducted using ABAQUS software. The results of the experimental test were compared with the finite element modeling as well as shear analogy method. Based on the results, there was a general tendency for both bending properties and rolling shear capacities to increase by changing the fiber orientation of the mid-layer from  $90^\circ$  to  $30^\circ$ .

# TABLE OF CONTENTS

	Page
ABSTRACT.....	v
LIST OF TABLES.....	x
LIST OF FIGURES .....	xi
TERMINOLOGY .....	xiv
CHAPTER	
1. INTRODUCTION .....	1
1.1 Overview.....	1
1.2 Objective and Scope .....	4
2. BACKGROUND .....	7
2.1 Cross Laminated Timber (CLT) .....	7
2.2 Rolling Shear Modulus and Shear Deformation.....	13
2.2.1 Rolling Shear Modulus .....	13
2.2.2 Shear Deformation.....	19
2.2.3 Determination of Rolling Shear Modulus.....	21
2.3 Standard & Design method.....	23
2.3.1 Shear Analogy Method .....	24
2.4 A summary of Classical Lamination Theory .....	27
2.4.1 Laminate Engineering Constants .....	29
3. PLANAR SHEAR PROPERTIES OF EASTERN HEMLOCK .....	32
3.1 Analyzing the Effect of Fiber Orientation .....	32
3.2 Materials and Methods.....	34
3.2.1 Specimen Preparation .....	34
3.2.2 Required Sample Size .....	34
3.3 Test Method .....	39

3.4 Results and Discussion .....	41
3.4.1 Failure Modes	41
3.4.2 Load-Displacement Curves.....	42
3.4.3 Planar Shear Properties .....	44
3.4.4 Effect of Fiber Orientation on Planar Shear Properties .....	47
3.4.5 Evaluation of CLT Panel Effective Shear Stiffness $GA_{eff}$ .....	50
3.5 Finite Element Analysis of Two-Plate Rolling Shear Properties.....	51
4. SHEAR PROPERTIES OF SYMMETRIC ANGLE PLY CLT .....	54
4.1 Materials and Methods.....	54
4.1.1 Manufacturing CLT .....	54
4.1.2 Three Point Bending Test Method.....	57
4.1.3 Analytical Model .....	59
4.1.4 Estimation of the Deflection .....	59
4.1.5 Evaluation of the Effective Shear Modulus .....	60
4.2 Test Results and Data Analysis.....	61
4.2.1 Failure Modes	61
4.2.2 Load-Displacement Data .....	63
4.2.3 Effective Shear Modulus and Rolling Shear Strength .....	64
4.3 Finite Element Model of Short-Span CLT Panel.....	67
4.3.1 Material property assumptions.....	68
4.3.2 FE Model Results and Discussion .....	70
5. SHEAR PROPERTIES OF ASYMMETRIC ANGLE PLY CLT .....	77
5.1 Materials and Methods.....	78
5.1.1 Dimensions and Fabrication of CLT.....	78
5.1.2 Test Method	81
5.2 Test Results .....	83
5.2.1 Failure Modes	83
5.2.2 Load-Displacement Data .....	85
5.2.3 Effective Shear Modulus and Rolling Shear Strength .....	86
5.3 Finite Element Model of Short-Span CLT Panel.....	89
5.3.1 Material property assumptions.....	90
5.3.2 Model Verifications .....	91
5.3.3 Investigation on Shear Stress of Asymmetric Layups of Panels .....	92
6. CONCLUSION.....	96

APPENDICES

A. SAMPLE CALCULATIONS FOR SHEAR PROPERTIES .....100

B. EVALUATION OF SHEAR PROPERTIES OF EASTERN HEMLOCK FOR  
DIFFERENT FIBER ORIENTATION.....104

C. IMPROVING THE ROLLING SHEAR PROPERTIES OF CROSS-LAMINATED  
TIMBER PANELS BY OPTIMIZING LAMINATE FIBER  
ORIENTATION.....130

BIBLIOGRAPHY .....160

## LIST OF TABLES

Table	Page
2.1. Dimensional Capabilities of CLT Panel .....	11
2.2. Mechanical Properties of Eastern Hemlock.....	19
3.1. Planar shear properties for different fiber orientations .....	45
3.2. Breakdown of the off-axis loading in the principal material coordinate .....	50
3.3. Comparison between effective shear stiffness of experimental test and CLT standard... 51	
3.4. Shear properties of Eastern Hemlock .....	52
4.1. Modulus of Elasticity and Shear Modulus of Eastern Hemlock for Different Fiber Orientation .....	60
4.2. Short Span Shear Test Experimental Result for Fiber Orientation of 30°,45°,60°,90° ....	66
4.3. Mechanical Properties input in FE Model .....	69
4.4. Comparison of FE Modeling with Experimental Test and Shear Analogy Method.....	72
5.1. Experimental result for asymmetric layups of 30°,and 60° .....	85
5.2. Shear properties of the 30°, and 60° asymmetric CLT panels.....	87
5.3. Breakdown of the off-axis loading in the principal material coordinate .....	89

## LIST OF FIGURES

Figure	Page
2.1. CLT Panel Configuration.....	8
2.2. Cost and Performance of CLT .....	8
2.3. Timeline of CLT Products .....	9
2.4. Examples of Possible CLT Panel Cross-Section .....	11
2.5. Direction of fiber of the outer layers for floor (left), Cross section of panel (right) .....	12
2.6. Failure due to rolling shear .....	14
2.7. Rolling Shear Deformation of CLT Panel .....	19
2.8. Proportion of shear and bending deformation versus span-to-depth ratio.....	20
2.9. Planar Shear Test Setup .....	22
2.10. Beam Modeling for Shear Analogy Method.....	24
2.11. Bending and Shear Stresses in Beam A and B (left & middle) .....	26
2.12. Sign Convention of lamina .....	28
2.13. Laminated plate geometry.....	29
2.14. In-Plane Loading of Laminate to Determination of Laminate Engineering Constant....	30
3.1. Longitudinal and Cross Section of CLT Floor Panel.....	33
3.2. Variation of Effective Engineering Constant with Respect to Orientation of Mid-Layer....	34
3.3. Fabrication process for two-plate shear test assembly.....	36
3.4. Size of the pieces for different fiber orientation in two-plate shear test .....	37
3.5. Test setup for compression perpendicular to grain test .....	38
3.6. Experimental setup for two-plate shear test.....	39
3.7. Typical failure appearances of specimens tested in 2 plate shear.....	41

3.8. Failure mode I .....	42
3.9. Load-displacement curves of specimens under two-plate shear test .....	43
3.10. Cumulative frequency and fitted Burr distribution for shear modulus .....	46
3.11. Cumulative frequency and fitted Burr distribution for shear strength.....	46
3.12. A comparison of Hankinson Formula with planar test .....	48
3.13. Biaxial stresses from off-axis loading.....	49
3.14. Finite element model of the two-plate shear test .....	53
4.1. The size of the three layers short-span CLT panel for different lumber orientation .....	56
4.2. The detailed fabrication process for short-span CLT panels .....	57
4.3. Longitudinal and cross-section of CLT floor panel.....	58
4.4. Typical test setup for short-span CLT test.....	59
4.5. Cross-section of 3-layer CLT.....	60
4.6. Typical failure of 90° CLT panels .....	62
4.7. Typical failure of angled CLT panels .....	63
4.8. Load-deflection response for short-span CLT panels .....	64
4.9. Comparison of effective shear Modulus, apparent bending modulus.....	66
4.10. Three Axes of Wood with Respect to Grain Direction.....	68
4.11. FEM Element Global Coordinates and Mesh .....	69
4.12. Comparison of the load-displacement curves of experiments with FE modeling and shear analogy method for 90°, 60°, 45°, 30° CLT .....	70
4.13. Comparison of FE Modeling with Experimental Test and Shear Analogy Method.....	73
4.14. Proportion of shear and bending deformation versus CLT with different fiber orientation in mid-layer for the short-span panel deformation .....	74
4.15. Distribution of shear stress along the length of the CLT panel .....	75

4.16. Distribution of shear stresses in cross-section of the CLT panel.....	75
5.1. Asymmetric angle-ply layups .....	78
5.2. The size of the four layers short-span CLT panel for asymmetric layups .....	80
5.3. The detailed fabrication process for short-span CLT panels .....	81
5.4. Typical test setup for short-span CLT test.....	83
5.5. Typical failure of short-span asymmetric panels .....	84
5.6. Load-deflection response for asymmetric 30° and 45° CLT panels.....	86
5.7. Biaxial shear stresses from off-axis loading .....	88
5.8. FEM Element Global Coordinates and Mesh .....	90
5.9. Comparison of the load-displacement curves of 30° asymmetric CLT with FE modeling 91	
5.10. Comparison of the load-displacement curves of 45° asymmetric CLT with FE modeling 92	
5.11. Contour plots of the in-plane shear ( $S_{12}$ ) for asymmetric four-layer CLT panel.....	93
5.12. Contour plots of the shear in the principal material directions ( $S_{13}$ ) for asymmetric four- layer CLT panel .....	94
5.13. Contour plots of the rolling shear in the principal material directions ( $S_{23}$ ) for asymmetric four-layer CLT panel.....	95
A.1. Cross Section of Three-Layers Short-Span Specimen.....	100
A.2. Short-span bending load-displacement graph for Specimen S1-90° .....	100

## TERMINOLOGY

### Abbreviations

CLT= Cross Laminated Timber

CLT= Classical Lamination Theory

LVL= Laminated Veneered Lumber

LSL= Laminated Strand Lumber

NDS= National Design Specification

PSL=Parallel Strand Lumber

Q (8) = Quadrilateral element

SCL=Structural Composite Lumber

### Symbols

L = Length of specimen;

W = width of specimen;

CV= coefficient of variation;

SD = standard deviation;

$\sigma_i$  = stress components;

$\delta$  = displacement;

$\tau$  = Shear stress;

$\tau_{ij}$ =in plane shear stress;

n = sample size;

$\alpha$  = estimate of precision, (0.05);

t: value of t statistic from table 1 ASTM D2915;

MC = Moisture Content;

$\nu_{ij}$  = Poisson's ratio;

$E_0$  = modulus of elasticity parallel to the grain (MPa);

$E_{90}$  = modulus of elasticity perpendicular to the grain (MPa);

$G_0$  = modulus of rigidity parallel to the grain (MPa);

$G_{90}$  = modulus of rigidity perpendicular to the grain (MPa);

$EI_{app}$  = Apparent Bending Modulus ( $10^6$  N-mm<sup>2</sup>/m);

$EI_{eff}$  = Effective Bending Modulus ( $10^6$  N-mm<sup>2</sup>/m);

$GA_{eff}$  = effective shear Modulus ( $10^6$  N/m);

$f_{v,max}$  = maximum shear stress (MPa);

$P_{Max}$  = Peak load (KN);

u, v, w = displacement in x, y, z directions;

### **Subscripts**

max = designates maximum value;

x, y, z = coordinate directions;

L, T, R = principal material directions;

# CHAPTER 1

## INTRODUCTION

### 1.1 Overview

Cross-laminated timber (CLT), is an innovative construction material which is composed of an uneven number of orthogonally bonded layers of solid lumber or structural composite lumber (in general three, five, seven or even more). Because of continuous bonding and, consequently, quasi-rigid composite action between the single layers, a very compact and versatile useable product arises. Product dimensions allow its application as large-sized wall and floor elements as well as for other large sized load-bearing plane-like, but also linear, structural components (Brandner, 2013). In this way, the product has opened new opportunities in timber engineering and allows architects and engineers to design monolithic mid-rise and even high rise buildings. This “solid timber construction technique with cross-laminated timber,” makes it possible to design and construct with timber to previously impossible dimensions and scales.

In comparison to a light frame wood floor, CLT floors offer numerous advantages. CLT floors have bi-directional strength and stiffness and can distribute concentrated loads in two orthogonal directions. Moreover, because of in-plane rigidity and dimensional stability, CLT panels provide an efficient lateral load resisting system. Test results also show that acoustic performance of CLT panels including airborne and impact sound transmission is in acceptable range (Gagnon and kouyoumji, 2011). In addition, the thickness of CLT floors creates effective fire resistance because panels char slowly (Frangi et.al 2007).

Many wood species for CLT production have been investigated around the world. Fortune and Quenneville (2010) investigated locally grown Radiata pine to use in CLT. Hindman and Bouldin measured the mechanical properties of CLT in bending using Southern pine wood and found these mechanical properties are superior to published values for the V3 grade (Hindman and Bouldin, 2015). These studies show that there is a high potential for creating an economic and sustainable market for low-value timber in the production of valuable and high-performance CLT products. Forests in the northeast region of the US supply many low-value species such as Eastern Hemlock. Due to their low quality, there is a lack of markets for these species and forest management in this region has resulted in the decline of the forest industry for many years. This condition is worsened by the infestation of a small insect called the Hemlock Woolly Adelgid (*Adelges tsugae*) causing tree death within 4 to 10 years (Webb et.al 2003, US Forest Service 2014). These concerns could be significantly reduced by using these low-grade species solely or in conjunction with high-grade species in CLT products.

One issue associated with CLT panels is their low shear properties arising from cross-directional fiber layup, so-called rolling shear, causing larger shear deformation and deflection in CLT floors (Fellmoser and Blab 2004). It is speculated that this issue is more prominent in CLT panels if low-grade species are used, specifically in the mid-layer. There is a benefit to using low-grade wood here due to low bending stress however, in this area, the shear stress is high. In this case, the low effective shear stiffness and strength of CLT may govern the design and performance of CLT panels.

Rolling shear relies on multiple aspects including sawn pattern configuration, species, moisture content, size, lamination thickness, and geometry of the lamination's

cross section. In Europe and Canada, experimental and numerical procedures have been recently established to calculate the rolling shear properties of wood in CLT panels. Aicher et al. (2016) estimated the rolling shear stiffness and strength of European Beech to be 53.6, 0.652 ksi respectively. They also evaluated these properties for Spruce wood 7.25, 0.130 ksi (Aicher et al. 2016). Other studies have shown that the shear modulus of wood varies between 1/12 and 1/20 of the major modulus of elasticity (Aicher and Dill 2000, Fellmoser and Blab 2004, Zhou et al. 2013). The CLT handbook also estimates the rolling shear modulus to be 10 percent of the main shear modulus parallel to the grain of laminations ( $G_r=G_0/10$ ). The rolling shear properties of softwood species are typically less than hardwood species which can cause large shear deformation and strength loss in CLT floors specifically for span-to-depth ratio less than 30 (Fellmoser and Blab 2004). Since CLT panels are vulnerable in rolling shear behavior, a deeper understanding of rolling shear properties of local species is necessary in order to use in CLT panels effectively.

Several analytical methods are recently developed to estimate and evaluate CLT behavior. These methods are: Mechanically Jointed Beams Theory or Gamma method (found in Eurocode 5 Appendix B (Eurocode 5 2004); Composite Theory (k Method) (Fellmoser and Blab 2004); Shear Analogy Method (developed by Kreuzinger, 1999); Classical Lamination Theory (CLT) Method (Gere et al. 2012); Orthotropic plate theories, including classical plate theory, first order shear deformation theory, Murakami's zigzag plate theory and Ren's plate theory (Stürzenbecher et al.2010). Since the shear analogy method is taken into account the shear deformation of cross layers, this method is deemed to be the most accurate to predict CLT properties (Fellmoser and Blab 2004). It is also recommended in the product standard of the United States and Canada (Standard for

performance-rated cross-laminated timber. ANSI/APA PRG, 320-2012) due to a close approximation of experimental test results. Although CLT panels with different ply-orientation cannot be analyzed by this method, the Classical lamination Theory (CLT) method, which is developed based on the analysis capability of different ply-orientations, is applicable to predict CLT properties prior to conducting experimental tests to measure the rolling shear properties of lumbers.

The goal of this research is to investigate the rolling shear stiffness and strength of CLT panels fabricated from locally grown species Eastern Hemlock. For this purpose, a CLT panel with different ply-orientation and configuration will be examined to determine the optimal mid-layer fiber orientation and layup configuration. It is my hypothesis that properties of CLT panels with orthogonal layups could be improved by reorienting the mid-layer fiber in the panel. This hypothesis originates from the conjecture that there is an optimal ply-orientation and layup configuration for CLT floor system considering specific loading condition and circumstances. This improvement in rolling shear properties of CLT provides the possibility for higher bending strength capacity in the major direction of CLT panels.

This research will also aid market development of local species CLT to make possible the establishment of manufacturing facilities in the region by using locally grown trees including Eastern Hemlock and White Pine, resulting in improvement of the forest management and creation of local jobs.

## **1.2 Objectives and scope**

It is the objective of this thesis to verify that the mechanical properties of CLT panel, especially the rolling shear modulus and strength, could be improved through

empirical and numerical investigation on the fiber orientation and configuration of CLT panels, specifically in the short span-to-depth ratio panels, where the shear deformation is significant. This thesis is also addressing the growing trend of using CLT products throughout the US, and specifically in the Northeast for heavy timber construction. To this end, specific objectives of this research are:

1. Investigate the effects of fiber orientation on mechanical properties of laminates
  - 1-1. Use Classical Lamination Theory (CLT) to analyze the effect of fiber orientation for 3 layer CLT
2. Measure mechanical properties of Eastern Hemlock for use in analytical models ( $G_0, G_r, E_0, E_{90}$ )
  - 2-1. Calculate the required sample size and specimen
  - 2-2. Conduct the two-plate shear test in fiber orientation of  $0^\circ, 30^\circ, 45^\circ, 60^\circ, 90^\circ$  to measure the shear modulus and strength as a function of fiber orientation.
3. Development of analytical models to predict the mechanical response of CLT panel layups following the procedures described in the CLT Handbook and ANSI/APA PRG-320.
4. Fabrication and preparation of symmetric and asymmetric three and four-layers of short-span CLT panels with the fiber orientation of  $30^\circ, 45^\circ, 60^\circ$ , and  $90^\circ$  in the mid-layer with respect to the major direction
5. Conducting three-point bending tests according to the procedures per ANSI/APA PRG-320-2012 and ASTM test standards to evaluate the shear properties (effective shear modulus ( $GA_{eff}$ ), apparent bending modulus ( $EI_{app}$ ) and shear strength ( $f_{vmax}$ )) of short-span CLT panel of CLT panels and comparison with ANSI/APA PRG 320 CLT grades.

6. Develop and validate finite element models to predict the behavior of short-span CLT panels

## **CHAPTER 2**

### **BACKGROUND**

This section is a summary of the body of knowledge which defines CLT properties, and standards for determination of shear properties of CLT panels to the foundation for this research.

#### **2.1. CROSS LAMINATED TIMBER (CLT)**

Cross-laminated timber (CLT) is a newly engineered wood panel product. It is composed of layers of lumber stacked and laminated in alternating orthogonal directions (Figure 2.1). Used worldwide in walls, roofs, floors, and bridge decking systems, it is found in both residential and non-residential structures. Using CLT, specifically in floor systems, is a growing trend that has structural benefits over traditional light-frame wood-joisted floors, such as bidirectional strength and stiffness allowing for open floor plans and other attractive architectural features (John W. Olver Design Building at the University of Massachusetts Amherst). As shown in figure 2.2, CLT could be cost-competitive with composite structural lumber (LSL, LVL, and PSL) and light framing in mid-rise construction where wood has not been traditionally used (Pöyry, 2017). The key advantages of the CLT panels which make fast project completion possible especially in the mid-rise building are easy handling and accurate prefabrication (Karacabeyli & Douglas, 2013). Although a concrete slab has an adequate capacity to meet the demand in the construction industry, there is a considerable opportunity for CLT capacity to meet the growing demand for future construction. However, currently CLT market is in an early stage of development both in Europe and in North of America.

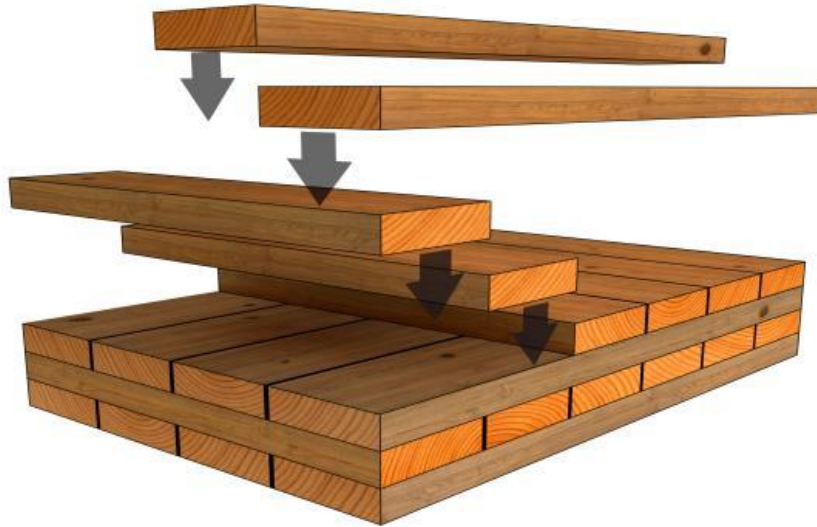


Figure 2.1: CLT Panel Configuration (Dietrich et al, 2016)

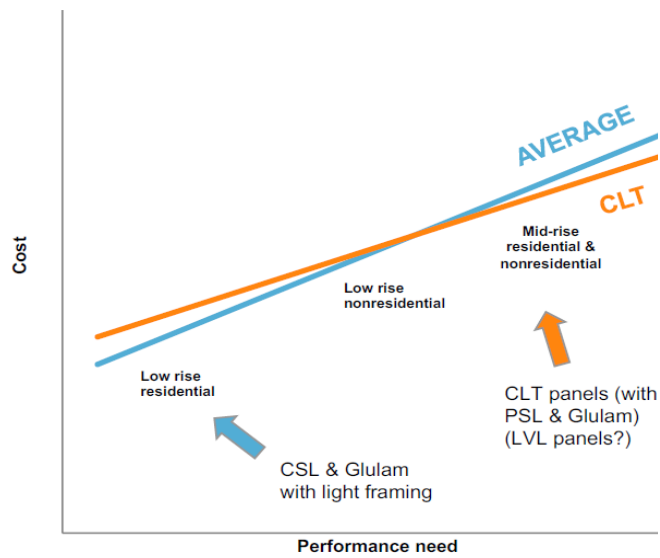


Figure 2.2: Cost and Performance of CLT (FP innovations)

The ideas and developments of CLT have been realized primarily in the early 1990s in Austria and Germany which is motivated by a missing market for the side-boards from sawmilling at that time and has been gaining popularity in many residential and non-

residential buildings in Europe (Gagnon & Pirvu, 2011). In a wider prospect, CLT can also be seen as a collaborative product or as further development of historical timber building style of logs, with the origination from Europe (Brandner, 2013). As can be seen in figure 2.3, the evolution of manufacture capacities is rapidly growing more than 15 % per year. In 2012, the volume of CLT product was estimated 500,000 m<sup>3</sup>/year in Austria and Germany while Austria has produced roughly 67 % of the market demand. Remarkable activities for installation of low, mid-rise and even high rise structures, are in the ongoing process around the world (Wegener, 1997).

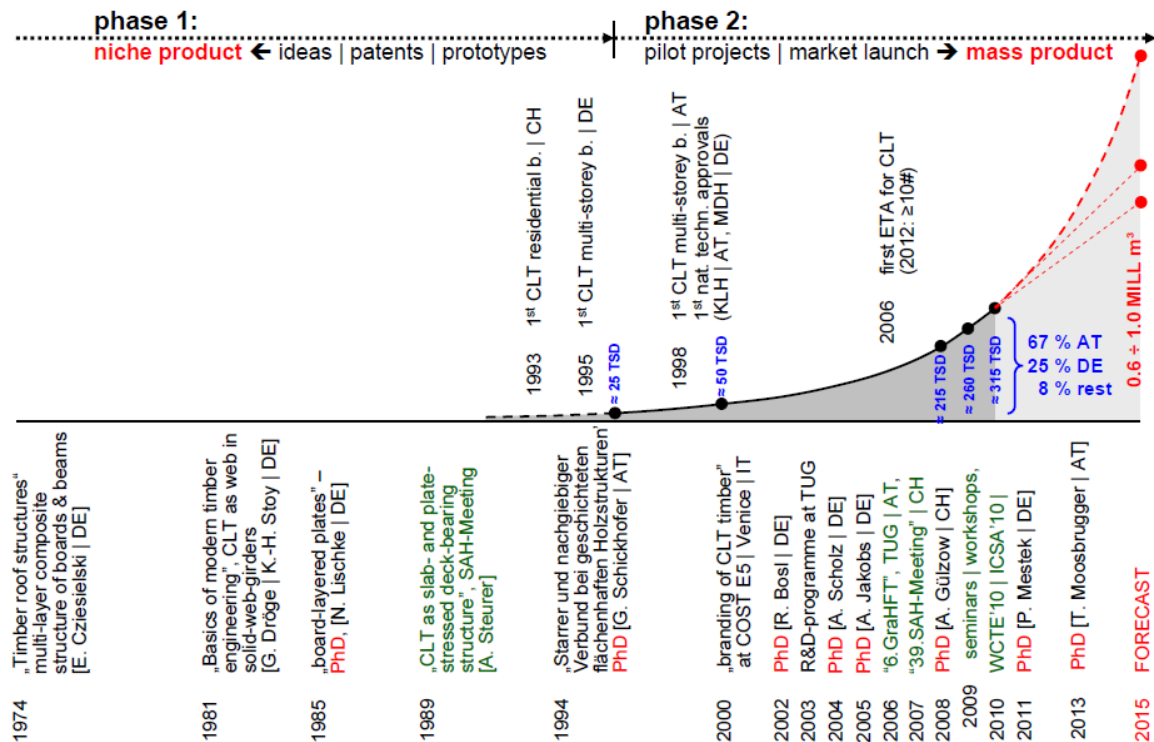


Figure 2.3: Timeline of CLT products (Schickhofer, 2010)

CLT can be used, as large-sized and panel-like solid timber construction elements for the building segments. The prefabrication capability, easy and fast installation (e.g., roughly one to two days per family house), and high dimensional stability which highlights

accuracy are several advantages of CLT panels (Brandner, 2013). Further structural advantages for this product are the ability to transfer loads in two-dimensional and the low mass, which make CLT ideal for retrofit and upgrading of existing buildings and also for seismic resisting exceptional loadings. There are more benefits for CLT in comparison with light-weight wood buildings including the high capacity to store moisture and temperature, acceptable fire resistance, controlling the air penetration, easy placement of openings, possibility of fastening non-structural members such as services and furniture (Frangi et al., 2007, Gagnon & Kouyoumji, 2011). Also some features such as biaxial bending strength capacity, considerable in-plane rigidity and the low weight of CLT makes it the perfect choice in multi-story residential, mid and even high-rise buildings, long-span structures and in conjunction with the concrete such as composite floor system (Kuilen et al., 2011, Yeoh et al., 2011).

A CLT panel has at least three layers of boards installed orthogonally alternating to adjacent layers. In a different configuration, successive layers can be installed in the same direction to achieve specific structural strength (see figure 2.4). The number of layers in CLT products are mainly built with an odd number; mostly three to seven layers are common. In table 2.1, the dimensional capabilities of CLT panel is shown according to ANSI/APA PRG-320-2012 standard product. This standard has been developed for Performance-Rated CLT contains the requirements and test methods for CLT qualification while providing quality assurance for production using solid-sawn lumber as well as structural composite lumber (SCL).

Table 2.1: Dimensional Capabilities of CLT Panel

		Dimensional Capabilities			
	Layers	Length	Width	Thickness	Lamellas
		(ft)	(ft)	(inches)	(inches)
CLT Panel	3-,5-,6-,7-,8-ply	Up to 60	2,4,8,10	Up to 20	5/8 to 2 inches, kiln dried, quality graded, finger jointed

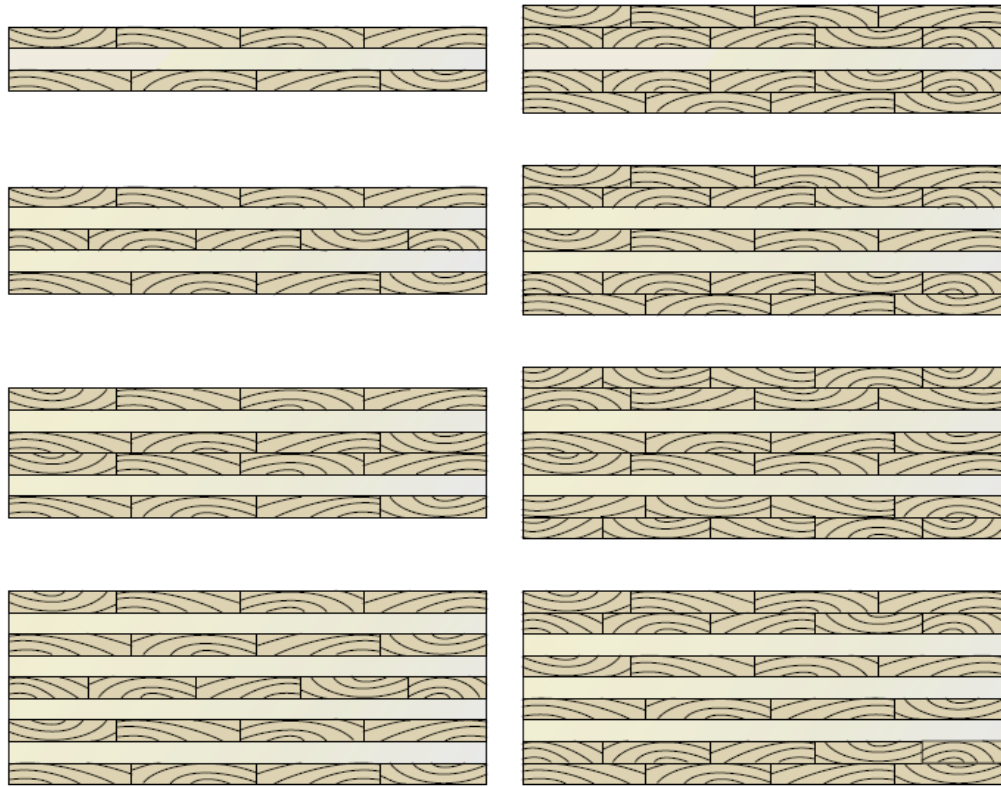


Figure 2.4: Examples of Possible CLT Panel Cross-Section (Karacabeyli & Douglas, 2013)

To achieve the maximum floor's strength capacities, the exterior layers must be placed parallel to major span direction (see figure 2.5). Likewise, for walls, the exterior layers of CLT panel must be oriented up and down, in direction of gravity loads. For the specific usage of the CLT floor and wall, the layers of CLT panel could be assigned a particular configuration due to the different distribution of shear and bending stresses.

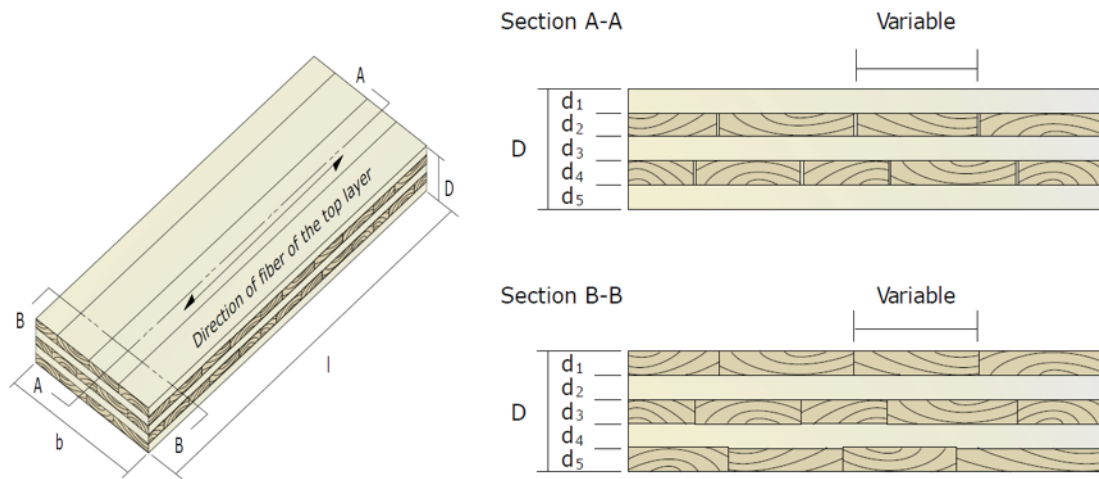


Figure 2.5: Direction of the fiber of the outer layers for floor (left), Cross section of panel (right) (Gagnon & Pirvu, 2011).

Recently, different species of wood for using in CLT production have been investigated in the world. Fortune and Quenneville (2010) explored locally grown Radiata pine to use in CLT production. Hindman and Bouldin, (2015) investigated Southern Pine wood to use in CLT panels. They calculated the mechanical properties of CLT and found these values are greater than the published values for the V3 grade.

Park et al. (2006) examined five different species (Sugi, Hinoki, Kiri, Katsura, and Buna) to use in three-layer CLT panel and realized the calculated modulus of elasticity parallel to grain was much higher than the modulus of elasticity obtained from experimental test due to the effect of shear deformation. In addition, there was an extremely

high positive correlation between the Modulus of Rupture (MOR) and the measured MOE parallel to the grain of the face laminate of CLT. Their findings are consistent with the study by Niederwestberg and Chui (2012), who explored material and structural characteristics of spruce boards with three different sizes (120×15mm, 76×15mm, 32×15mm) and their effects on the overall characteristics of CLT using modal testing and static testing. They estimated that MOE from static test are nearly 50% lower than MOE calculated from shear analogy method.

Buck et al. (2016) studied CLT panel with  $\pm 45^\circ$  alternating layers, against regular panel of  $90^\circ$  orientation. They tested 40 panels of 5-layers fabricated in two configuration with the dimensions of 95 mm in thickness, 1200 mm in width and 4136 mm in length. The results of the four-point-bending test exhibited 35% and 15% increasing in the bending strength and modulus of elasticity, respectively, compared to the CLT panel with  $90^\circ$  orientation.

There are few markets for low-value wood species such as Eastern Hemlock and White Pine in the northeast region of the US. This concern also is intensified by an attack of small insect pest called the Hemlock Woolly Adelgid (*Adelges tsugae*) causing tree death within 4 to 10 years (Webb et.al 2003, US Forest Service 2014). Previous studies have been shown that there is a high potential for using local wood species in CLT products, however, to date, there is no published research that examines the use of locally grown species of northeast wood in CLT products.

## **2.2. Rolling Shear Modulus and Shear Deformation**

### **2.2.1. Rolling Shear Modulus**

Rolling shear is described as shear stress across the grain in which deformation occurs in the radial-tangential plane. As can be seen in figure 3.6, large shear deformation and rolling shear failure are frequently observed in bending tests because of low rolling shear stiffness of timber (Fellmoser & Blass, 2004). Therefore, rolling shear strength and stiffness in CLT is a key issue that can control design criteria. Many studies confirmed that the laminations oriented crosswise similar to plywood affect the load bearing behavior since the properties of the material and products are anisotropic (Mestek et al., 2008). The work conducted by Bejtka and Lam on CLT panel with Canadian pine lumber confirmed this finding (Bejtka & Lam. 2008). Several researchers have been reported that the value of effective bending stiffness of floor panel and stress distribution in the layers depends on the rolling shear modulus of the cross-wise layers (Bejtka & Lam. 2008, Fellmoser & Blass, 2004).

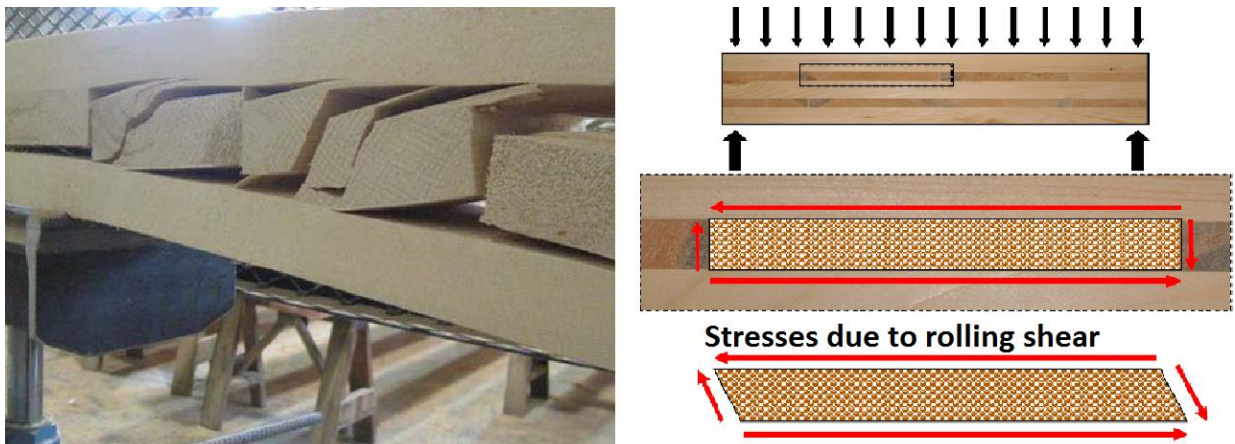


Figure 2.6: Failure due to rolling shear (Mohammad & Gagnon 2012)

Rolling shear properties relies on multiple factors including: specific density of cross-layer, growth ring orientation, species, moisture content, size, layers thickness, span to depth ratio, shrinkage, and geometry of the lamination's cross section (Brandner 2013, Gagnon and Pirvu 2011, Yawalata and Lam 2011, Flores et al. 2015). Moreover, CLT

floors with span-to-depth ratios below 30 are particularly vulnerable to large shear deformation (Fellmoser and Blaß 2004, Aicher et.al 2016). To measure the rolling shear properties of CLT, different procedures have been recently developed.

Munthe and Ethington (1968) used the two-plate shear test to evaluate the shear properties of Sitka spruce (*Picea sitchensis*) plank. The rolling shear strength was estimated to be 1.77 MPa, which is 20% of the longitudinal shear strength.

Aicher and Dill (2000) predicted the rolling shear modulus of 3-layer Norway spruce between 50 MPa and 200 MPa by finite element method. They found that the rolling shear modulus highly depend on the growth ring orientation of laminate and the rolling shear modulus is at maximum value when growth ring of cross-layer is 45 degree. In a recent study, they also calculated the rolling shear modulus of European Beech and Spruce to be 370, 53 MPa, which is  $2/9$ ,  $1/24$  of tensile modulus of elasticity respectively  $G/E_t$  (Aicher et al., 2016).

Görlacher (2000) used an analytical model to study the influence of annual ring orientation on rolling shear modulus and modulus of elasticity perpendicular to the grain. He found the rolling shear modulus for annual ring orientation of  $0^\circ$  and  $90^\circ$  remains almost constant, however, the modulus of elasticity perpendicular to the grain is decreasing significantly and for an annual ring orientation of about  $45^\circ$  the rolling shear modulus is increasing significantly (up to a factor of about 4), and the modulus of elasticity perpendicular to the grain remains almost constant.

According to the numerical and experimental method, Blass and Görlacher (2000) suggested the 1 and 50 MPa for the characteristic value of the rolling shear strength and

stiffness of European spruce respectively, independent of the strength class of timber. However, these values may differ slightly depending on some wood properties such as density and annual ring orientation (Fellmoser & Blass, 2004).

Steiger developed an analytical method to determine the shear modulus for three direction of 3-layer CLT panel and the bending modulus for two perpendicular direction. They used the resonance frequencies and mode shapes of the panel to determine the shear modulus in three direction for 3-layer CLT panel. The values of their analytical method were validated by the static bending test (Steiger et al., 2008).

Zhou et al. (2014) observed that cross layers with growth ring orientation in rift-sawn could increase the rolling shear modulus in comparison to flat-sawn or quarter-sawn. In another study, they used two methods bending tests and two-plate shear test to compare the rolling shear modulus and strength of the cross-layer in CLT. Their finding shows that the results of the two-plate shear test can accurately estimate the deflection of CLT specimens. Their CLT panels were made of Black Spruce (*Picea mariana*) timber using fast-curing epoxy one-component PUR. The average rolling shear strength of 3-layer down-scaled CLT was 2.69 MPa under three-point bending tests at a span-to-depth ratio of 6. Furthermore, they suggest that the bending test might be the most appropriate test method for the determination of the shear strength of CLT because it can produce a rolling shear failure mode that is encountered under bending (Zhou et al., 2014).

Moreover, Li (2015) in his PhD thesis showed that the mean rolling shear strength value for Pine Beetle varies from 1.4 MPa to 1.76 MPa and confirmed previous claims that the rolling shear strength relies on specimen size, loading type, and loading protocol. In another research, Saavedra Flores et al. (2015) studied the influence of edge-gluing, wood

density and span-to-depth ratio on the rolling shear capacity. They developed a numerical model to predict the rolling shear capacity of CLT panels. Their numerical model predicts 40% reduction of the failure load if cross-layers does not have edge gluing. In addition, their model predict 21% increase of the failure load, when wood density increases 37.5%.

Lam et al. (2016) measured the rolling shear properties of Mountain Pine Beetle through the torque loading tests on small blocks. The rolling shear strength values for three- and five-layer CLT tube specimens were 3.8 and 4.8 MPa, respectively, which are much higher compared to the previous study, likely due to size effect and pure shear. Yawalata and Lam (2011) studied the effects of manufacturing process variables on the rolling shear strength of three-layer spruce-pine-fir (SPF) and hem-fir CLT panels. Their findings revealed that the rolling shear strength of three-layer SPF panels produced under 0.4 MPa of pressure was 2.22 MPa, which was higher than the 1.85 MPa result achieved under 0.1 MPa of pressure, suggesting that higher manufacturing pressure produces stronger panels, resulting in higher shear strength. Pirvu (2011) studied the effects of edge gluing and larger sectional size (using cross-sectional sizes of 38×38 mm, 38×89 mm and 38×140 mm) on the rolling shear modulus of laminates using planar shear tests on lodge pole pine specimens. According to his finding, using a larger size of the specimen is more effective for increasing shear modulus than edge gluing specimen. Additionally, he found that increasing the specimen's width had no notable effect on the rolling shear modulus.

Many studies have been conducted to establish wood shear property relationships. For example, some experimental and numerical research studies have found that in general terms, shear modulus to elastic modulus ratio for wood varies from 1/12 to 1/20 (Fellmoser and Blaß 2004, Holzbrettern et al. 2000, Zhou et al. 2014). Similarly, product standards

(ANSI/APA PRG320) have suggested that the rolling shear modulus is approximately 10% of the longitudinal shear modulus ( $G_r=G_0/10$ ). Munthe and Ethington (1968) found that, for Sitka spruce specifically, rolling shear strength was 20% of the longitudinal shear strength. Along the same lines, Aicher and Dill (2016) calculated the rolling shear modulus of European Beech and Spruce to be 370 MPa and 53 MPa, respectively, which is 2/9ths and 1/24th of the tensile modulus of elasticity ( $G/E_t$ ). In 2000, the same authors found that the rolling shear modulus depends highly on the growth ring orientation of the laminate, is at a maximum value when the growth ring of the cross-layer is 45 degrees, and that the modulus of 3-layer Norway spruce was between 50 MPa and 200 MPa.

To date, there is no published study that measures the rolling shear modulus of locally grown northeast wood species including Eastern Hemlock, however, the other mechanical properties of this species are presented as average mechanical properties of species in the wood handbook (2010). In table 2.2, specific gravity, modulus of elasticity and shear strength (parallel to grain) of three species are presented. Other properties such as shear modulus and rolling shear modulus are estimated according to the suggested relation in the ANSI/APA PRG-320-2012. This product standard assumed the shear modulus  $G$  of lumbers in major direction is 1/16 of modulus of elasticity ( $E/G_0 = 1/16$ ). It is also suggested the width of the cross-layer to thickness shall be more than 3.5 for not edge bonded if not testing is done to assess the rolling shear strength. In figure 2.7, the deformation and relationship between rolling shear modulus and major shear modulus for 5-layer CLT cross-section is shown.

Table 2.2: Mechanical properties of Eastern Hemlock

	Specific Gravity	Modulus of Elasticity (MPa)	Shear Strength parallel to grain (MPa)	Shear Modulus parallel to grain (MPa)	Rolling Shear Modulus (MPa)
Eastern Hemlock	0.4	8300	7.3	518	51.8

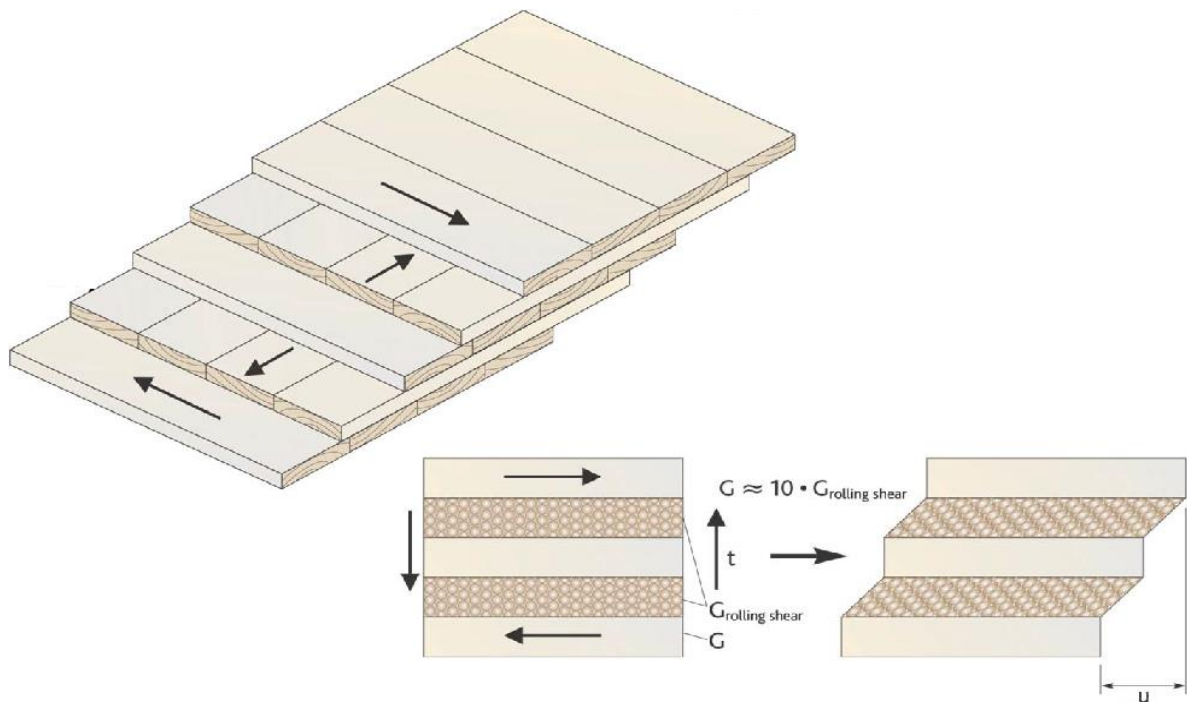


Figure 2.7: Rolling Shear Deformation of CLT Panel (Karacabeyli & Douglas, 2013)

### 2.2.2. Shear Deformation

Shear deformation for CLT panel is greater than for other wood products. It is because of the low rolling shear modulus of the cross-lamination. Many factors such as loading, span length to depth ratio, and end fixity of panels are controlling the amount of deformation. Fellmoser and Blass, (2004) analyzed a CLT panel with variety span to depth

ratio using shear analogy method to determine the shear deformation effect. According to their finding, the proportion of shear deformation significantly increases when the span to depth ratio reduces. For example, according to the figure 2.8, while the contribution in shear deformation to the total deformation of a panel for a uniformly-loaded, simply supported slab with the span-to-depth ratio of 15 was about 30%, it was 11% for a panel with the span-to-depth ratio 30. Same results were obtained by Saavedra Flores et al. (2015), who developed analytical models to predict the behavior of CLT panels for different span-to-depth ratios. They also performed several experimental tests on CLT panels made of Chilean radiata pine to measure the effect of span-to-depth ratio on rolling shear capacity. They found the failure load decreases by 50% when the span-to-depth ratio increases 2.5 times.

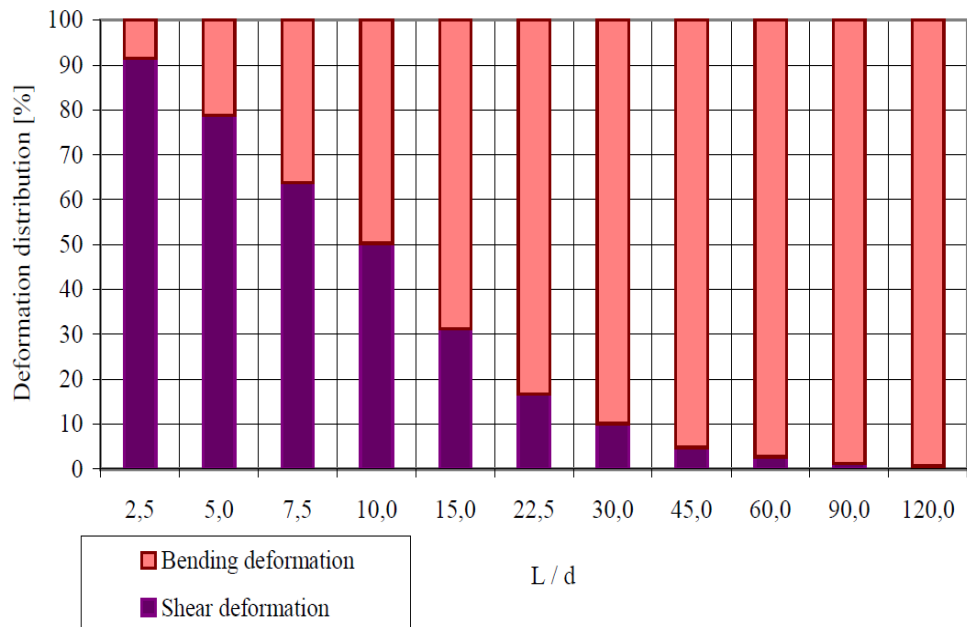


Figure 2.8: Proportion of shear and bending deformation versus span to depth ratio (Fellmoser and Blass, 2004)

### 2.2.3 Determination of Rolling Shear Modulus

There is no international standard test for direct determination of rolling shear and apparent shear modulus of lumbers and CLT panels. In the European product standard EN 16351 (2015) there is a two type of shear detailed instructions test for determination of the rolling shear properties of a cross-layer of boards. The first method in European standard EN 789 (2004) is the so-called two-plate shear test which is designed for the determination of in-plane shear properties of specimens. The second method is an improved type of the two-plate shear test method which is intended for a broader dimensional variability of the panels. It also avoids the lateral steel plates by transfer of the loads via lengthwise oriented boards.

There are two more two-plate shear tests:

- 1) European standard EN 408 (2012) on the determination of shear strength parallel to the fiber of solid wood
- 2) ASTM standard D 2718 (2011)

ASTM standard D 2718 (2011) is served for the determination of in-plane shear properties of panels. In this standard, there are two test methods, 1- planar shear loaded by plates and 2-planar shear induced by five-point bending.

In the planar shear loaded by plates, the load would be created by using steel plates which are adhered to rectangular panel section. Then a gage measures slip between the steel plates (see figure 2.9). In this method, shear strength and modulus of structural panels associated with shear distortion of the planes parallel to the edge planes of the panels can be obtained. Essentially, the tests measure the shear in-plane (rolling shear for 90-degree

orientation) strength developed in the plane of the panel. Consequently, shear strength is computed from the maximum load, and effective shear modulus for the specimen is determined from a plot of load versus slip. Although this test method does not produce pure shear, the specimen length is prescribed so that the secondary stresses have a minimum effect.

ASTM D2718 suggested either (a) the use of larger specimens with 15 cm width and 45 cm length, or (b) the use smaller specimens if the width and length are more than four and twelve times the thickness of the wood (ASTM D2718-2011).

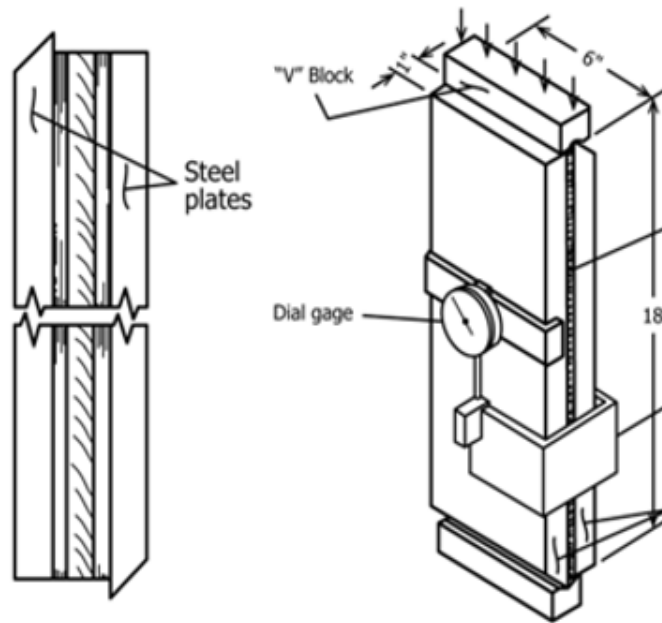


Figure 2.9: Planar Shear Test Setup (ASTM D2718-2011).

The slip between steel plates due to shear deformation is measured through two gages on both sides. Then the rolling shear modulus of samples can be obtained by Eq (1)

$$G = \frac{P}{\Delta} \left[ \frac{t}{L \times w} \right] \quad (1)$$

Where  $t$  is the thickness of specimen,  $L$  and  $w$  are the specimen length and width respectively,

,  $P/\Delta$  is the slope of the force-deformation curve below the proportional limit load,

Shear strength ( $f_v$ ) of a specimen can be calculated according to the peak load.

$$f_v = \frac{P_{max}}{L \times W} \quad (2)$$

Where  $P_{Max}$  is the peak load in the shear test.

### **2.3. Standard & Design Method**

For analysis and design of CLT, several approaches have been created and are commonly used around the world. These methods are:

- 1- Mechanically Jointed Beams Theory (Gamma Method)
- 2- Composite Theory (k Method)
- 3- Shear Analogy Method
- 4- Simplified Design Method
- 5- Classical Lamination Theory (CLT)

The CLT code (Standard for performance-rated cross-laminated timber. ANSI/APA PRG, 320) in the United State and Canada has accepted shear analogy method to obtain mechanical properties of composite panels. The simplified design method has also been accepted for bending strength of panels; however, shear analogy method is more accurate than others. In the following section, a summary of the shear analogy method and classical lamination theory is illustrated.

### 2.3.1- Shear Analogy Method

The “shear analogy” is a new method has been specially developed by Kreuzinger, (1999) for solid panel floors with cross layers. In this method, the shear deformation of cross layers is taken into account and can be applied to the unlimited number of layers within a panel (Karacabeyli & Douglas, 2013). In this method, the characteristic of multi-layer CLT panels are considered as two virtual beams A and B. While beam A represent the bending and shear stiffness of each ply along their center, beam B is representing the “Steiner” points or increased moment of inertia due to the distance from the natural axis. As can be seen in figure 2.10, these beams are rigidly linked with members, so that equal deflection for both beams is obtained. Then the final results for the whole cross-section can be calculated by overlaying the bending and shear stress/stiffness of both beams (Fellmoser & Blass, 2004)

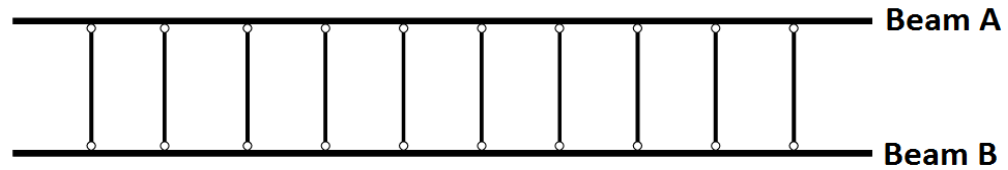


Figure 2.10: Beam Modeling for Shear analogy method

A bending stiffness equal to the sum of the inherent bending stiffness of all the individual layers assigned to beam A as shown in Eq.3.

$$(B)_A = \sum_{i=1}^n E_i \cdot I_i = \sum_{i=1}^n E_i \cdot b_i \cdot \frac{h_i^3}{12} \quad (3)$$

The bending stiffness of beam B is obtained using the parallel axis theorem.

$$(B)_B = \sum_{i=1}^n E_i \cdot I_i \cdot z_i^2 \quad (4)$$

Furthermore, beam B has a shear stiffness  $(S_B)=(GA)_B$  and can be obtained as:

$$\frac{1}{S_B} = \frac{1}{a^2} \cdot \left[ \frac{h_1}{2 \cdot G_1 \cdot b_1} + \sum_{i=2}^{n-1} \frac{h_i}{G_i \cdot b_i} + \frac{h_n}{2 \cdot G_n \cdot b_n} \right] \quad (5)$$

Where modulus of elasticity parallel to the grain direction is  $E_0$  and  $E_{90}$  is a modulus of elasticity perpendicular to the grain direction ( $E_{90}=E_0/30$ ). Also, in these equations, the longitudinal shear modulus is  $G$ , while for cross laminations are called rolling shear  $G_R$  ( $G_R \approx G/10$ ).

The continuity of deflection between beam A and B must be valid at every point ( $\Delta_A=\Delta_B$ ), then the virtual section size of beam A and B and the values for  $M_A$ ,  $M_B$ ,  $V_A$  and  $V_B$  are obtained. Bending moments and shear forces of each layer beam A can be calculated by Eq.6 and 7.

$$M_{A.i} = \frac{E_i \cdot I_i}{B_A} \cdot M_A \quad (6)$$

$$V_{A.i} = \frac{E_i \cdot I_i}{B_A} \cdot V_A \quad (7)$$

Bending and shear stresses of each individual layer of beam A can be obtained by Eq. 8 and 9, respectively

$$\sigma_{A.i} = \pm \frac{M_{A.i}}{I_i} \cdot \frac{h_i}{2} \quad (8)$$

$$\tau_{A.i} = \frac{E_i \cdot I_i}{B_A} \cdot 1.5 \cdot \frac{V_A}{b \cdot h_i} \quad (9)$$

Axial forces and normal stresses of each layer of beam B and shear stresses at the interface of two layers of beam B can be obtained by Eqs.10, 11, 12, respectively.

$$N_{B,i} = \frac{E_i \cdot A_i \cdot Z_i}{B_B} \cdot M_B \quad (10)$$

$$\sigma_{B,i} = \frac{M_{B,i}}{b_i h_i} = \frac{E_i \cdot Z_i}{B_B} \cdot M_B \quad (11)$$

$$\tau_{B,i,i+1} = \frac{V_B}{B_B} \cdot \sum_{j=i+1}^n E_j \cdot A_j \cdot Z_j \quad (12)$$

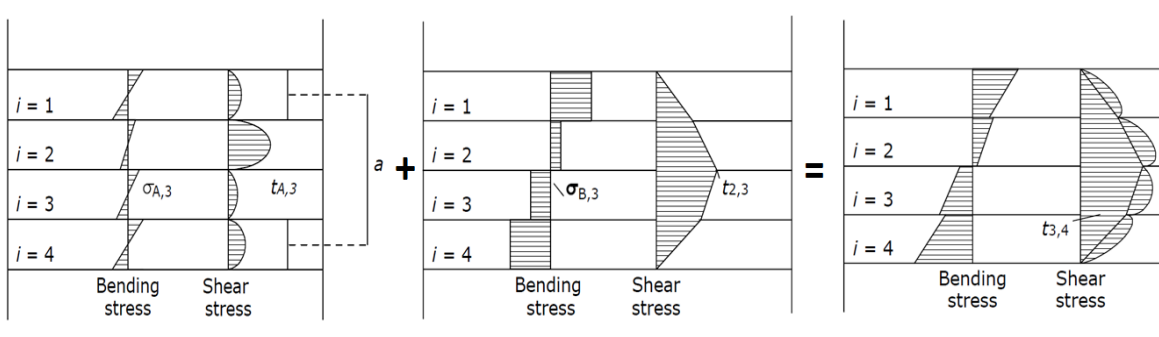


Figure 2.11: bending and shear stresses in beam A and B (left & middle), final stress distribution results from beam A and B (right) using shear analogy method (Karacabeyli & Douglas, 2013).

As can be seen from Figure 2.11 from the superposition law, the final stress distribution for beam A and B can be obtained. Using shear analogy method, the maximum deflection  $\Delta_{max}$  in the CLT panel under the uniformly distributed load with the contribution of both bending and shear stresses can be calculated using Eq.13.

$$\Delta_{max} = \frac{5}{384} \cdot \frac{w \cdot l^4}{EI_{eff}} + \frac{1}{8} \cdot \frac{wL^2 k}{GA_{eff}} \quad (13)$$

The effective bending stiffness ( $EI_{eff}$ ) and effective shear stiffness ( $GA_{eff}$ ) can be obtained from Eqs. 14, 15, respectively,

$$(EI)_{eff} = \sum_{i=1}^n E_i \cdot b_i \cdot \frac{h_i^3}{12} + \sum_{i=1}^n E_i \cdot A_i \cdot Z_i^2 \quad (14)$$

$$(GA)_{eff} = \frac{a^2}{\frac{h_1}{2 \cdot G_1 \cdot b} + \sum_{i=2}^{n-1} \frac{h_i}{G_i \cdot b} + \frac{h_n}{2 \cdot G_n \cdot b}} \quad (15)$$

#### 2.4. A Summary of Classical Lamination Theory

The Classical laminated theory (CLT) has apparently developed from work in the 1950s and 1960s. The only difference between this theory and classical theory of homogenous, isotropic plate is in the form of laminated stress-strain relationship. Another parts of the theory such as the deformation hypothesis, the equilibrium equations, and strain-displacement relationship is the same (Gere et al., 2012). In this method, a laminate is defined as a formed stack of singular filament direction instead of intertwined template. The layer orientation of each filament is determined as a stack. This method provides the analysis capability for the CLT panels with different fiber orientation and layup configuration.

In the CLT theory, it is assumed that individual laminae are fully bonded together so that their behavior is as a unitary, nonhomogeneous, anisotropic plate, so there is no interfacial slip among layers, which means that displacement across laminae interfaces is assumed to be continuous (Gibson, 2016). Figure 2.12 shows the sign convention for lamina.

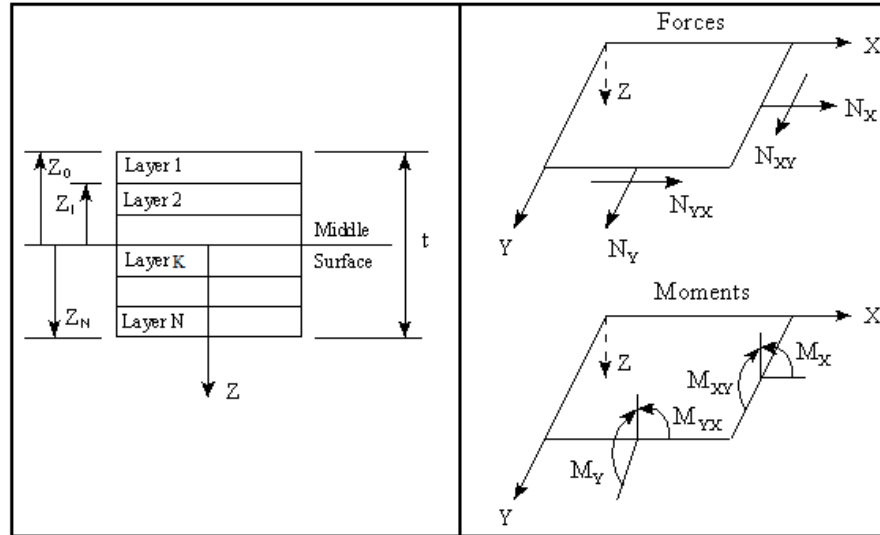


Figure 2.12: Sign Convention of the lamina

The subscript k, as can be seen in figure 2.13 refers to the  $k_{th}$  layer from above with the all number of N layers.

The elastic constitutive equation for laminate is presented here.

$$\begin{Bmatrix} \mathbf{N} \\ \mathbf{M} \end{Bmatrix} = \begin{bmatrix} \mathbf{A} & \mathbf{B} \\ \mathbf{B} & \mathbf{D} \end{bmatrix} \begin{Bmatrix} \boldsymbol{\varepsilon}^0 \\ \boldsymbol{\kappa} \end{Bmatrix} \quad (16)$$

Where A is named the extensional stiffness, B is named the coupling stiffness, and D is named the bending stiffness of the laminate. The components of these stiffness matrices are determined here:

$$\begin{aligned}
A_{ij} &= \sum_{k=1}^N (\bar{C}_{ij})_k (z_k - z_{k-1}) = \sum_{k=1}^N (\bar{C}_{ij})_k t_k \\
B_{ij} &= \frac{1}{2} \sum_{k=1}^N (\bar{C}_{ij})_k (z_k^2 - z_{k-1}^2) = \sum_{k=1}^N (\bar{C}_{ij})_k t_k \bar{z}_k \\
D_{ij} &= \frac{1}{3} \sum_{k=1}^N (\bar{C}_{ij})_k (z_k^3 - z_{k-1}^3) = \sum_{k=1}^N (\bar{C}_{ij})_k \left( t_k \bar{z}_k^2 + \frac{t_k^3}{12} \right)
\end{aligned}$$

(17)

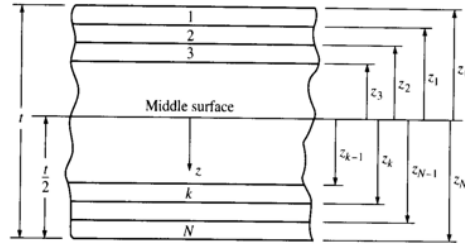


Figure 2.13: laminated plate geometry

Where  $t_k$  is the thickness of the  $k$ th layer and  $z_k$  is the distance of the center of the plate to the centroid of the  $k$ th layer. Creating the matrices of stiffness, A, B, and D, is the most important stage in the analysis of composite laminates.

A laminate with the nonzero  $B_{ij}$  will bend or twist under loads. This laminate will also display mid-plane stretching under bending loads. The symmetry of laminate geometry and material properties with respect to the middle surface leads to the condition that all  $B_{ij} = 0$ . Therefore, to avoid the stretching or warping of CLT panels, all laminates will be symmetrically configured.

#### 2.4.1. Laminate Engineering Constants

Sometimes it is more appropriate to use effective laminate engineering constants rather than the laminate's stiffness defined in equations 17. These constants are derived from laminate compliances. The effective longitudinal and transverse modulus of elasticity,  $E_x$  and  $E_y$  defined as the response of laminates under the single axial load per unit length when the other axial loads are zero. Figure 2.14 shows the in-plane loading of laminate for defining laminate engineering constants.

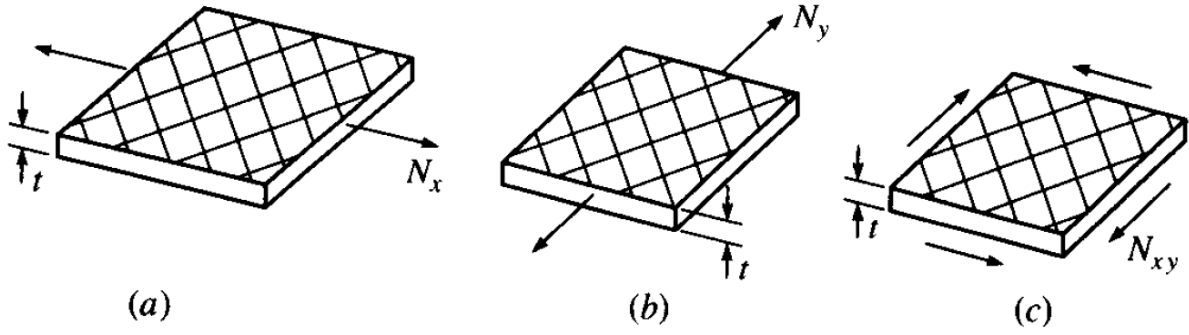


Figure 2.14: in-plane loading of laminate to determination of laminate

engineering constant. a) single axial load  $N_x$  with  $N_y=N_{xy}=0$ , b) single axial load  $N_y$  with

$N_x=N_{xy}=0$ , c) pure shear load  $N_{xy}$  with  $N_x=N_y=0$

$$\begin{cases} \epsilon_x^0 \\ \epsilon_y^0 \\ \gamma_{xy}^0 \end{cases} = \begin{bmatrix} A'_{11} & A'_{12} & A'_{16} \\ A'_{12} & A'_{22} & A'_{26} \\ A'_{16} & A'_{26} & A'_{66} \end{bmatrix} \begin{cases} N_x \\ N_y \\ N_{xy} \end{cases} \quad \begin{aligned} E_x &= \frac{\sigma_x}{\epsilon_x^0} = \frac{N_x/t}{A'_{11}N_x} = \frac{1}{tA'_{11}} \\ E_y &= \frac{\sigma_y}{\epsilon_y^0} = \frac{N_y/t}{A'_{22}N_y} = \frac{1}{tA'_{22}} \\ G_{xy} &= \frac{\tau_{xy}}{\gamma_{xy}^0} = \frac{N_{xy}/t}{A'_{66}N_{xy}} = \frac{1}{tA'_{66}} \end{aligned} \quad (18)$$

Similarly, the effective laminate flexural moduli can be expressed in terms of flexural compliances.

$$\begin{cases} \kappa_x \\ \kappa_y \\ \kappa_{xy} \end{cases} = \begin{bmatrix} D'_{11} & D'_{12} & D'_{16} \\ D'_{12} & D'_{22} & D'_{26} \\ D'_{16} & D'_{26} & D'_{66} \end{bmatrix} \begin{cases} M_x \\ M_y \\ M_{xy} \end{cases} \quad \begin{aligned} E_{fx} &= \frac{12}{t^3 D'_{11}} \\ E_{fy} &= \frac{12}{t^3 D'_{22}} \end{aligned} \quad (19)$$

For all laminate orientation and configuration, the laminates stiffness A, B and C are meaningful, however, the effective laminate stiffness may not valid for all configuration. It can clearly be recognized this constant are meaningful for symmetric laminates which  $B=0$  this means that bending moments will not generate stress and deformation at the middle surface of CLT panels and also warping under in-plane load

will not occur. So the deformation of laminates would be similar to the equivalent homogenous material.

In December 2011, ANSI/APA PRG 320, a standard for Performance-Rated CLT was published by the ANSI/APA CLT standard committee and updated in 2018 (ANSI 2018). This standard motivated acceptance and harmonization of CLT panels in North America (US & Canada). The ANSI/APA PRG 320 standard has been approved by the Structural Committee of the International Code Council (ICC) and is included in the 2015 International Building Code (IBC 2015) and also there is a chapter assigned to CLT in 2015 edition of National Design Specification (NDS) For Wood Construction (American Wood Council 2015). ANSI/APA PRG 320 considers Shear Analogy method as the main analytical method for evaluating mechanical properties of CLT panels. This study follows methods and instructions provided in ANSI/APA PRG 320 as the broadly accepted standard to evaluate the structural performance of CLT panels.

## **CHAPTER 3**

### **PLANAR SHEAR PROPERTIES OF EASTERN HEMLOCK**

The goal of this study is to evaluate the planar shear properties of Eastern Hemlock for different fiber orientations in order to increase its potential for use in CLT products. To this end, a planar shear test (also called two-plate shear test) was conducted according to ASTM 2718 (ASTM 2011). The technical content of this chapter has been submitted to the ASCE Journal of Materials in Civil Engineering as provided in Appendix B.

#### **3.1 Analyzing the Effect of Fiber Orientation Using Classical Lamination Theory (CLT)**

According to classical laminated theory, a case study analysis was performed to compare effective laminate moduli for short span-to-depth ratio of CLT panels in variety of orientations. For this purpose, the laminator software was used to estimate the laminate engineering constant. This software has been developed according to the classical lamination theory can analyze the laminates for different orientations and configurations.

The lumbers for the CLT panels are 2x4 Eastern Hemlock in all layers. According to IBC 2015, the concentrated load to be 8.9 KN which is suggested for the live load of office building is assigned to middle span of CLT panel. The material properties of wood is specified from wood handbook (2010), ANSI/APA PRG320 and National Design Specification (NDS) (2015).

Figure 3.1 shows a three layer CLT panel with the 609 mm length, 305 mm width and 99 mm thick (each layer is 33 mm). The direction of top and bottom laminates fiber are parallel to the direction of loads, however, the orientation of mid-layer is changing from zero to 90 degree with the step of 10 degrees. Because of symmetric configuration of laminates, the effective engineering constants are meaningful. In other words, these effective stiffness values could be real representative of CLT panels under the real loading.

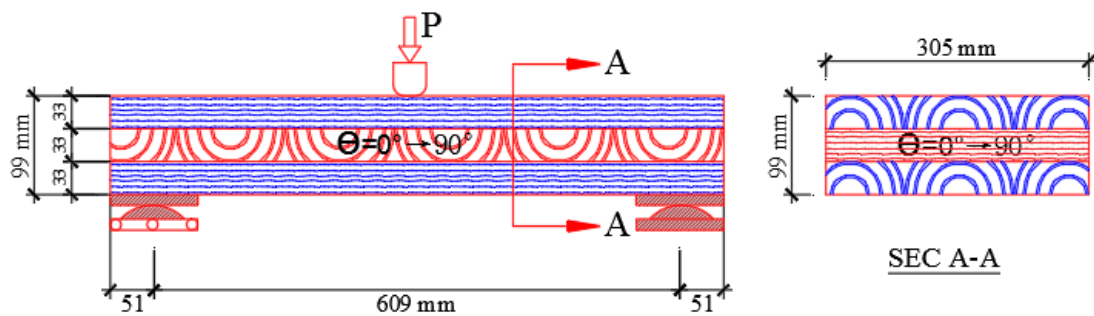


Figure 3.1: Longitudinal and Cross Section of CLT Floor Panel

The results of analysis are summarized in figure 3.2. As can be seen, with increasing the orientation of mid-layer, the effective longitudinal young's modulus and flexural modulus are dropping. Conversely, the effective modulus in transverse direction are rising by increasing the orientation of mid-layer. More importantly, the effective in-plane shear modulus is at the highest value for 30 degree. Therefore, it would be expected the mechanical properties of CLT panels specifically rolling shear strength improve in this fiber orientation

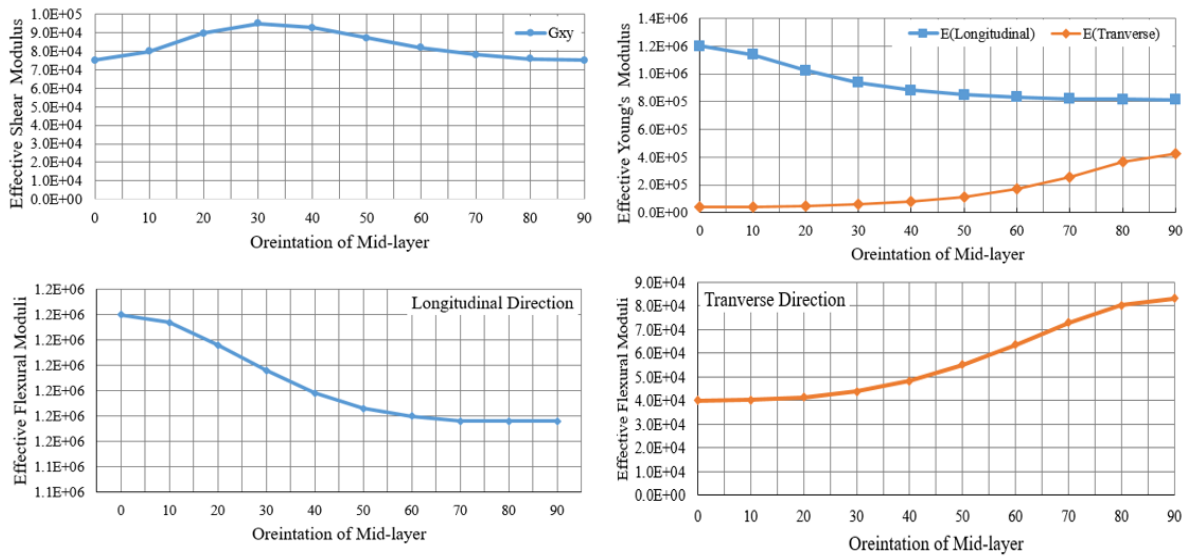


Figure 3.2: Variation of Effective Engineering Constant with Respect to Orientation of Mid-Layer

### 3.2 Materials and Methods

#### 3.2.1 Specimen Preparation

A total of 20 kiln dried Eastern Hemlock 2x4s of lengths between 2 to 3.5 m were purchased from a local mill in Massachusetts. The boards arrived planed and joined to dimensions of 33mm x 84mm. The first author graded the boards according to NELMA (Northeastern Lumber Manufacturers Association) grading rules and found all boards to be flat-sawn, and either No.1 and No.2 grade. The specific gravity was measured in accordance with ASTM D 2395 (ASTM 2014), and ranged from 0.37 to 0.5 with a mean value of 0.42. The boards were placed in an environmental conditioning chamber set at a temperature of  $20 \pm 3^\circ\text{C}$  and relative humidity of  $65 \pm 2\%$  to maintain equilibrium moisture content of about 12%.

#### 3.2.2 Required Sample Size

The sample size required for each orientation is estimated by two-stage method using following equation (ASTM D2915-2010). This equation assumes the data is normally distributed and the mean is to be estimated to within 5% with specified confidence:

$$n = \left( \frac{t}{\alpha} \cdot CV \right)^2 \quad (20)$$

where:

n = sample size,

CV = coefficient of variation,

$\alpha$  = estimate of precision, (0.05),

t = value of the statistic,

The value of t and CV are not known before begins the testing program. However, the value of CV for shear test can be approximated by using the results of other shear test program. So the coefficient of variation for shear strength is assumed to 14% (Wood Handbook, 2010, p.5-26). Considering the 75 % for confidence interval, the t value is obtained 1.17,

$$n = \left( \frac{1.17}{0.05} \times 0.14 \right)^2 = 12$$

According to this calculation, 12 sample size for each group of shear test was required. Finally, the sample size has been adjusted based on the new results. Then a total of 75 specimens were prepared into five groups in terms of fiber orientation.

Figure 3.3 depicts the basic process used to fabricate the two-plate assembly: cutting the wood pieces to size, edge gluing the pieces together, preparing the steel plates (not shown), and then pressing the assembly in a mechanical press. The following sections describe the process in detail.

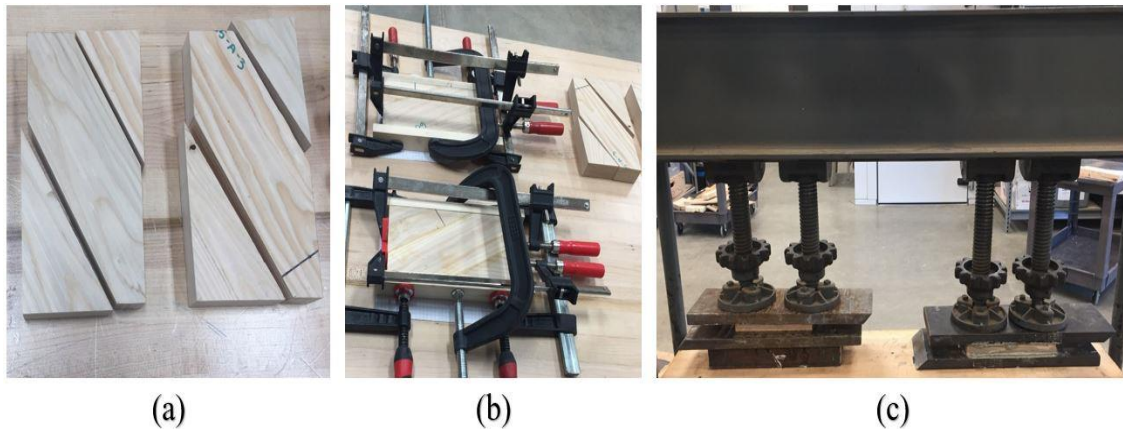


Figure 3.3: Fabrication process for two-plate shear test assembly: (a) Wood cutting, (b) edge gluing and surface preparation, (c) specimen pressing, curing

The dimensions of the wood pieces used in making the specimens for each fiber orientation is given in figure 3.4. Although each orientation is made up of different size pieces, the overall volume of wood used is consistent for each orientation (33mm thick  $\times$  119 mm wide  $\times$  237mm long). Specimen lengths and widths were measured to the nearest 0.25 mm, and thickness was measured to the nearest 0.025 mm. Due to limitations of the testing machine, the width and length dimensions were slightly less than suggested by ASTM D2718 (ASTM 2011), which is either (a) 150mm width  $\times$  450 mm length, or (b) smaller dimensions, if the width and length are more than four and twelve times, respectively, the thickness of the wood. The growth ring orientations of the adjacent pieces were alternated and edge bonded to optimize shear strength performance.


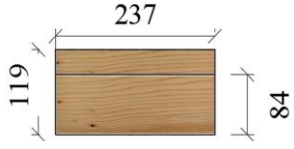

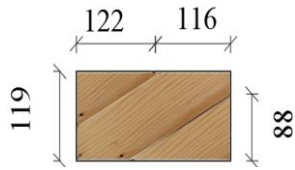

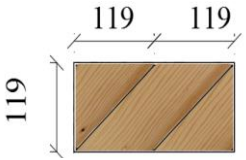

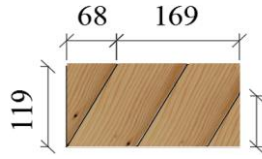

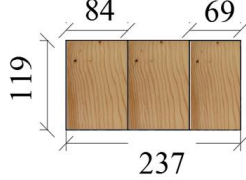
Fiber Orientation (degrees)	Sketch of wood pieces glued to steel plates	Wood dimensions (in mm)
0		
30		
45		
60		
90		

Figure 3.4: Size of the pieces for different fiber orientation in two-plate shear test

Preliminary compression perpendicular to grain tests (ASTM D143-2000) were conducted to assess the capacity of the Eastern Hemlock prior to gluing the specimens. This was done to ensure no damage would occur to the wood from pressure needed to cure the glue. In total, 15 specimens were milled to 33×84×203 mm and load was applied

through bearing plates to the tangential surface of the specimen (Figure 3.5). The mean compressive strength perpendicular to the grain was 4.1 MPa with extreme values ranging from 2.6 to 5.8 MPa.

The steel plates were prepared by first scrubbing them with a clean bristle brush under cold running tap water to remove residue from any previous test. The steel plates were then heated in an oven at 150°C for 1 hour to dry completely and to avoid any oxidation of the metal surfaces. Three types of adhesives were assessed for bonding the wood to the steel: 1) Loctite PL Premium Fast Grab Polyurethane, (LOCTITE®) 2) System Three G-2 epoxy, and 3) System Three T-88 epoxy (SYSTEMTHREE). In the end, Loctite PL Premium adhesive, with the spread rate of 1500 g/m<sup>2</sup> and an assembly time 20 min, was used for bonding the specimens to avoid glue failure during the shear tests.

The two-plates shear test assembly was finally formed by applying a uniform pressure of 1.0 MPa through a mechanical press for 48h at 25°C. Specimen thickness was measured before and after pressing to be sure that the thickness of the specimen did not change.

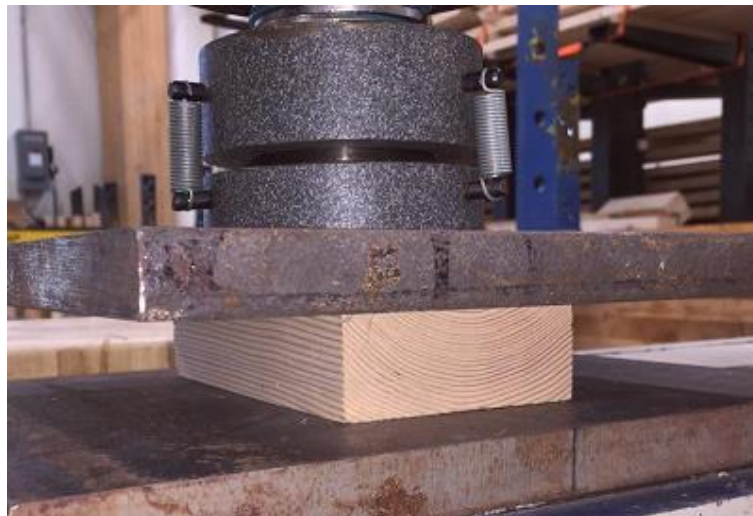


Figure 3.5: Test setup for compression perpendicular to grain test

### 3.3 Test Method

Figure 3.6 shows the test setup whereby the compressive load is applied through steel blocks with grooves which concentrically load the knife edges of the steel plates. The knife-edge of the plates provides pin support during loading of the specimen. The angle of specimen inclination ( $\alpha$ ), between the direction of the applied shear force ( $V$ ) and the bond line of the specimen, is a function of the steel plate size and the specimen size. In our case, the angle of inclination was 8 degrees.

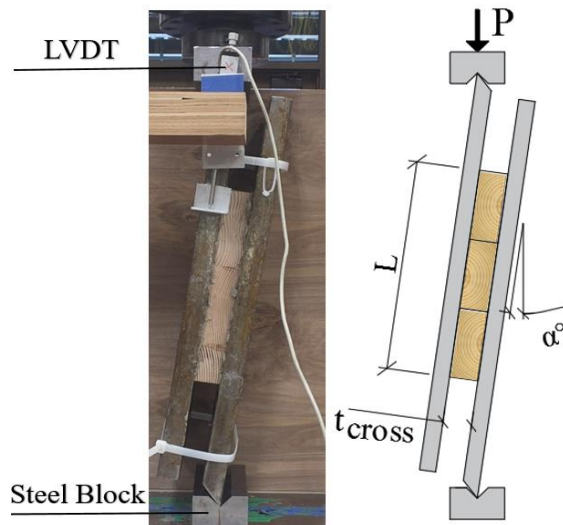


Figure 3.6: Experimental setup for two-plate shear test

In accordance with ASTM D2718 (ASTM 2011), failure should occur in the range of 3 to 12 minutes elapsed time from start of loading. The shear force should be continuously applied to the steel plate at a constant rate as follows:

$$N = 0.0075 \times R \times \sum t \quad (21)$$

where N is the crosshead speed, R is a ratio of the shear modulus of the parallel plies to the shear modulus of the perpendicular plies and t is the total thickness of laminates. In our case, the crosshead speed of 0.508 mm/min lead to specimen failures within 5 to 9 minutes depending on the fiber orientation of specimens.

Shear modulus (G) was calculated based on the equation provided in ASTM D2718 (ASTM 2011) adjusted to account for the angle of specimen inclination ( $\alpha$ ) as follows:

$$G = \frac{P \times \cos \alpha}{\Delta} \left[ \frac{t}{L \times W} \right] \quad (22)$$

Where t is the thickness of the specimen, L and W are the specimen length and width respectively, and P/ $\Delta$  is the slope of the linear range of the load-deformation curve below the proportional limit (i.e. within a load range of 10% to 40% of the maximum load). Linear Variable Differential Transformers (LVDTs) were employed to measure the relative displacement of the movable steel plate (on the left in figure 3.6) to the supported one during the test to the nearest 0.002 mm.

The shear strength ( $f_v$ ) of the specimens was calculated based on the maximum load as follows:

$$f_v = \frac{P_{max} \times \cos \alpha}{L \times W} \quad (23)$$

where  $P_{max}$  is the peak load.

### 3.4 Results and Discussion

#### 3.4.1 Failure modes

Figure 3.7 displays typical failure surfaces of specimens for each fiber angle tested. Not surprisingly, the predominant failure mode for the parallel to grain ( $0^\circ$ ) specimens (in horizontal shear) was distinctly different than that of the angled specimens (in combined horizontal and rolling shear) or the  $90^\circ$  specimens (in rolling shear). The  $0^\circ$  specimens (Figure 3.7a) failed in a brittle manner along the fiber direction without any obvious pre-cracking developing in the specimens during the test. However, for specimens with fiber angles from  $30^\circ$  to  $90^\circ$  (Figs. 3.7 b, c, d, e), an initial inclined shear crack generally appeared at approximately 50% to 60% of the peak load (Figure 3.8a). The crack propagated along the growth ring with increasing load until the entire specimen fractured (Figure 3.8b) precipitating a nonlinear maximum loading range.

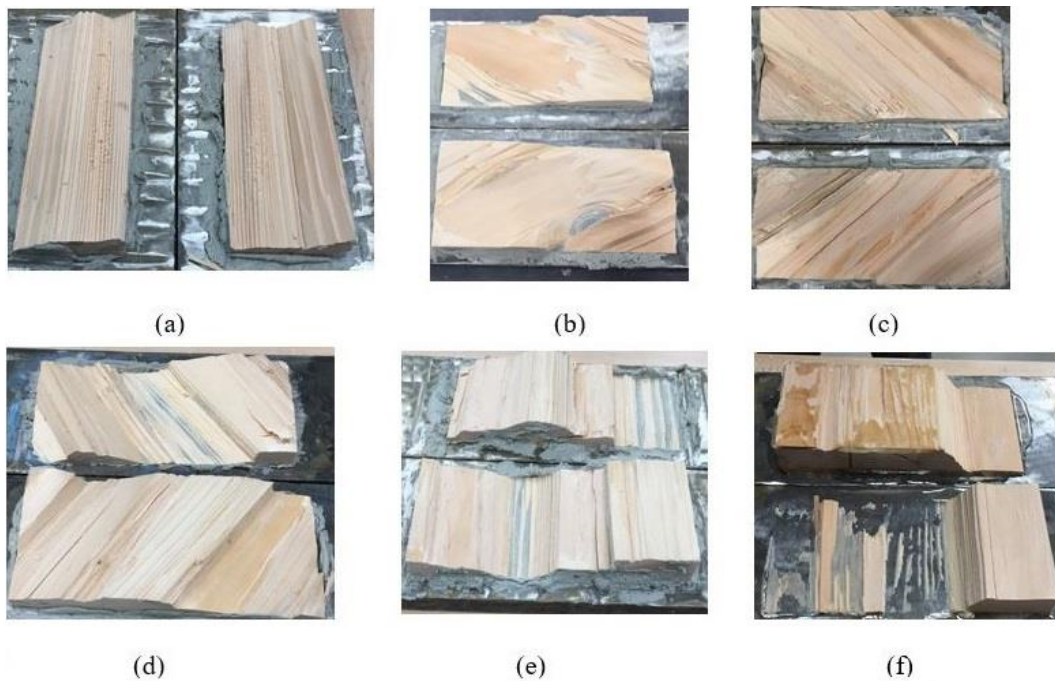


Figure 3.7: Typical failure appearances of specimens tested in 2 plate shear: (a)  $0^\circ$ , (b)  $30^\circ$ , (c)  $45^\circ$ , (d)  $60^\circ$ , (e)  $90^\circ$ , (f) glue failure

No glue failure was observed for the  $30^\circ$  to  $60^\circ$  specimens. Glue failure did occur, however, for two  $0^\circ$  specimens and three  $90^\circ$  specimens (Figure 3.7f). In total, 80 specimens were tested and five of them were excluded from the data analysis due to glue failure.



Figure 3.8: Failure mode I: (a) formation of the first crack (b) propagation of cracks along growth rings at final failure

### 3.4.2 Load-Displacement Curves

Figure 3.9 presents the full range of the load-displacement curves of the specimens. The mechanical behavior of the five data sets is clearly different. Most obvious is that the pure rolling shear failure of the  $90^\circ$  specimens is much weaker than the pure horizontal shear failure of the  $0^\circ$  specimens; moreover, the  $90^\circ$  specimens are far more ductile with large deformation after peak load than the  $0^\circ$  specimens which fail consistently in an abrupt, brittle manner with the yield load and ultimate load being consistently coincident.

For the mixed mode specimens, with fiber angles of 30°, 45°, and 60°, it can generally be seen that with increasing fiber angle, there is decreasing initial stiffness and strength. A common behavior observed for these specimens was a type of sequential fiber failure and corresponding load peaks and drops evident in their curves. After the formation of the first failure crack, the shear stress was redistributed until the next crack initiated. This pattern repeated several times before the ultimate peak load and the slope of curves progressively decreased, gradually reducing the stiffness of the specimens, with increased displacement.

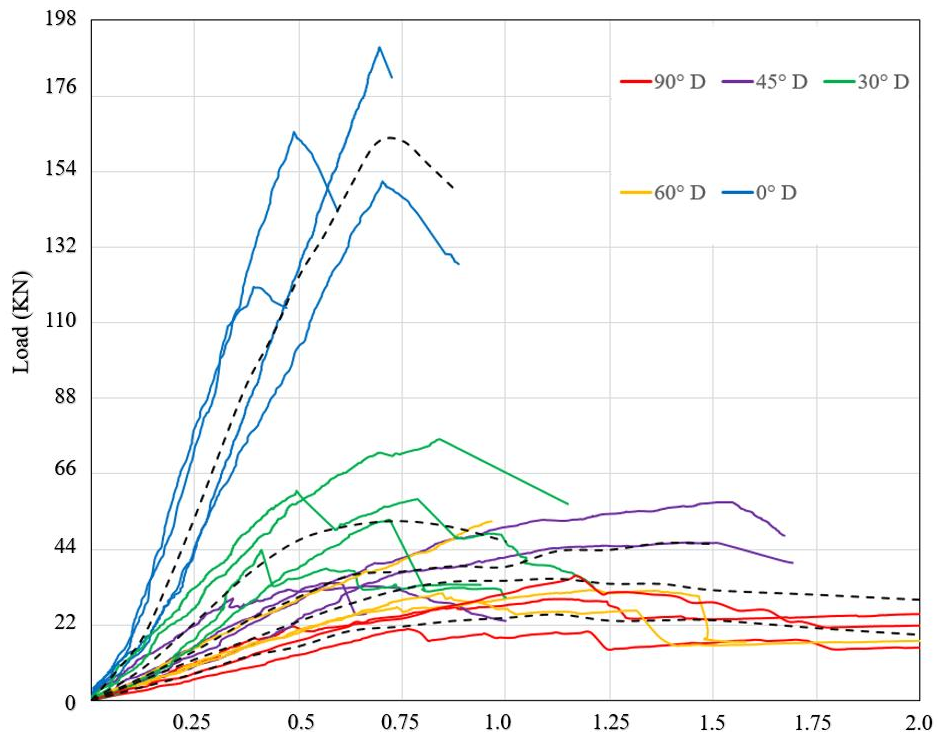


Figure 3.9: Load-displacement curves of specimens under two-plate shear test for different fiber orientations

### 3.4.3 Planar Shear Properties

Descriptive statistics for planar shear properties of Eastern Hemlock, for all fiber orientations tested, are provided in Table 3.1. The shear moduli ( $G$ ) were evaluated in accordance with Equation 2 and the shear strength ( $F_v$ ) were evaluated at peak load per

Equation 3. Figures 3.10 and 3.11 present the data visually for moduli and strength respectively, as cumulative frequencies with fitted Burr cumulative distribution curves. The Burr distribution has been used to fit a wide variety of experimental data, including failure data.

A one-way analysis of variance (ANOVA) was performed at the 5 percent significance level between the five fiber orientations for both stiffness and strength. The results confirmed that there were highly significant differences among the means of these groups (p-values < 0.001), indicating that fiber orientation had a statistically highly significant effect on both stiffness and strength.

The mean rolling shear modulus  $G_{90}$  (45 MPa) was 11% of the mean longitudinal shear modulus  $G_0$  (398 MPa) which is consistent with the ratio suggested in ANSI/APA PRG-320 for rolling shear to longitudinal shear moduli ( $G_{90}=0.10G_0$ ). Meanwhile, the mean  $G$  values of the specimens with  $60^\circ$ ,  $45^\circ$ , and  $30^\circ$  fiber orientation were approximately 35%, 95% and 244% higher values, respectively, than  $G$  perpendicular-to-grain, demonstrating a progressive increase in shear modulus when fiber orientation decreases with respect to load direction.

The findings are similar for shear strength: the mean longitudinal shear strength  $F_{v0}$ , is 5.5 times more than the rolling shear strength  $F_{v90}$  and for the angles in between the mean strengths were 33%, 50%, and 100% more. Referencing figure 3.11, one can compare the characteristic design strength values of each angle (i.e. the 5<sup>th</sup> percentile with 75% confidence). The characteristic rolling shear strength  $F_{vr,05}$  (0.89 MPa), is approximately 20% of the characteristic longitudinal shear strength  $F_{v,05}$  (4.5 MPa). This ratio is in agreement with Bendtsen (1976), who studied five western and four eastern softwood

species and found rolling shear strength is about 20-25% of longitudinal shear strength. Also, it is within the range of 18% to 28% which is given in the Wood Handbook (Ross 2010). For reference, ANSI/APA PRG-320 suggests the rolling shear strength to be one-third (33%) of the longitudinal shear strength. The characteristic shear strength for perpendicular and parallel direction is 12% and 89% higher than characteristic shear strength requirement for CLT grade E3.

The characteristic shear strength for 60°, 45°, and 30° fiber orientation is 1.17, 1.42, and 1.77 MPa respectively, which is 26%, 31% and 39% of the longitudinal shear strength value.

Table 3.1: Planar shear properties for different fiber orientations

Fiber Orientation	0		30		45		60		90	
Mechanical Prop.	$f_v$ (MPa)	$G_r$ (MPa)	$f_v$ (MPa)	$G_r$ (MPa)	$f_v$ (MPa)	$G_r$ (MPa)	$f_v$ (MPa)	$G_r$ (MPa)	$f_v$ (MPa)	$G_r$ (MPa)
Mean	6.6	398	2.4	151	1.8	88	1.6	61	1.2	45
SD	0.86	54.6	0.36	22.7	0.30	10.3	0.30	8.2	0.17	6.9
COV (%)	12.9	13.8	15.3	15.1	16.6	11.7	18.1	13.4	14.2	15.1
Min	4.94	307	1.88	120.7	1.22	71.4	1.17	49.6	0.85	37.2
Max	7.79	520.6	3.11	191.7	2.08	104	2.14	83.4	1.49	61.4
Count	15		15		15		15		15	

Note: COV = coefficient of variation.

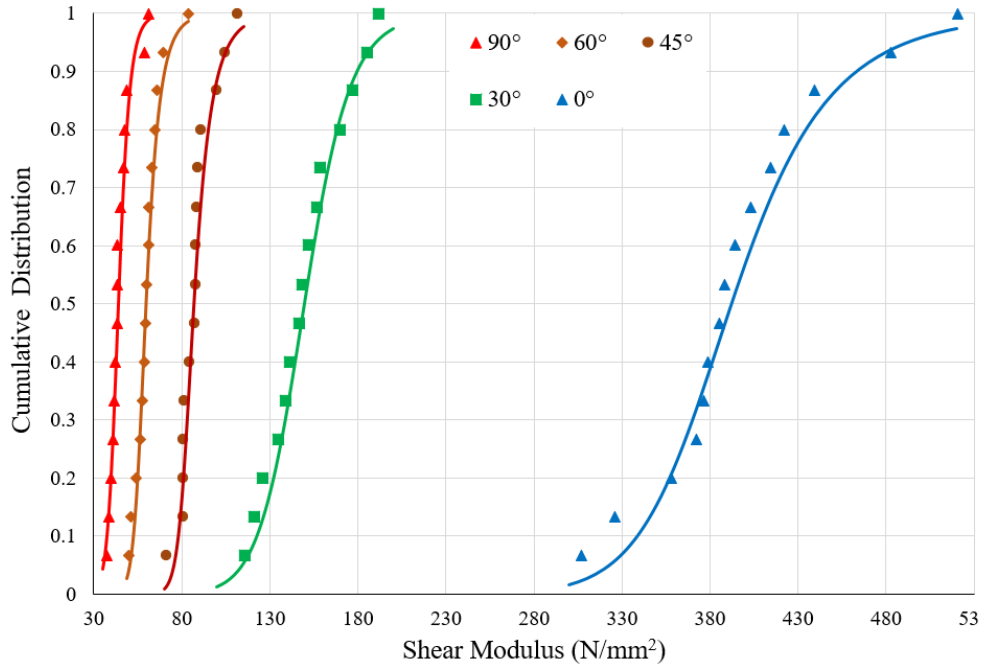


Figure 3.10: Cumulative frequency and fitted Burr distribution for shear modulus from 0° to 90° fiber orientation

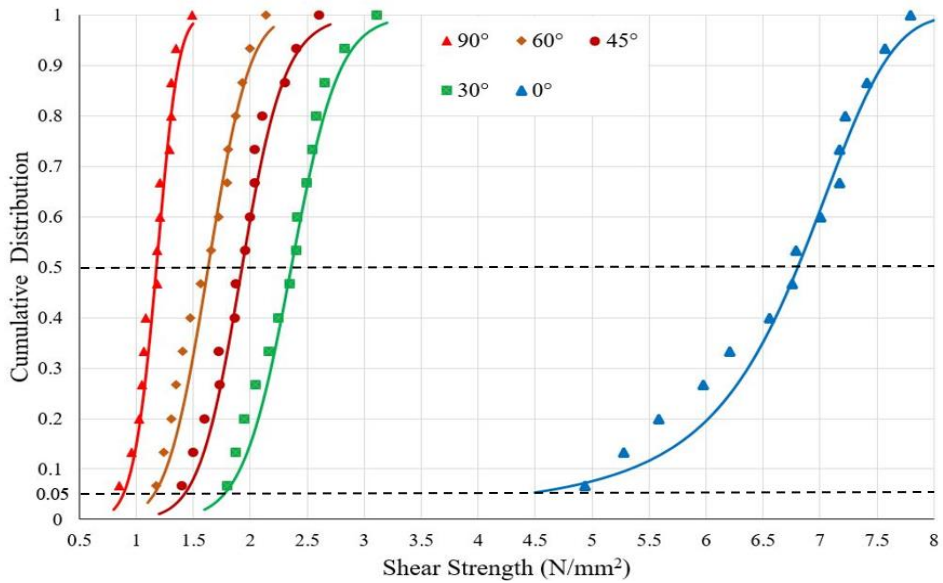


Figure 3.11: Cumulative frequency and fitted Burr distribution for shear strength from 0° to 90° fiber orientation

### 3.4.4 Effect of Fiber Orientation on Planar Shear Properties

Figure 3.12 visually depicts the relationship between fiber orientation and shear modulus (left) and between fiber orientation and shear strength (right). Also plotted on these graphs is Hankinson formula to gauge its effectiveness in predicting moduli and strength based on fiber orientation. The Hankinson formula was developed by the U.S. Army in 1921, and is widely used for estimating the off-axis uniaxial compressive strength of wood (Kim, 1986). When determining shear stresses values at an angle to grain, Hankinson formula takes the following form:

$$F_{V\theta} = \frac{F_{V0} \times F_{V90}}{F_{V0} \times \sin^2 \theta + F_{V90} \times \cos^2 \theta} \quad (24)$$

where  $F_{V\theta}$  is the shear stresses at angle  $\theta$ , and  $F_{V0}$  and  $F_{V90}$ , are stresses parallel and perpendicular to the grain, respectively. The formula appears to fit the data fairly well, particularly for shear modulus. The largest difference from the mean is for the 30° specimens in both cases: for shear modulus, the predicted value is 135MPa (10% lower than experimental mean) and for shear strength, the predicted value is 3.05 MPa (27% higher than experimental mean).

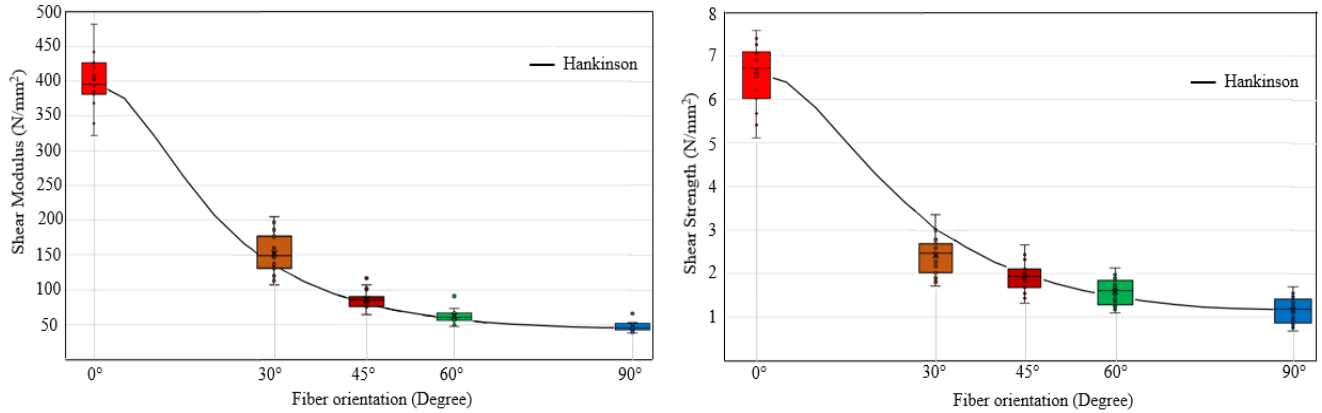


Figure 3.12: A comparison of Hankinson Formula with planar test for shear properties of Eastern Hemlock in different fiber orientation: (left) modulus, (right) strength

It is well understood that the 0° specimens are stiffest and strongest owing to wood’s natural resistance to fibers sliding past each other in the longitudinal direction; and in contrast, the 90° specimens are the least stiff and least strong due to the wood’s natural low resistance to the fibers rolling over each other. What happens in between these two ‘pure’ shear stress states, in the angled specimens, is a mixed stress state that is part longitudinal shear and part rolling shear.

Referring to figure 3.13, an applied shear force at an angle to grain produces the theoretical components of stress along the principal material directions. The off-axis shear stress ( $\tau_{zx}$ ) at  $\theta^\circ$  to the fibers can be broken down into bi-axial shear stress components in the principal material directions according to Eq. 25, as follows:

$$\begin{aligned} \tau_{13} = \tau_{31} &= \tau_{zx} \cdot \cos\theta \\ \tau_{23} = \tau_{32} &= \tau_{zx} \cdot \sin\theta \end{aligned} \quad (25)$$

Table 3.2 summarizes these components for different fiber orientations. For the perpendicular-to-grain specimen ( $\theta=90^\circ$ ), the stress state is pure rolling shear so  $\tau_{13} = \tau_{31}$

$=0$ ,  $\tau_{23}=\tau_{zx} = F_{v90}=1.2$  MPa. For the parallel-to-grain specimen ( $\theta=0^\circ$ ), the stress state is pure longitudinal shear so  $\tau_{23}=\tau_{32}=0$ ,  $\tau_{13}=\tau_{zx}=F_{v0}=6.6$  MPa. For the angled specimens ( $\theta=30^\circ, 45^\circ$ , and  $60^\circ$ ), both stresses  $\tau_{13}$  and  $\tau_{23}$  are present in the coordinates of the material, and a failure criteria should be considered for evaluation of the shear capacity. Because the shear strength perpendicular-to-grain is much lower than shear parallel-to-grain, it is expected the shear strength of the angled specimens are significantly influenced by the rolling shear strength ( $F_{v90}$ ). For example, considering angled specimens with  $\theta=60^\circ$ , the estimation of shear strength based on the rolling shear strength is calculated to be 1.38 MPa, which is close to the mean shear strength value obtained from the planar test ( $F_{v60}=1.6$  MPa).

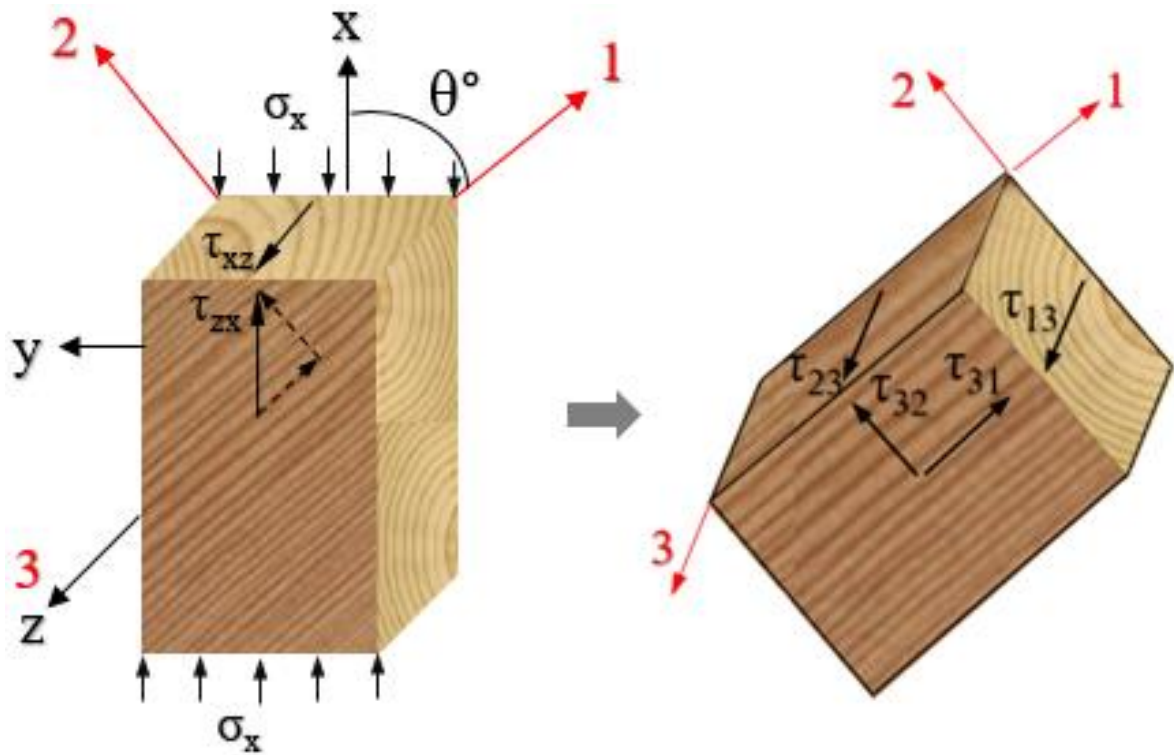


Figure 3.13: Biaxial stresses from off-axis loading

Table 3.2: Breakdown of the off-axis loading in the principal material coordinate

Stress	Fiber Orientation (Degree)				
	0°	30°	45°	60°	90°
$\tau_{13}$	$\tau_{zx}$	$0.87\tau_{zx}$	$0.71\tau_{zx}$	$0.5\tau_{zx}$	0
$\tau_{23}$	0	$0.5\tau_{zx}$	$0.71\tau_{zx}$	$0.87\tau_{zx}$	$\tau_{zx}$

### 3.4.5 Evaluation of CLT Panel Effective Shear Stiffness $GA_{eff}$

To assess the rolling shear moduli ( $G_{90}$ ) and determine the potential for Eastern Hemlock use in ANSI/APA PRG-320 grades, we can estimate the effective shear stiffness  $(GA)_{eff}$  for different CLT layups using Eq. 26:

$$(GA)_{eff} = \frac{a^2}{\left(\frac{h_1}{2G_1 \cdot b} + \frac{h_2}{G_2 \cdot b} + \frac{h_3}{2G_3 \cdot b}\right)} \quad (26)$$

where  $b$  is a width of the layers,  $a$  is the distance from centroid of top layer to the centroid of bottom layer,  $h$  and  $G$  are thickness and shear modulus of each layer, respectively.

The results for three, five and seven layers of CLT panel using Eastern Hemlock are given in Table 3.3. As shown, these values for all layups just exceed the standard requirement for CLT grade E3. The mean values of both longitudinal and rolling shear modulus from the two-plate shear tests were used for calculation of the effective shear stiffness  $(GA)_{eff}$ . Although the effective shear modulus of different panel layups using Eastern Hemlock meet the requirement of the standard, the superior results of the angled specimens show there is potential for significantly improved shear performance by using angled layers in CLT panels.

These values are less than that estimated from the relations suggested in the ANSI/APA PRG-320. As can be seen in table 3.4, while the CLT standard estimates the longitudinal and rolling shear Moduli to be 517 and 51.7 MPa, respectively, the mean values of 398 and 45 MPa are obtained from the planar tests which slightly differ from the 50 percentile of the Burr distribution curves. The other mechanical properties presented in table 3.4, including compressive perpendicular to the grain, modulus of elasticity, parallel and rolling shear strength are the average of small clear specimens per the Wood Handbook (Ross 2010).

Table 3.3 Comparison between effective shear stiffness of experimental test and CLT standard

CLT Grade	CLT thickness (mm)	Number of Layers	$GA_{eff}$ ( $10^6$ N/m)	
			ANSI/APA PRG-320	Two-Plate Shear Test
E3	105	3	5.3	5.54
	175	5	11	11.07
	245	7	16	16.6

### 3.5 Finite Element Analysis of 2 plate rolling shear properties

In order to provide insight into the complex stress distribution in the specimen of the two-plate shear test, a numerical Finite Element (FE) analysis was developed using ABAQUS finite element software. The model geometry was built following the test setup dimensions of the study. While the boundary conditions of the knife-edge for one steel plate was assumed pinned, the other knife-edge of the steel plate was subjected to the

compressive load in the form of displacement. The shear specimen was modeled as linear elastic, orthotropic material with the constitutive rolling shear property values taken from table 4. A 2D plane strain model was developed using 8-node biquadratic plane strain quadrilateral (CPE8R) elements. This 2D simulation is only valid for modeling the longitudinal and rolling shear specimens. The state of the plane strain assumption is not valid for angled specimens due to the interaction of mixed mode and out-of-plane deformation.

Table 3.4: Shear properties of Eastern Hemlock

Species	Mechanical Properties(MPa)				
	Compression Strength Perpendicular to Grain ( $F_{C\perp}$ )	Shear Strength Parallel to Grain ( $f_v$ )	Rolling Shear Strength ( $f_v$ )	Parallel Shear Modulus ( $G_0$ )	Rolling Shear Modulus ( $G_{90}$ )
Eastern Hemlock	4.5	7.3	1.31	517	51.7

Figure 3.14, shows 2D rolling shear modeling of planar test subjected to the 1-mm displacement. As can be seen in the right figure, the shear stresses are distributed nearly uniformly in most part of the shear plane ( $\tau_{12} = 1.25$  MPa). Moreover, the stresses perpendicular to the shear plane are relatively low (Figure 3.14, left). The normal stresses in the plane are around 0.1 MPa which are 8% of the uniform shear stresses; however, local stress concentration zones were observed in the corner area close to free edges. Therefore, it can be concluded that the effect of the secondary stresses is minimum on the determination of the specimen's shear properties, although this test setup does not create pure shear.

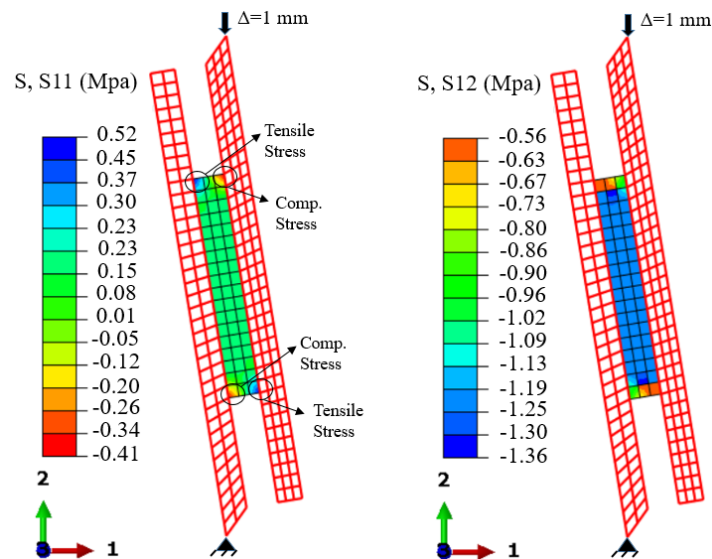


Figure 3.14: Finite element model of the two-plate shear test: normal stresses (left) and shear stresses (right)

## CHAPTER 4

### SHEAR PROPERTIES OF SYMMETRIC ANGLE PLY CLT PANELS

The research goal of this chapter is to examine the effect of the fiber orientation on the shear properties of short-span CLT panels made from local Eastern Hemlock and to determine the potential load-bearing capacity, thus improving the rolling shear properties of CLT panels. This alignment has not been evaluated on industrially manufactured CLT products to date. The mechanical properties of angled CLT panels for three-layers were compared with the 90° CLT regarding effective shear modulus, rolling shear strength and apparent bending modulus. The technical content of this chapter has been submitted to the Elsevier Journal as provided in Appendix C.

#### 4.1 Materials and Methods

##### 4.1.1 Manufacturing CLT

Eastern Hemlock was obtained from a local supplier in Massachusetts, which included No.1 and No.2 grade 2x4 board, sawn flatwise, planed and joined to the 84 mm × 33 mm. To target equilibrium moisture content of about 12%, all wood was placed in a standard room set at a temperature of 20±3°C and relative humidity of 65±2% prior to CLT manufacturing. After conditioning, the measured moisture content of the boards was in the range of 9.1%-12.4%.

All of the CLT panels in these tests were three-layered, each 33 mm in thickness, with each panel having a panel thickness of approximately 99 mm. The width of each board was approximately 84 mm, with each panel having four boards in width with an average full panel width of 336 mm after pressing. The adhesive used between the layers was

LOCTITE HB X452 PURBOND single-component polyurethane adhesive. The glue spread rate for each panel was  $180 \text{ g/m}^2$ , which was within the recommended rate of 120 to  $195 \text{ g/m}^2$ . This adhesive system is recommended for wet-use or dry-use exposure and meets the requirements of AITC 405-2008 (Standard for Adhesives for Use in Structural Glued Laminated Timber). Prior to adhesive application, a surfactant primer was sprayed with a ratio of 5% concentration to 95% water, and approximately  $20 \text{ g/m}^2$  (light spray) on the surface of the board. The wood was dried for 15 minutes before gluing. The adhesive was applied with a paint roller and the total assembly time of each test specimen was less than 45 minutes, measured from the start of the adhesive application to the time of the total pressure being applied to the panel.

To achieve higher shear strength and to prevent possible movement of cross-layers, the growth ring orientations of adjacent board were arranged alternatively and edge-bonded. Three-layer CLT panels were laid up for each of four configurations as described in figure 4.1. As shown in this figure, all top and lower layers of the CLT panel were parallel to the major direction, but the mid-layers were oriented in  $0^\circ$ ,  $30^\circ$ ,  $45^\circ$ , and  $60^\circ$  with respect to the major direction. Following the application of adhesive, a vertical pressure of 0.69 MPa was applied by the hydraulic press for 24 hours. The required pressing time for the adhesive was approximately 135 min, which was always met or exceeded. To squeeze the panels in the transverse direction and avoid gaps between the boards, the side pressure was applied by clamps.

Figure 4.2 shows the fabrication layup of the short-span CLT panels. ANSI/APA PRG-320 suggests using the specimen's width of not less than 305 mm and a span-to-depth ratio of 5 to 6 could produce a high percentage of shear failures. To meet the requirement

of the short span-to-depth ratio of 6 and obtain straight edges, the 3048 mm long continuous CLT panels were cut to 686 x 305 mm short-span panels using a large band saw. In total, 16 short-span CLT panels were prepared into four groups according to fiber orientation in mid-layer. Specimen lengths and widths were measured to the nearest 0.25 mm and thickness to the nearest 0.025 mm.

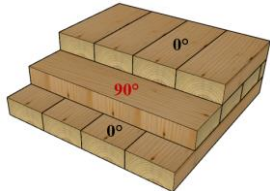
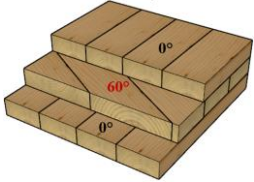
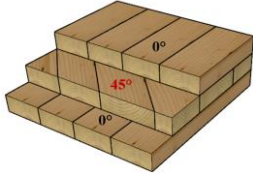
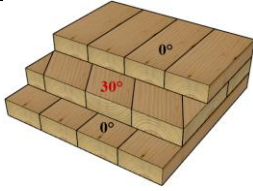
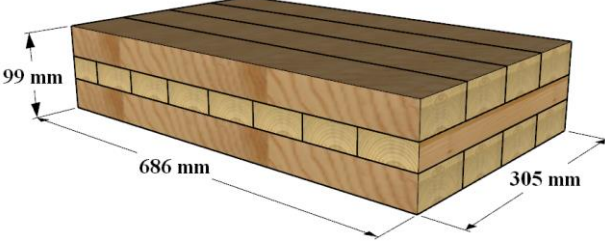
Treatment	Layups	Fibers Orientation
1	[0/90/0]	
2	[0/60/0]	
3	[0/45/0]	
4	[0/30/0]	
		

Figure 4.1: The size of the three layers short-span CLT panel for different board orientation



Figure 4.2: Fabrication process for short-span CLT panels

#### 4.1.2 Three Point Bending Test Method

The shear tests were performed according to the ANSI/APA PRG 320 (ANSI/APA 2018), which refers back to the three-point bending test illustrated in the ASTM D198. These tests were used to determine the shear properties of short-span CLT panels. As

shown in figures 4.3 and 4.4, the load was applied to the middle of the 0.619 m span with a single 200 mm radius wooden load head. The specimen span was 610 mm, measured between the centerline of the supports. Each support had a steel top plate that rested on a roller allowing free rotation. To minimize the support effect and avoid bearing failure, the bearing length was 76 mm, which was less than the specimen depth suggested in the ANSI/APA PRG 320. Two yokes, one on each side, were supported at the neutral axis over the supports. To measure the neutral axis mid-span deflection using two linear variable differential transformers LVDTs ( $\pm 25.4$  mm range,  $\pm 0.25\%$  sensitivity), the mean value of two readings from LVDTs was recorded as the beam deflection. Testing was conducted in two phases. Initially, to determine the shear and bending stiffness, the center point loading was applied up to 60% of estimated maximum load using an MTS universal testing machine with a load rate of 5 mm/min, ensuring specimen failure within 6–20 min as specified by ASTM D198. In the second phase, both LVDTs were removed to prevent damage. The point loading was then applied to failure at a constant rate of displacement and the peak load of the shear test recorded.

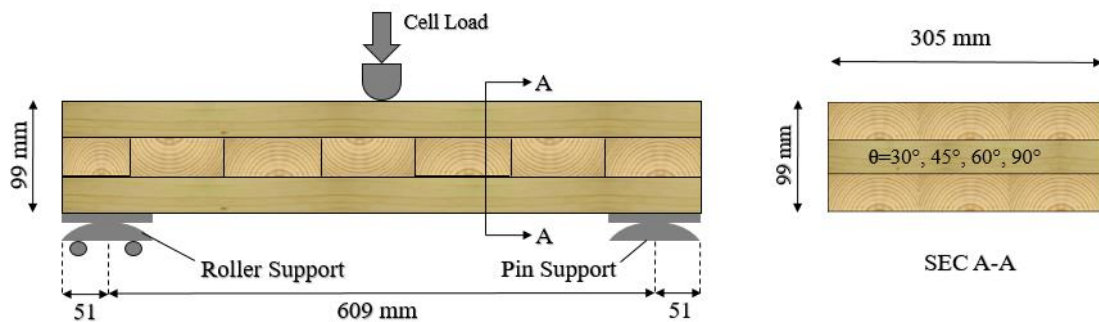


Figure 4.3: Longitudinal and cross-section of CLT floor panel



Figure 4.4: Typical test setup for short-span CLT test

#### **4.1.3 Analytical Model**

In this study, shear analogy method, as explained in CLT Handbook (US Edition) was used to create an analytical model to evaluate structural performance of short-span panels with different fiber orientation.

#### **4.1.4 Estimation of the Deflection**

As shown in table 4.1, for each group of CLT panels, the material properties of laminates, including modulus of elasticity and shear modulus, were used to predict the deflection of the panels under the three-point bending test. The shear modulus values in different orientations were obtained from a two-plate shear test. The mid-span deflection value can be estimated in accordance with Eq. (27) from ASTM D198 (ASTM 2015). Figure 4.5 shows the schematic of a cross-section of 3-layer CLT.

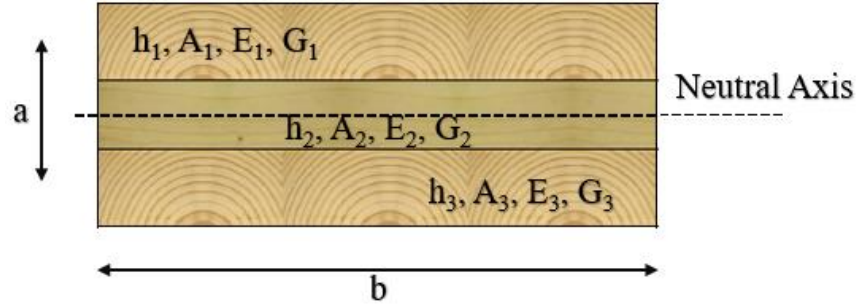


Figure 4.5: Cross-section of 3-layer CLT

Table 4.1: Modulus of Elasticity and Shear Modulus of Eastern Hemlock for Different Fiber Orientation

Species	Elastic Properties(MPa)						
	$E_L$	$E_T$	$G_{0^\circ}$	$G_{30^\circ}$	$G_{45^\circ}$	$G_{60^\circ}$	$G_{90^\circ}$
Eastern Hemlock	8300	276	520.56	191.68	104.11	83.43	61.36

$$\Delta_{Mid} = \frac{1}{48} \times \frac{Pl^3}{EI_{eff}} + \frac{1}{4K} \times \frac{Pl}{GA_{eff}} = \frac{1}{48} \times \frac{Pl^3}{EI_{app}} \quad (27)$$

where P is the load applied, L is the CLT span, and K is equal to 5/6 for the rectangular section.

The effective bending stiffness ( $EI_{eff}$ ) and effective shear stiffness ( $GA_{eff}$ ) can also be obtained from Eqs. (14) and (15), respectively from shear analogy method explained in CLT Handbook (2013)

#### 4.1.5 Evaluation of the Effective Shear Modulus Using the Three-Point Bending Test

The mid-span deflection was calculated in the elastic range of the load-displacement curves following Eq. (28).

$$\delta_e = \frac{P}{K_e} \quad (28)$$

where P is a load in the elastic range, and  $K_e$  is the slope of the force-deformation curve below the proportional limit load obtained from the linear regression of data.

The effective shear modulus ( $GA_{\text{eff}}$ ) and apparent bending modulus ( $EI_{\text{app}}$ ) of short-span CLT panel were computed from the mid-span deflection of the three-point bending test, using Eqs. (29) and (30) explained in the ASTM D198 (ASTM 2015).

$$EI_{\text{app}} = \frac{1}{48} \times \frac{PL^3}{\delta_e} \quad (29)$$

$$GA_{\text{eff}} = \frac{PL}{4K \times \left( \delta_e - \frac{1}{48} \times \frac{PL^3}{EI_{\text{eff}}} \right)} \quad (30)$$

To determine shear stress at the peak load of the short-span CLT panels, Eqs. (3) through (12) were used according to the shear analogy method.

## 4.2 Test Results and Data Analysis

### 4.2.1 Failure Modes

Two failure modes were observed in the bending tests. As expected, the main type of failure mode was rolling shear failure that occurred in 90° CLT panels. In this type of failure, the first rolling shear crack with 30° to 45° inclined angle started between the supports and loading area and, as the load increased, it propagated along the length of the panel toward the support areas, where the final fracture occurred following the nonlinear maximum loading range (Figure 4.6).

The failure type of the angled panels was similar to the regular panels, except that the out-of-plane shear deformation along the angle-fibers occurred in the mid-layer of the CLT due to the biaxial shear stresses from off-axis loading. Figure 4.7 shows typical mixed failure mode (a) along the angle-fibers, and (b) rolling shear of the mid-layer in the angled panels. Due to symmetric layups of the laminates, there is a bending-twisting coupling in the mid-layer. In this type of the deformation, the panel twisting about the longitudinal axis, in addition to the CLT's major flexure (Jones 2014, Gibson 2016) . This type of deformation will be discussed in the following chapter.

At the last stage of failure, the mixed mode of the bending and rolling shear failure were observed, especially for 30° CLT, indicating greater shear strength resistance than in other samples.



Figure 4.6: Typical failure of 90° CLT panels: formation of first crack (top) and its propagation of crack along the length of the panel at the final failure step (bottom)

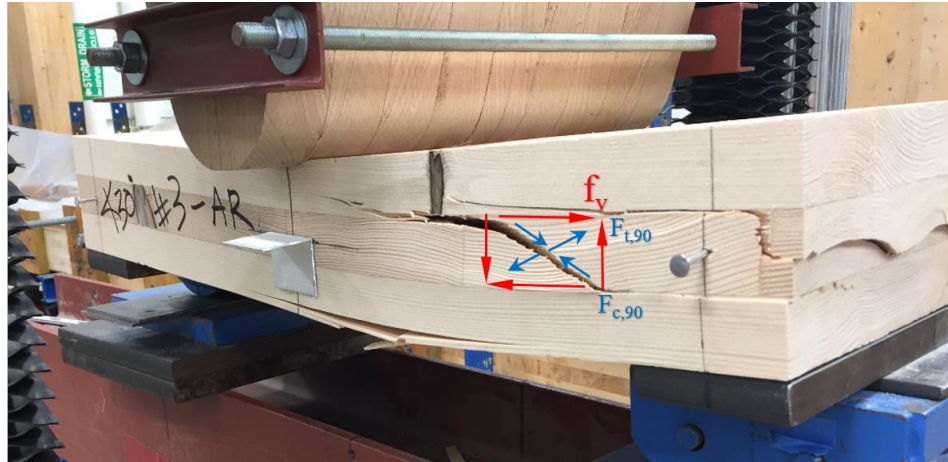


Figure 4.7: Typical failure of angled CLT panels

#### 4.2.2 Load-Displacement Data

Figure 4.8 presents the load-deflection curve of the short-span CLT panels for four data sets under the three-point bending test. Data mapping was performed on the 90° specimens to remove machine setup related displacement. The mean peak load of angled CLTs is clearly higher than regular CLT (90°), having the lowest mean value of 88.3kN for 90° and 122.2kN for 30° which indicates the higher strength of the angled CLT panels. Also, it can be seen that the slope of the curves increases as the fiber orientation of the mid-layer changes from 90° to 30°, indicating that the mechanical properties are enhanced by reorientation of the fibers.

There is a minor load drop around 60-70% of peak load showing the formation of the first crack for most of the specimens. Increasing the load, the slope of curves, which reflects the apparent bending stiffness of the specimens, progressively decreases. For the

90° CLT, several load peaks and drops occurred before the major drop, indicating that shear stress was redistributed. However, fewer sequential load drops and fiber failure occurred by changing the fiber orientation toward 30°. In other words, for 90° CLT, the shear stress was better redistributed along the length of the panel. This behavior is in agreement with the two-plate shear test finding, which has shown that angled specimens have a higher failure load with the brittle failure mechanism compared to the shear perpendicular-to-grain specimens with the large deformation and lower failure loads.

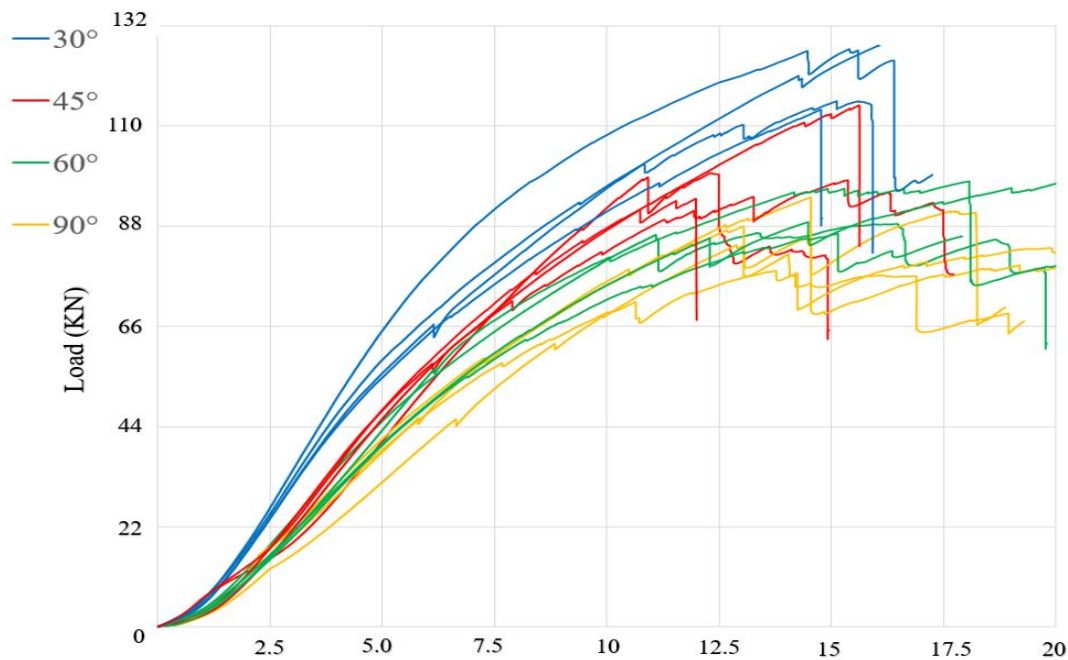


Figure 4.8: Load-deflection response for short-span CLT panels

#### 4.2.3 Effective Shear Modulus and Rolling Shear Strength

Summary test results for the bending tests are shown in table 4.2. These include the apparent bending modulus, effective shear modulus, and peak load for each specimen, which were evaluated using Equations (5) and (6). The comparison of these properties for different fiber orientation which are normalized to 90° are presented in figure 4.9. As can

be seen, the specimens generally exhibited the lowest degree of variability in both strength and stiffness, which may be attributed to their being made entirely from No.1 flat sawn boards in CLT panel. The 90° CLT panels generally exhibited the lowest stiffness in both bending and shear modulus. For this type of panel, the mean apparent bending modulus and effective shear modulus were  $177.3 \times 10^9$  N-mm<sup>2</sup>/m and  $9.49 \times 10^6$  N/m, respectively. The mean values for 60° CLT panels were 61% and 209% greater than for 90° CLT. Comparing 45° with 90° CLT, the values grow by 212% and 368%, respectively, and the highest values were calculated from 30° CLT, with a 274% and 829% growth rate compared to the 90° CLT.

Table 4.2 and figure 4.9 also give the average rolling shear strength at peak load for the short-span specimens calculated from the shear analogy method. As shown in the table and figure, the mean rolling shear strength value of 3-layer 30°, 45°, and 60° CLT specimens is 2.83, 2.36 and 2.2 MPa, respectively; they are 39%, 16%, and 8% higher than the 90° CLT panel.

It is well recognized that as the fiber orientation of the mid-layer varies from 90° to 30°, the mean effective shear modulus and shear strength values per unit width increase. The highest values in the investigated specimens were recorded for the 30° CLT panels with the  $78.7 \times 10^6$  N/m effective shear modulus and 3 MPa shear strength. What occurs in the angled specimens is a mixed stress state that is part longitudinal shear and part rolling shear. In this case, the contribution of longitudinal shear stress increase as fiber orientation decrease. For the 90° specimens, these properties are the lowest, due to the wood's natural low resistance to the fibers rolling over each other.

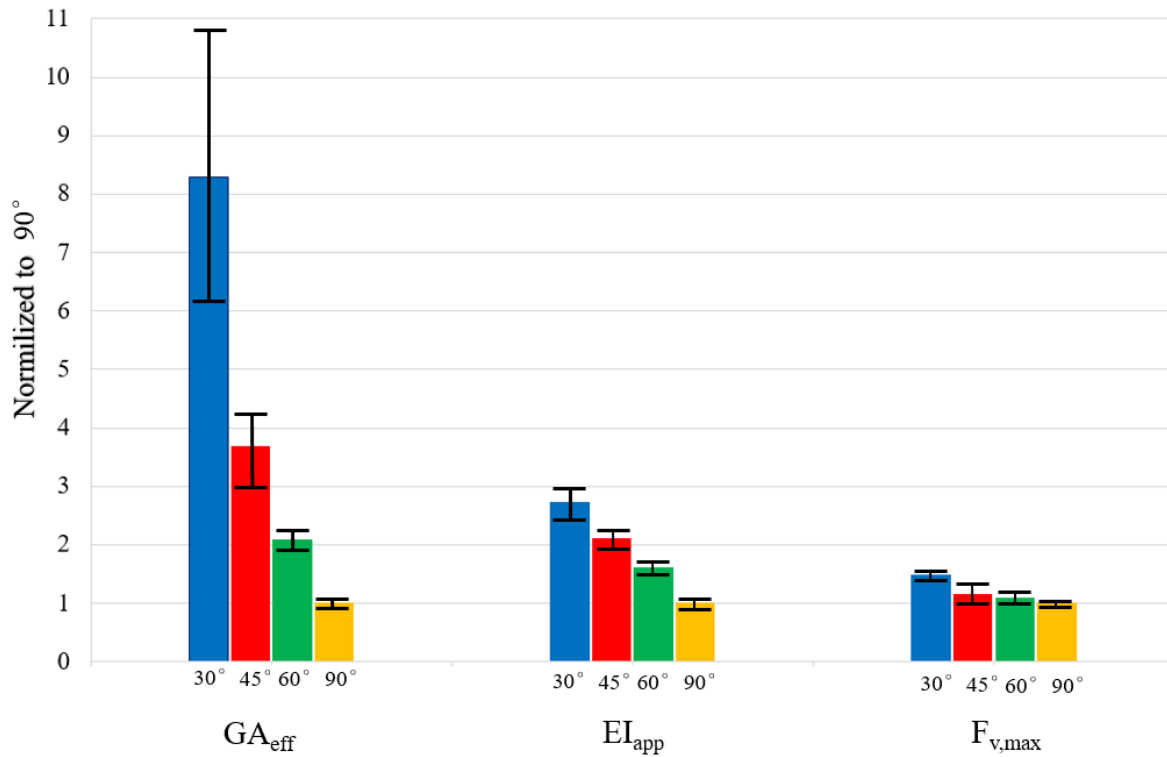


Figure 4.9: Comparison of effective shear modulus ( $GA_{\text{eff}}$ ), apparent bending modulus ( $EI_{\text{app}}$ ), and shear stress ( $f_v$ ) for fiber orientation of  $30^\circ, 45^\circ, 60^\circ$  &  $90^\circ$

Table 4.2: Short Span Shear Test Experimental Result for Fiber Orientation of  $30^\circ, 45^\circ, 60^\circ$  &  $90^\circ$

Specimen	Failure Load (kN)	MC (%)	$EI_{\text{app}}$ ( $10^6$ N-mm <sup>2</sup> /m)	$GA_{\text{eff}}$ ( $10^6$ N/m)	$f_{v,\text{max}}$ (MPa)	Failure Mode
S1-90°	88.95	8.9	165.34	8.61	2.05	Shear
S2-90°	95.35	11.1	188.69	10.33	2.19	Shear
S3-90°	84.14	12.5	185.72	10.10	1.94	Shear
S4-90°	84.70	11.2	169.47	8.90	1.95	Shear
<b>Mean 90°</b>	<b>88.29</b>	<b>10.9</b>	<b>177.31</b>	<b>9.49</b>	<b>2.03</b>	-
S1-60°	89.49	9.1	286.93	19.98	2.06	Shear
S2-60°	108.14	12.9	276.69	18.74	2.50	Shear

S3-60°	87.34	11.4	294.73	20.98	2.01	Bending+Shear
S4-60°	98.88	10.8	286.93	19.98	2.28	Shear
<b>Mean 60°</b>	<b>95.96</b>	<b>11.05</b>	<b>286.32</b>	<b>19.92</b>	<b>2.21</b>	-
S1-45°	95.08	8.9	344.54	28.47	2.19	Bending+Shear
S2-45°	100.76	9.7	382.44	36.11	2.32	Shear
S3-45°	99.13	12.1	378.18	35.14	2.28	Shear
S4-45°	115.75	12.8	398.75	40.10	2.66	Shear
<b>Mean 45°</b>	<b>102.68</b>	<b>10.8</b>	<b>375.98</b>	<b>34.96</b>	<b>2.36</b>	-
S1-30°	131.22	12.4	487.68	75.15	3.05	No Failure
S2-30°	130.49	13.1	534.82	115.70	3.03	Bending+Shear
S3-30°	129.53	9.9	478.22	69.67	3.01	Bending+Shear
S4-30°	124.99	10.1	444.51	54.21	2.91	Shear
<b>Mean 30°</b>	<b>129.05</b>	<b>11.3</b>	<b>486.31</b>	<b>78.68</b>	<b>3.00</b>	-

(MC = moisture content;  $EI_{app}$  = apparent bending modulus;  $GA_{eff}$  = effective shear Modulus;  $f_v^{max}$ =maximum shear stress).

### 4.3 Finite Element Model of Short-Span CLT Panel

To investigate the shear stress distribution in the short-span shear CLT panel and predict the behavior of the panel in the elastic range, further numerical finite element (FE) analysis was developed on the 686 mm short-span CLT and subjected to three-point bending using ABAQUS finite element software. The model geometry, consisting of three layers of orthotropic plies illustrated in figure 4.10, was modeled as a linear elastic. A 2D plane strain model was developed with an 8-node biquadratic plane strain quadrilateral (CPE8R) elements with side lengths of 12.7 mm. As shown in figure 4.11, because the geometry is symmetric about the mid-span, half of the CLT panel was modeled considering the boundary condition of zero displacement component perpendicular to the centerline and rotational component parallel to centerline, however the displacement along the centerline is free to move ( $U_x = 0$ ;  $U_y = free$ ;  $R_z=0$ )

### 4.3.1 Material property assumptions

For 2D plane strain conditions, such as in a shell element, the values of  $E_L$ ,  $E_R$ ,  $E_T$ ,  $\nu_{LR}$ ,  $\nu_{LT}$ ,  $\nu_{TR}$  and  $G_{LR}$  are required to define an orthotropic material. For plane-strain problem we have:

$$\begin{bmatrix} \boldsymbol{\varepsilon}_L \\ \boldsymbol{\varepsilon}_R \\ \boldsymbol{\varepsilon}_T = 0 \\ \boldsymbol{\gamma}_{LR} \end{bmatrix} = \begin{bmatrix} \frac{1}{E_L} & -\frac{\nu_{LR}}{E_R} & -\frac{\nu_{LT}}{E_T} & 0 \\ -\frac{\nu_{RL}}{E_L} & \frac{1}{E_R} & -\frac{\nu_{RT}}{E_T} & 0 \\ -\frac{\nu_{TL}}{E_L} & -\frac{\nu_{TR}}{E_R} & \frac{1}{E_T} & 0 \\ 0 & 0 & 0 & \frac{1}{G_{LR}} \end{bmatrix} \begin{bmatrix} \boldsymbol{\sigma}_L \\ \boldsymbol{\sigma}_R \\ \boldsymbol{\sigma}_T \\ \boldsymbol{\sigma}_{LR} \end{bmatrix} \quad (31)$$

$\boldsymbol{\varepsilon}_T$  is the strain in direction T due to uniaxial stress  $\boldsymbol{\sigma}_L$

Each layer was modeled as a linear elastic, orthotropic material with constitutive properties collected for Eastern Hemlock from two-plate shear test results and wood handbook which are displayed in table 4.3 (Ross 2010). For angled short-span CLT, shear modulus of mid-layer obtained from angled specimens under two-plate shear test (Bahmanzad et al. 2019). A supporting plate was modeled as isotropic steel plate (modulus of elasticity and Poisson's ratio were set to 200 GPa and 0.25, respectively)

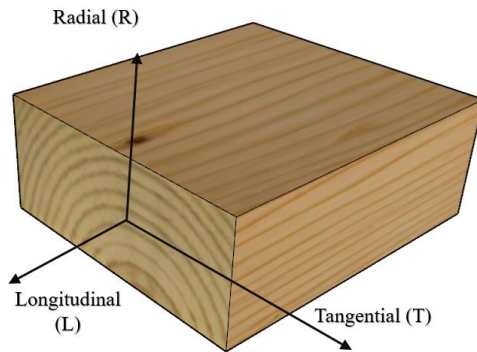


Figure 4.10: Three Axes of Wood with Respect to Grain Direction

Table 4.3: Mechanical Properties input in FE Model

Specie	$E_L$ (MPa)	$E_R$ (MPa)	$E_T$ (MPa)	$\nu_{LR}$	$\nu_{LT}$	$\nu_{TR}$	$G_{LR}$ (MPa)	$G_{LT}$ (MPa)	$G_{TR}$ (MPa)
Eastern Hemlock	8300	276	276	0.485	0.423	0.442	520.56	61.36	61.36

The Poisson's ratio  $\nu_{RL}$  is implicitly given as  $\nu_{RL}=(E_L/E_R) \nu_{LR}$ .

In orthotropic materials, both stiffness and compliance must be positive definite to reach the solution (Jones, 1999). ABAQUS checks all these restrictions by using input values (ABAQUS, 2016).

$$E_L, E_R, E_T, \nu_{LR}, \nu_{RT}, \nu_{LT}, G_{LR}, G_{LT}, G_{TR} > 0, \quad (32)$$

$$|\nu_{RL}| < (E_L/E_R)1/2$$

The material axes directions were modeled to coincide with the global axes directions.

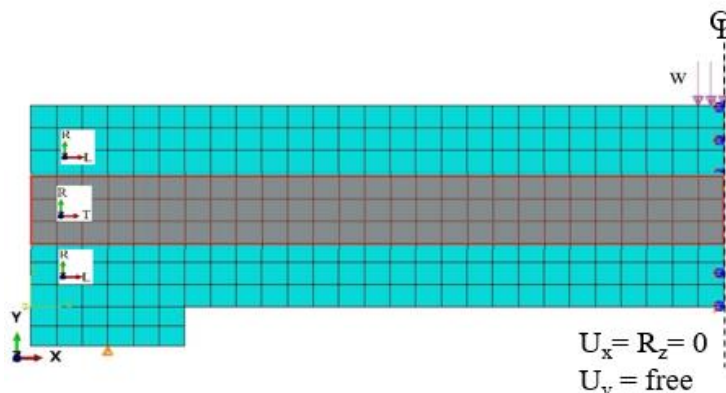


Figure 4.11: FEM Element Global Coordinates and Mesh

### 4.3.2 FE Model Results and Discussion

In figure 4.12, the results of the load-displacement curves for all CLT panels obtained from experiments are compared with the finite element analysis results. In the elastic range, the finite element model predicts deformation better than the shear analogy method.



Figure 4.12: Comparison of the load-displacement curves of experiments with FE modeling and shear analogy method for 90°, 60°, 45°, 30° CLT

The results of the FE model for mid-span deflection of short span panels and maximum shear stress are compared in table 4.4 and figure 4.13 to the experimental test and shear analogy method. In the table 4.4, the maximum shear stresses are calculated based on peak load, but mid-span deflections of numerical analysis are calculated in the

range of 0 to 44.5 KN. For the experiments, the slope of the curves between 15 KN and 44.5 KN (where the load-displacement curves are linear) were used to calculate the panels' mid-span deflection. Referencing figure 4.13, for 90° CLT specimens the discrepancy between the average deflection of mid-span calculated from the experimental test and FE simulation is the lowest (around 8%), and in contrast, for the 30° specimens this discrepancy are the highest (44%). This discrepancy proportionally increases with changing the mid-layer fiber orientation from 90° to 30°.

The shear analogy method generally predict higher deflection values than either the FE model or the experimental results. Specifically, the shear analogy method predicts the 49%, 96%, 100%, and 93% higher deflection for 90°, 60°, 45°, 30° than the experiments, respectively.

According to these analyses, for 90° CLT, the prediction of the FE model is in fair agreement with the experimental results. However, for angled CLT, the prediction accuracy of stiffness proportionally decreases with changing the mid-layer fiber orientation from 90° to 30°. This proportional difference can be attributed to the biaxial shear stresses from the off-axis loading and bending-twisting coupling which are typically present in the symmetric angle-ply laminates. In the bending-twisting coupling deformation, the CLT not only bends along the direction of the span but also twists about the neutral axis of the CLT, causing out-of-plane deformation (XZ-plane in figure 4.11). Neither the 2D finite element model nor the shear analogy method considered this deformation, resulting in conservative prediction in stiffness of angled specimens. In the three layered angled specimens, due to the low bending stresses in the mid-layer, the bending-twisting coupling is minimal for practical purposes, but for five layers and more, this type of deformation should be

investigated. Considering a portion of deformation occurring in the minor axis of the specimens, the assumption of plane strain condition is not valid for data analysis and for more accurate prediction, the behavior of angled specimens should be investigated in a 3D model.

Figure 4.14 shows the ratios of shear and bending deformation for a short-span panel in different fiber orientation. Due to the low rolling shear modulus of 90° specimens, the proportion of shear deformation is 73% of the total deformation. In contrast, for the 30° specimens the contribution of shear deformation is 25% of the total deformation, indicating the effective shear modulus increasing as the fiber orientation of mid-layer varies from 90° to 30°.

Table 4.4: Comparison of FE Modeling with Experimental Test and Shear Analogy Method for Short-Span CLT Panel with 90° Specimens

Specimen	Experimental Test		FE Model		Shear Analogy Method	
	Mid-span Deflection (mm)	Peak Load (KN)	Mid-span Deflection (mm)	$f_{v, \max}$ (MPa)	Mid-span Deflection (mm)	$f_{v, \max}$ (MPa)
CLT -30°	1.42	122.2	2.04 (44%)	2.87	2.74 (93%)	2.83
CLT -45°	1.84	102.7	2.48 (35%)	2.19	3.68 (100%)	2.36
CLT -60°	2.4	96.0	2.92 (22%)	1.95	4.72 (96%)	2.21
CLT-90°	3.9	88.3	3.58 (8%)	1.71	5.84 (49%)	2.03

Note: numbers in percentage represent the deflection difference of analysis with the experimental test

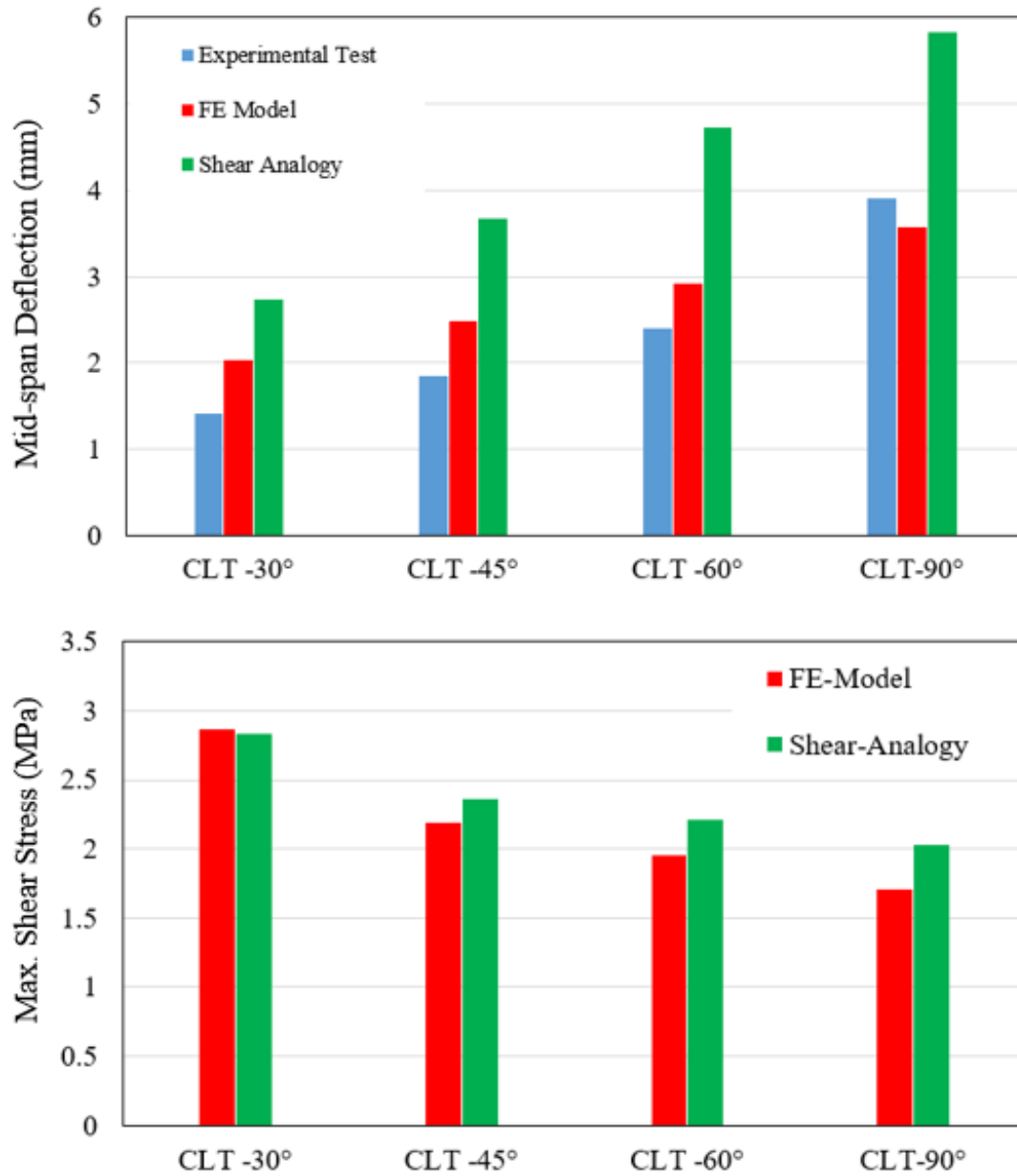


Figure 4.13: Comparison of FE Modeling with Experimental Test and Shear Analogy Method

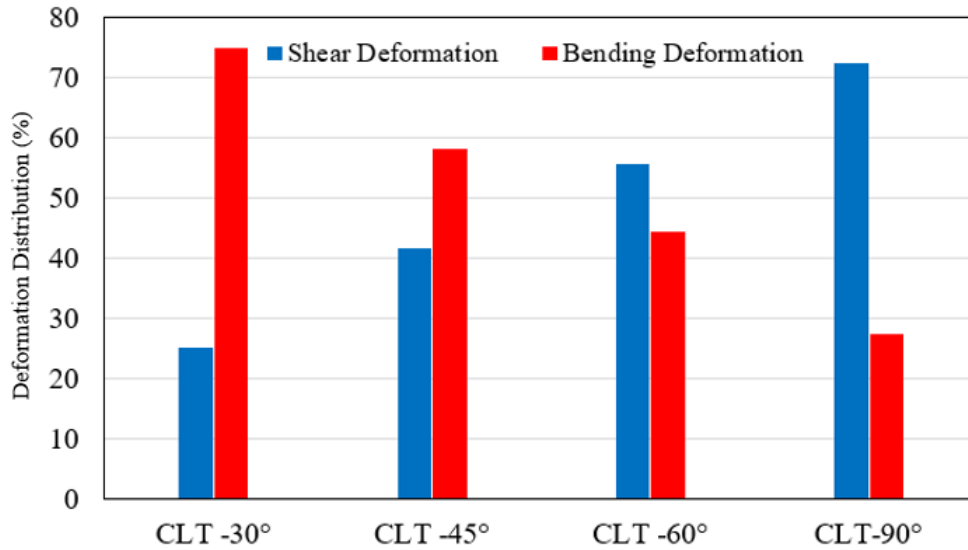


Figure 4.14: Proportion of shear and bending deformation versus CLT with different fiber orientation in mid-layer for the short-span panel

Table 4.4 and figure 4.14 also give the average maximum shear stress calculated from the shear analogy method and FE model at peak load. As can be seen, the shear analogy method estimated higher values than the FE model. Since the FE model predicted the experimental deflection more accurately, we can consider that the stress distribution from the FE model is more realistic than the shear analogy method, especially for 90° CLT.

Accordingly, the shear stresses distribution from the FE model for one of the 90° specimen (with a peak load of 89 KN) in both cross-section and longitudinal directions are compared to the shear analogy analysis. Figure 4.15 and 4.16 depict the shear stress distribution in both longitudinal and cross section of CLT panel using shear analogy method and FE model. As shown in figure 4.15, for FE analysis, the shear stress distribution along the length of the CLT panel, ranging from 0.05 to 1.83 MPa, is not uniform. However, the shear analogy method estimated higher than the constant shear stress values ( $f_{Max}=2.05$  MPa).

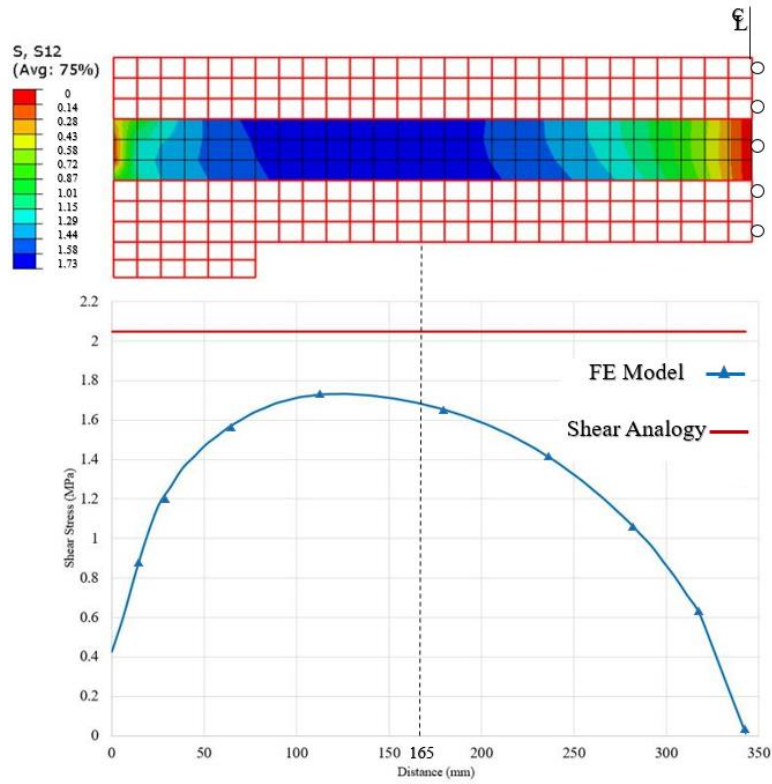


Figure 4.15: Distribution of shear stress along the length of the CLT panel (dashed line indicates the location of the line profiles of distribution for Figure 4.16).

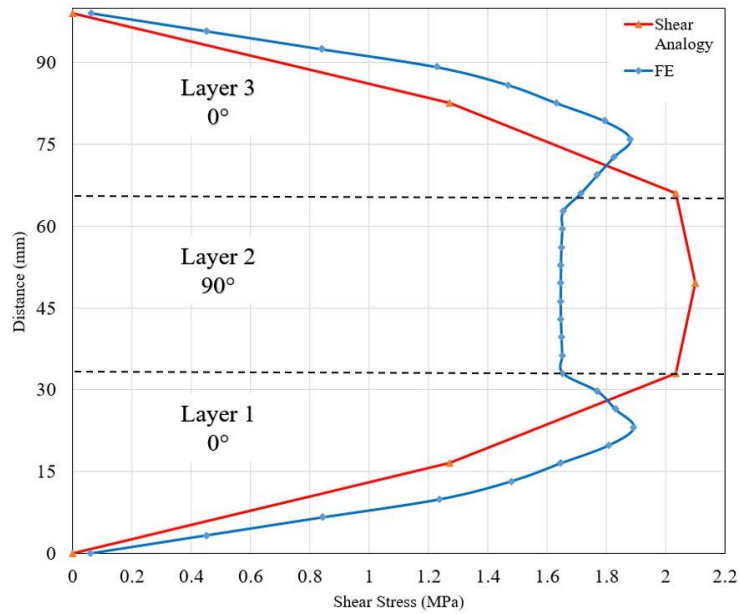


Figure 4.16: Distribution of shear stresses in cross-section at distance 165 mm of the CLT panel.

Clearly, in figure 4.15, the shear stress is maximum in the region between the support and loading area where the first rolling shear crack formed. This is the region, where the secondary stresses are low and as the load increase, the rolling shear crack propagates along the length of the panel toward the support areas, where eventually the interaction of shear and secondary stresses cause the final fracture.

For shear stress distribution in the cross-section (Figure 4.16), the stresses of FE model in the top and lower layers are estimated higher values than in shear analogy method. However, the FE model's prediction for mid-layer is lower than in the shear analogy method. Although the shear stress is maximum at the top and lower layers, due to the higher longitudinal shear strength, the rolling shear cracks form only in the mid-layer of the specimens.

## CHAPTER 5

### SHEAR PROPERTIES OF ASYMMETRIC ANGLE PLY CLT

The standard procedure of CLT construction includes a  $0^\circ / 90^\circ$  laminate; which means that the board layers are interchangeably configured in a longitudinal and transverse order (ANSI/APA PRG320). However, there is a potential for using alternating layers, taking advantage of the anisotropic properties of wood. From the results of the two-plate shear test, it is well understood, that there is a high potential of using the angle-ply of  $30^\circ$ , and  $45^\circ$  in the layups of the CLT panels in order to improve the rolling shear properties of the panels. It was also recognized that the  $0^\circ$  angle-ply is the stiffest and strongest in shear owing to wood's natural resistance to fibers sliding past each other in the longitudinal direction. According to this finding, there is another more suitable way to align the boards in CLT to achieve the required mechanical properties while using less wood. Therefore, in this chapter, different configuration layups including asymmetric four-layers of CLT panels with the fiber orientation of  $30^\circ$ , and  $45^\circ$  in the mid-layer were examined in order to evaluate the shear properties of asymmetric layups configuration. As shown in figure 5.1, an asymmetric laminate has plies of identical material and thickness at equal positive and negative distances from the middle surface, but the ply orientations are asymmetric with respect to the middle surface. That is if the ply orientation at a positive distance  $z$  is  $+$  $\theta$ , the ply orientation at an equal negative distance  $z$  is  $-\theta$ .

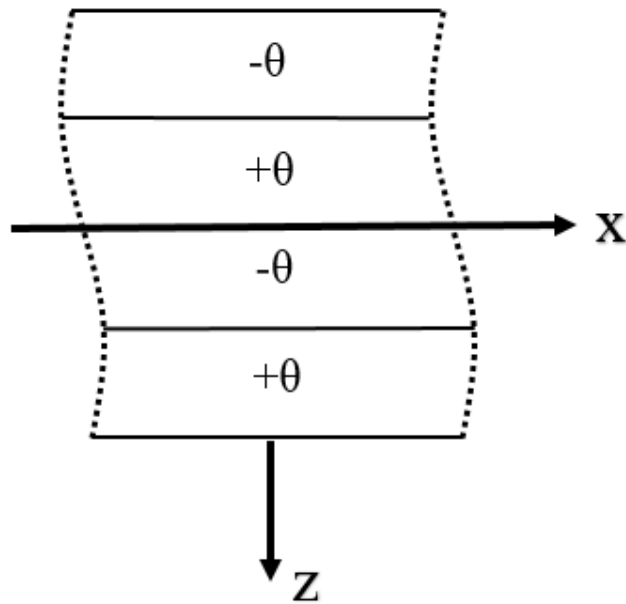


Figure 5.1: Asymmetric angle-ply layups

It is expected of the higher rolling shear properties in these types of the configuration since the longitudinal fibers are contributing in the shear transferring of the layers.

## 5.1 Materials and Methods

### 5.1.1 Dimensions and Fabrication of CLT

For this study, No.1 and No.2 grade 2x4 Eastern Hemlock lumber was used for the CLT panels. The nominal cross-section dimension of the lumber was 84 mm  $\times$  33 mm. Before CLT manufacturing, all boards were in the environmental chamber in BCT Wood Mechanics Lab and maintained at the average MC of 12% and a temperature of 70°F. After conditioning, Lumber were cut into the specified length and angle, then all lumber pieces were individually numbered and tracked for their position in the CLT layup. To create four-layered asymmetric layups, the top and lower layer were 33 mm in thickness, and mid-

layers were cut to half in thickness with each panel having a four lumber thickness totaling a panel thickness of approximately 99 mm. The width of each lumber was approximately 84 mm, with each panel having four boards in width with an average full panel width of 336 mm after cold pressing. The adhesive used between the layers was LOCTITE HB X452 PURBOND single-component polyurethane adhesive. Following the application of adhesive, vertical pressure of 0.69 MPa was applied by the hydraulic press for 24 hours. Four-layer CLT panels were laid up for each of two configurations as described in figure 5.2. As shown in this figure, all top and lower layers of the CLT panel were parallel to the major direction, but the mid-layers were asymmetrically oriented in 30°, 45° with respect to the major direction.

Figure 5.3 shows the fabrication process of short-span CLT panels. To meet the requirement of the short span-to-depth ratio of 6 suggested in the ANSI/APA PRG-320, the 3048 mm long continuous CLT panels were cut to 686 x 305 mm short-span panels using a large band saw. In total, 12 short-span CLT panels were prepared into two groups according to fiber orientation in mid-layer. Four specimens were cut out of two CLT panels and eight specimens cut out of two continuous CLT panels. Specimen lengths and widths were measured to the nearest 0.25 mm and thickness to the nearest 0.025 mm.

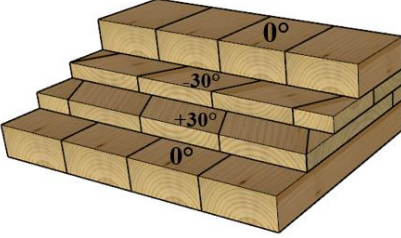
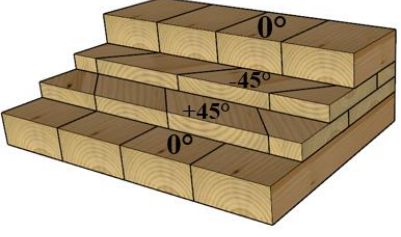
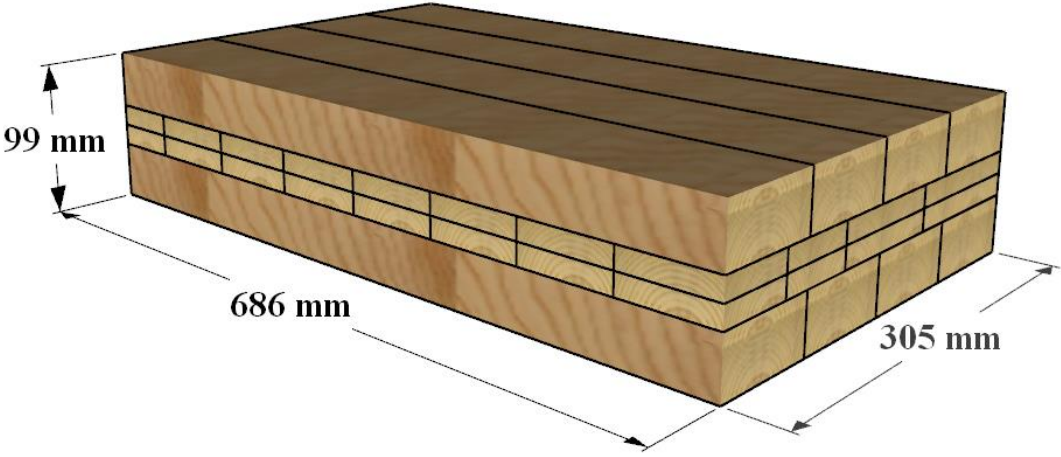
Treatment	Layups	Fibers Orientation
1	[0/+30/-30/0]	
2	[0/+45/-45/0]	
		

Figure 5.2: The size of the four layers short-span CLT panel for asymmetric layups



Figure 5.3: The detailed fabrication process for short-span CLT panels

### 5.1.2 Test Method

Three-point bending test was performed on twelve short-span CLT panels using a 30K Material Test System (MTS<sup>®</sup>) screw-driven universal testing machine. Tests were conducted as instructed in ASTM D198.

To eliminate the effects of specimen settling on the supports, a cycle load was incorporated into the test protocol. The initial loading was ramped up to 27 kN, set back to 9 kN and then loading continued up to failure for each CLT specimen.

As shown in figure 5.4, the load was applied to the middle of the 0.619 m span with a single 200 mm radius wooden load head. The specimen span was 609 mm, measured between the centerline of the supports. Each support had a steel top plate that rested on a roller allowing free rotation. Two yokes, one on each side, were supported at the neutral surface over the supports. To measure the neutral axis mid-span deflection using two linear variable differential transformers LVDTs ( $\pm 25.4$  mm range,  $\pm 0.25\%$  sensitivity), the mean value of two readings from LVDTs was recorded as the beam deflection. Testing was conducted in two phases. Initially, to determine the shear and bending stiffness, the center point loading was applied up to 60% of estimated maximum load using an MTS universal testing machine with a load rate of 5 mm/min, ensuring specimen failure within 6–20 min as specified by ASTM D198. In the second phase, both LVDTs were removed to prevent damage. The point loading was then applied to failure at a constant rate of displacement and the peak load of the shear test recorded.

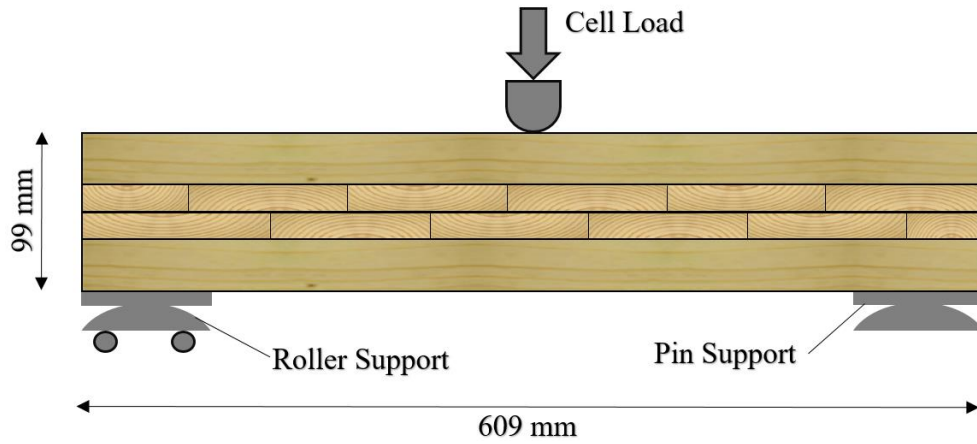


Figure 5.4: Typical test setup for short-span CLT test

## 5.2 Test Results

### 5.2.1 Failure Modes

Summary test results for the bending tests are shown in table 5.1. As expected, rolling shear was the dominant failure mechanism for 45° CLT, however for four out of the six 30° CLT specimens, the mixed mode of the bending and rolling shear failure were

observed. The first rolling shear crack with  $30^\circ$  to  $45^\circ$  inclined angle started in the second and third (angled) layers and, as the load increased, it propagated along the length of the panel toward the support areas. Final fracture was observed in the mid-span of the panel as a bending failure occurred in the bottom layer of most  $30^\circ$  specimens (see figure 5.5). This indicates that greater shear strength was achieved with  $30^\circ$  than with  $45^\circ$  specimens.



Figure 5.5: Typical failure of short-span asymmetric panels:  $45^\circ$  CLT (top)  $30^\circ$  CLT (bottom)

Table 5.1: Experimental Result for Asymmetric layups of 30°, and 60°

Specimen	Failure Load (kN)	MC (%)	Failure Mode
AS1-45°	104.22	8.9	Shear
AS2-45°	109.95	11.1	Shear
AS3-45°	107.45	12.5	Shear
AS4-45°	108.81	11.2	Shear
AS5-45°	110.03	8.9	Bending+Shear
AS6-45°	104.67	9.1	Shear
<b>Mean 45°</b>	<b>107.52</b>	<b>10.28</b>	-
AS1-30°	123.54	8.9	Bending+Shear
AS2-30°	126.31	10.7	Shear
AS3-30°	128.84	11.1	Bending+Shear
AS4-30°	113.35	8.8	Bending+Shear
AS5-30°	116.77	9.8	Shear
AS6-30°	123.71	9.3	Bending+Shear
<b>Mean 30°</b>	<b>122.09</b>	<b>9.77</b>	-

(MC = moisture content)

### 5.2.2 Load-Displacement Data

Figure 5.6 presents the load-deflection curve of the short-span CLT panels for two data sets under the three-point bending test. The mean peak load of 30° CLTs is clearly higher than 45° CLT, having the lowest mean value of 107.5kN for 45° and the highest mean value of 122.1kN for 30°. Also, it can be seen that the slope of the 30° curves are greater than 45°, indicating that the mechanical properties are enhanced by orienting the fibers at 45°.

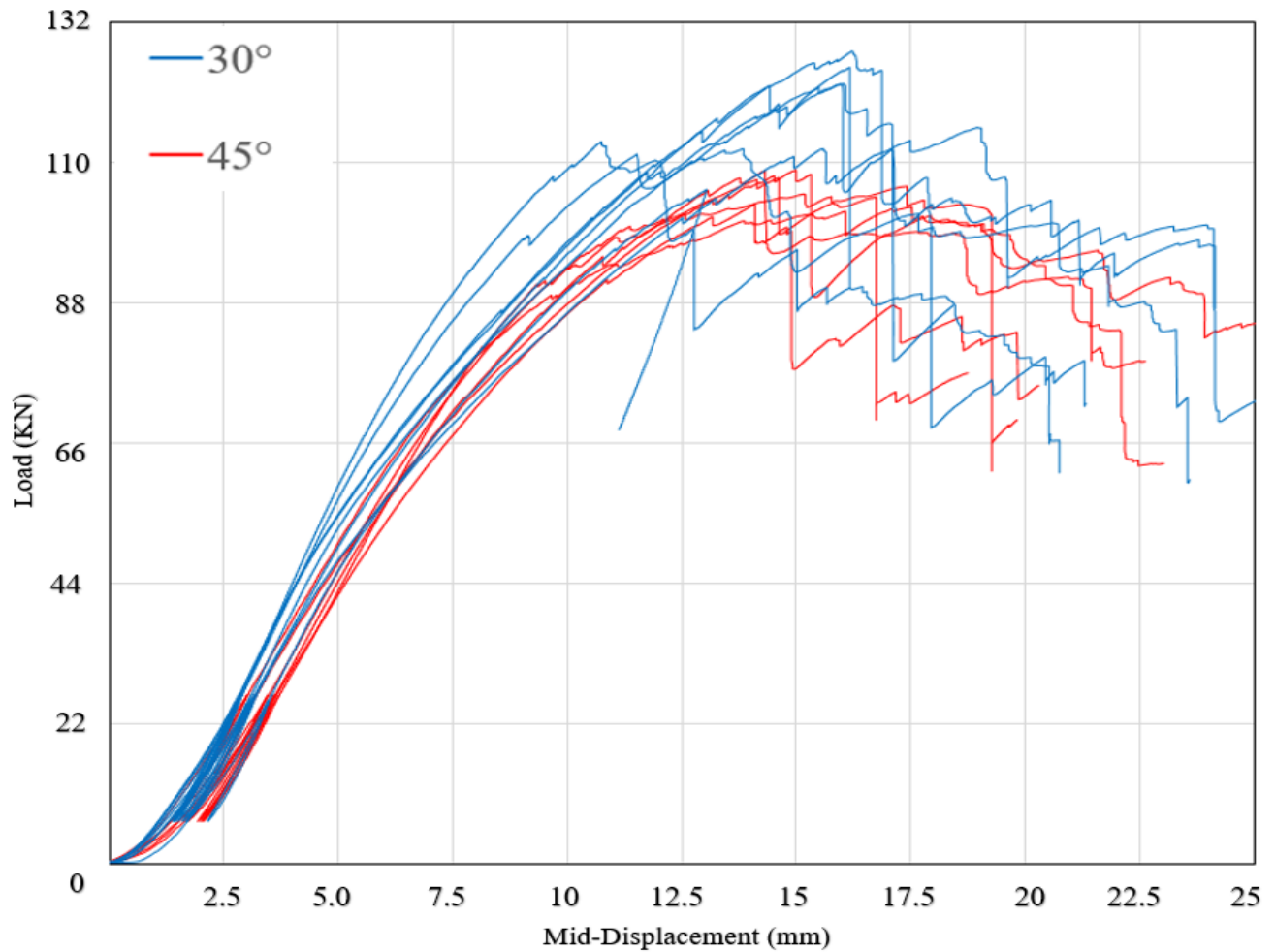


Figure 5.6: Load-deflection response for asymmetric 30° and 45° CLT panels

### 5.2.3 Effective Shear Modulus and Rolling Shear Strength

Shear properties of the asymmetric panels are shown in table 5.1. These include the apparent bending modulus, effective shear modulus, and failure mode for each specimen, which were evaluated using Equations (5) and (6). The asymmetric 30° CLT panels generally exhibited the higher stiffness in both bending and shear modulus. The mean apparent bending modulus and effective shear modulus were  $453.7 \times 10^9$  N-mm<sup>2</sup>/m and

$61.6 \times 10^6$  N/m, respectively which are 35% and 126% greater than for asymmetric 45° CLT.

Table 5.2 also gives the average rolling shear strength at peak load for the short-span specimens calculated from the shear analogy method using Equations (7) and (8). As shown in the table, the mean rolling shear strength value of asymmetric 30° CLT specimens is 2.86 MPa, which is 15% higher than the asymmetric 45° CLT panel.

Table 5.2: Shear properties of the 30°, and 60° asymmetric CLT panels

Specimen	$EI_{app}$ ( $10^9$ N-mm <sup>2</sup> /m)	$GA_{eff}$ ( $10^6$ N/m)	$F_{v,max}$ (MPa)
AS1-45°	326.00	25.47	2.41
AS2-45°	333.08	26.61	2.54
AS3-45°	354.12	30.32	2.48
AS4-45°	346.47	28.91	2.52
AS5-45°	316.09	23.95	2.54
AS6-45°	340.31	27.83	2.42
<b>Mean 45°</b>	<b>336.01</b>	<b>27.18</b>	<b>2.49</b>
AS1-30°	506.75	88.37	2.90
AS2-30°	486.69	74.55	2.96
AS3-30°	478.48	69.81	3.03
AS4-30°	449.68	56.25	2.66
AS5-30°	411.86	43.39	2.74
AS6-30°	388.61	37.32	2.90
<b>Mean 30°</b>	<b>453.68</b>	<b>61.61</b>	<b>2.86</b>

( $EI_{app}$  = apparent bending modulus;  $GA_{eff}$  = effective shear Modulus;  $f_v^{max}$  = maximum shear stress).

It is well understood that asymmetric 30° specimens are stiffer and stronger than 45° specimens. In the mid-layers of the specimens, a mixed stress state that is part longitudinal shear and part rolling shear are active. Referring to figure 5.7, a theoretical analysis of shear force due to bending at an angle to grain produces the components of stress along with the principal material directions. This figure shows how the off-axis shear stress ( $\tau_{zy}$ ) at  $\theta^\circ$  to the fibers can be broken down into bi-axial shear stress components in the principal material directions. These shear stress components can be calculated according to equations 33, as follows:

$$\tau_{13}=\tau_{31}=\tau_{zx}.\text{Cos}\theta$$

$$\tau_{23}=\tau_{32}=\tau_{zx}.\text{Sin}\theta \quad (33)$$

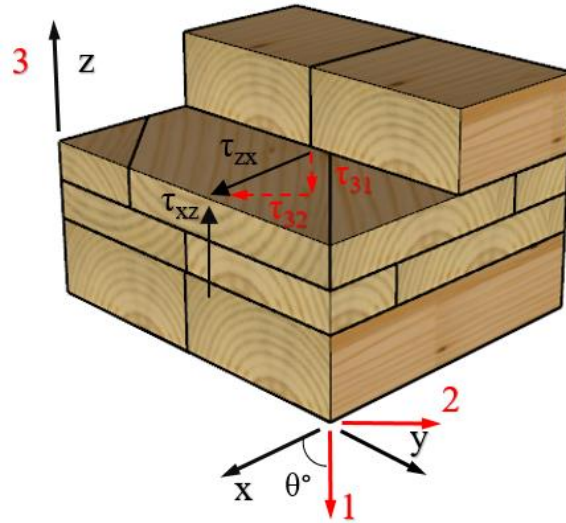


Table 5.3 summarizes these components for fiber orientations of 30° and 45°. As can be seen, although the shear stress parallel-to-grain ( $\tau_{13}$ ) of 30° is 23% higher than 45°, the shear stress perpendicular-to-grain ( $\tau_{23}$ ) of 30° is 30% lower than 45° for the same loading. It is expected that the shear strength of the angled composite specimens are limited

by the rolling shear strength ( $F_{v90}$ ) because it is much lower than the strength parallel-to-grain.

Table 5.3. Breakdown of the off-axis loading in the principal material coordinate

Stress	Fiber Orientation (Degree)	
	30°	45°
$\tau_{13}$	$0.87\tau_{zy}$	$0.71\tau_{zy}$
$\tau_{23}$	$0.5\tau_{zy}$	$0.71\tau_{zy}$

### 5.3 Finite Element Model of Short-Span CLT Panel

To investigate the coupling effect of the asymmetric short-span panel and predict the behavior of the panel in the elastic range, further numerical finite element (FE) analysis was conducted on the 686 mm short-span CLT and subjected to three-point bending using ABAQUS/CAE finite element software. The model geometry, consisting of four layers of orthotropic plies illustrated in figure 5.2, was modeled as linear elastic. As can be seen, the ply orientation of top and lower layers was  $0^\circ$  with respect to the major direction; however, the second and third layers were oriented in the  $\pm 30^\circ$  and  $\pm 45^\circ$  for the asymmetric layups. A 2D conventional shell composite layups were created with an 8-node doubly curved thick shell elements (S8R) with side lengths of 12.7 mm. Conventional shell composite layups are composed of plies made of different materials in different orientations. A layup contains a different number of plies in different regions.

The boundary conditions were assigned as simply supported beams, similar to the experiment, restraining the displacement on all directions on one support and restraining the displacement on the z-axis and the y-axis but allowing for free movement about the x-axis on the other support. Figure 5.8 shows the meshed model for which a 19-mm (0.75-in.) element size was selected. Surface pressures were applied at the center of the panel with the width of the 38-mm (1.5-in.), similar to the experiments, as shown in figure 5.8.

### 5.3.1 Material property assumptions

The material properties used for each layer are presented in table 4.3. These mechanical properties were obtained from planar tests or from the relationships of material properties described in the Wood Handbook (Ross et al. 2010). Supporting plates of the support were modeled as an isotropic steel plate with the width of the 76-mm (modulus of elasticity and Poisson's ratio were set to 200 GPa and 0.25, respectively)

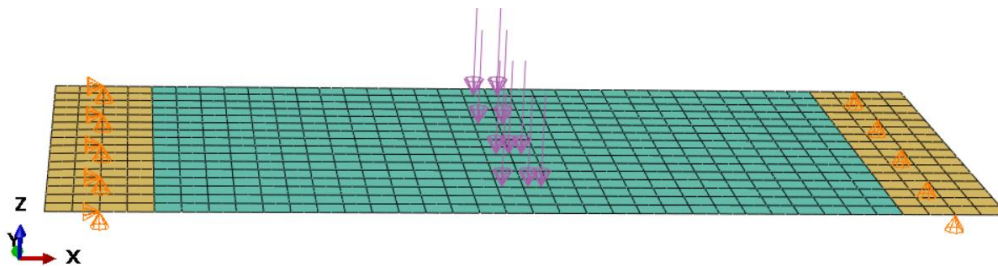


Figure 5.8: FEM Element Global Coordinates and Mesh

### 5.3.2 Model Verifications

The FE results were verified by comparing the load-deflection curves of the FEA and experiments, which were based on the same configuration. As observed from the curves shown in figures 5.9 and 5.10, very good agreement was found between the FEA results and experimental data. The error between the FEA result and the average maximum deflection value for asymmetric 30° and 45° panels were calculated as 13% and 11% respectively, which could be considered to be within an acceptable range.

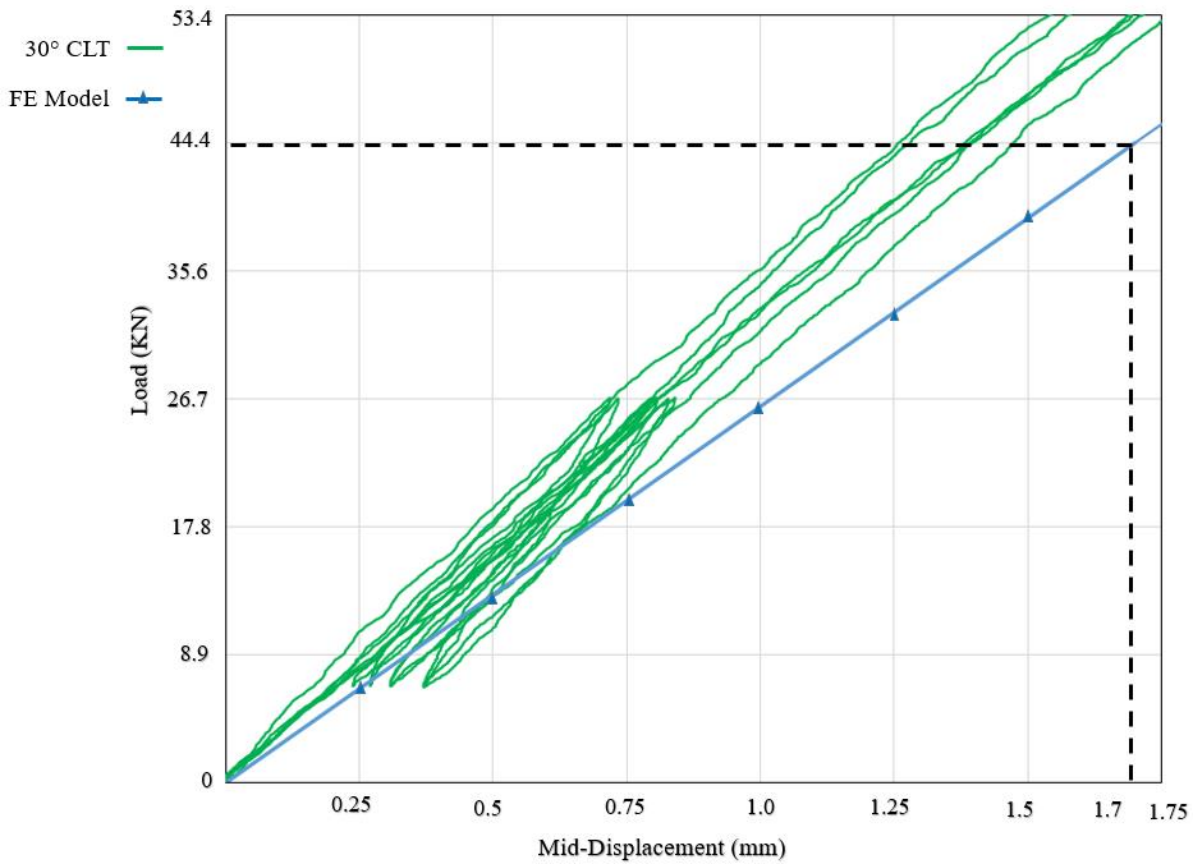


Figure 5.9: Comparison of the load-displacement curves of 30° asymmetric CLT with FE modeling

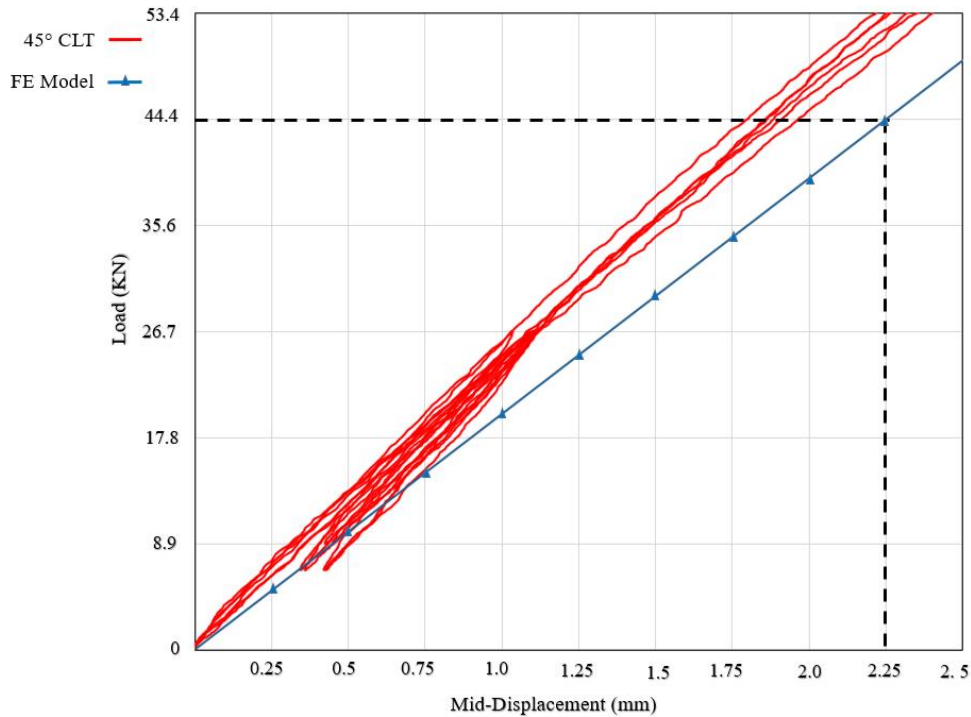


Figure 5.10: Comparison of the load-displacement curves of 45° asymmetric CLT with FE modeling

### 5.3.3 Investigation on Shear Stress of Asymmetric Layups of Panels

Angled asymmetric CLT are characterized in terms of their response to mechanical loading, which is associated with a description of the coupling behavior, unique to this type of layup. The coupling behavior relevant to asymmetric layups of 30° and 45° is presented in figure 5.11. It is clearly seen that asymmetric layups possess coupling between out-of-plane bending and in-plane shearing. This means that out-of-plane bending stresses cause in-plane shear stresses. As shown in figure 5.11, for both asymmetric layups, the maximum in-plane shear stresses ( $s_{12}$ ) occur simultaneously at the interfaces between layers 1 and 2 and layers 3 and 4, which are 18% of the bending stress of the layers. Clearly, contour plots of the shear in-plane stresses at the layers conform to the contour plots of the bending stresses.

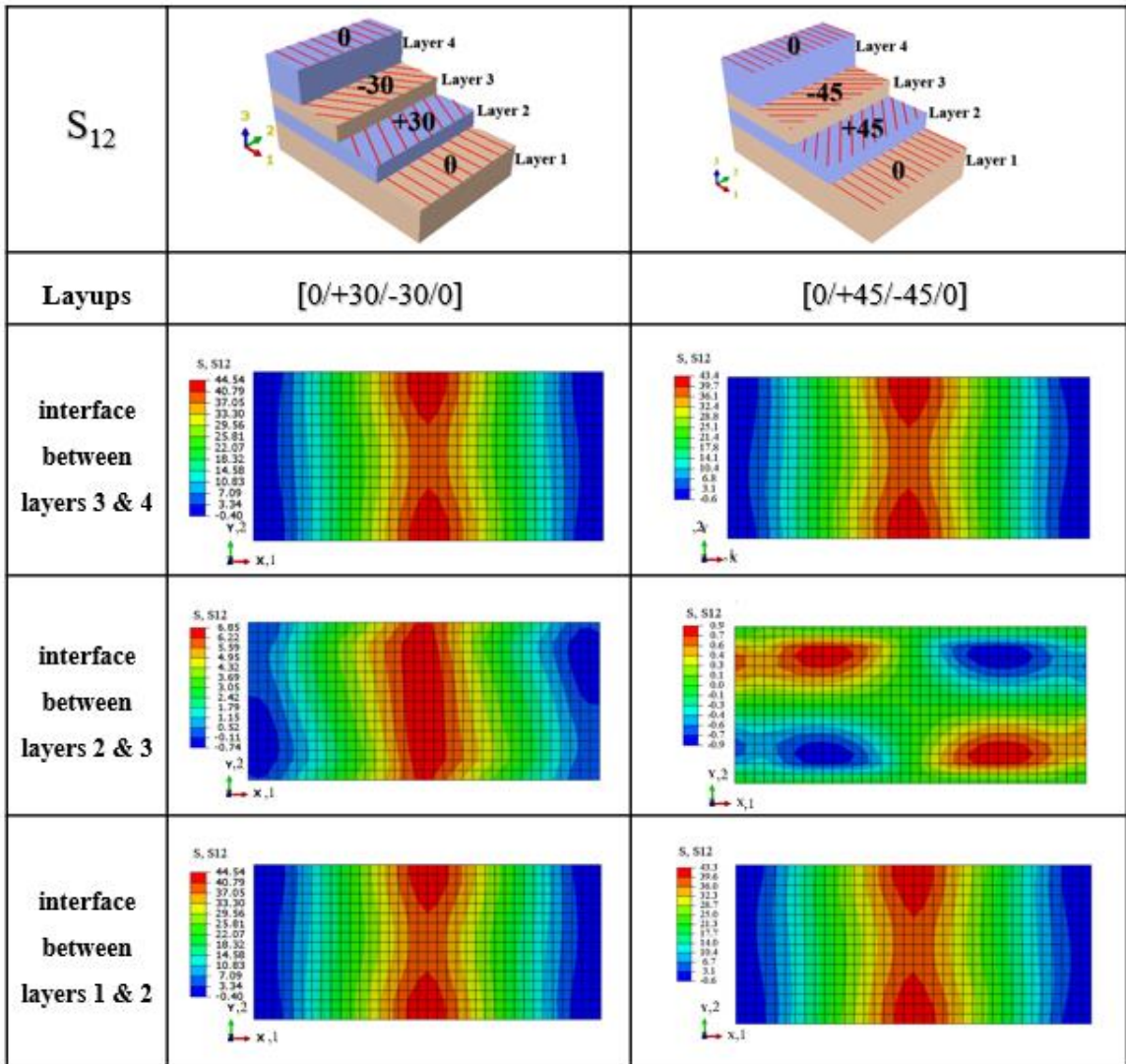


Figure 5.11: Contour plots of the in-plane shear ( $S_{12}$ ) for asymmetric four-layer CLT panel

Figures 5.12 and 5.13, show contour plots of the shear stress in the principal material directions ( $S_{13}$  and  $S_{23}$ ) for asymmetric four-layer CLT panels. The results of the FE model is in agreement with the analytical model and equations illustrated in the previous section. For example, the maximum off-axis shear stress ( $\tau_{zy}$ ) at  $30^\circ$  to the fibers was calculated 1.18 Mpa (171 psi) which occurs at the middle surface of the layups, and it can be seen from FE model (figures 5.12 and 5.13), the bi-axial shear stress components is obtained to be 1.02 Mpa (148 psi) and 0.59 Mpa (86 psi) for the shear stress parallel-to-grain ( $\tau_{13}$ ) and shear stress perpendicular-to-grain ( $\tau_{23}$ ), respectively.

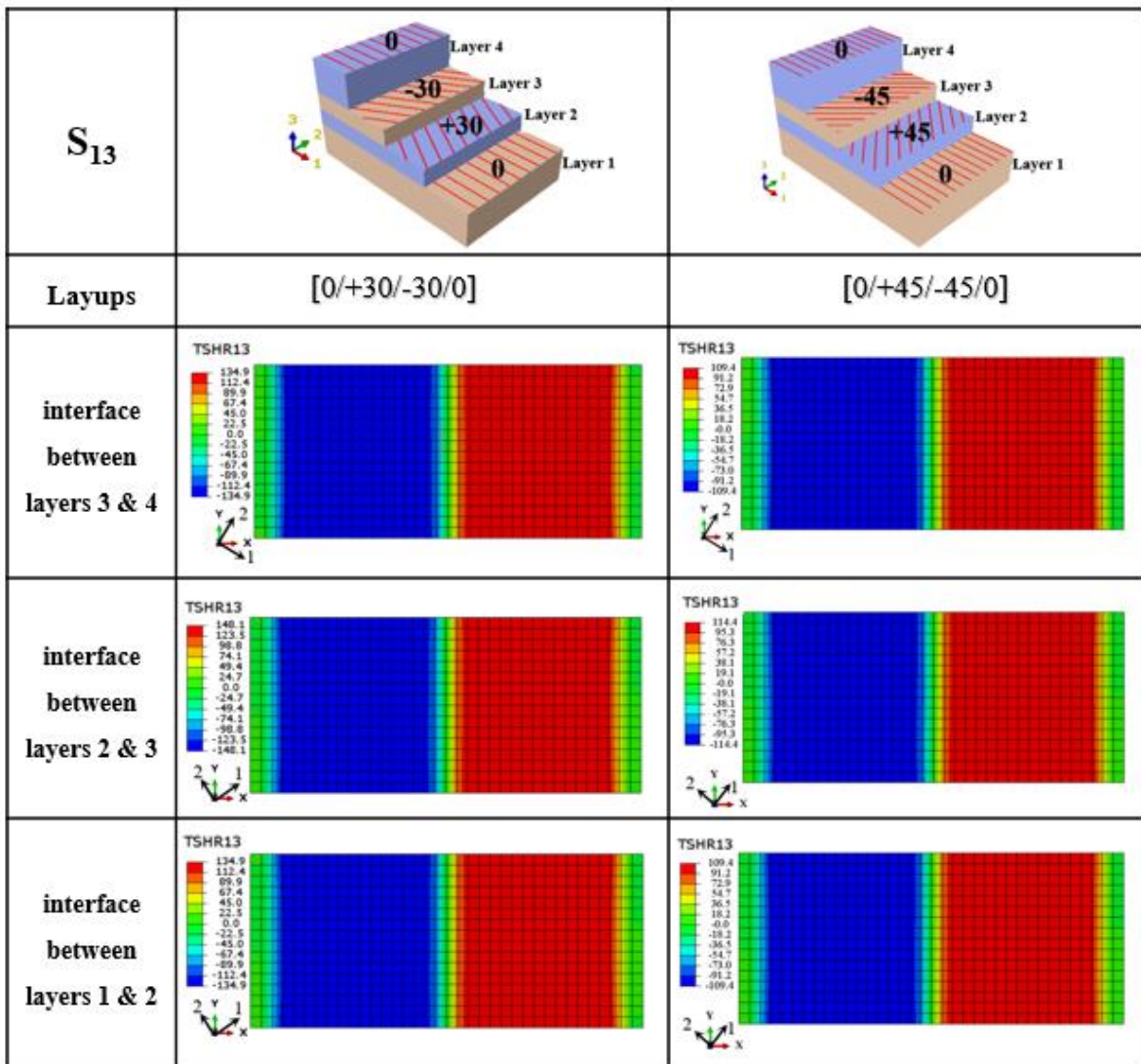


Figure 5.12: Contour plots of the shear in the principal material directions ( $S_{13}$ ) for asymmetric four-layer CLT panel

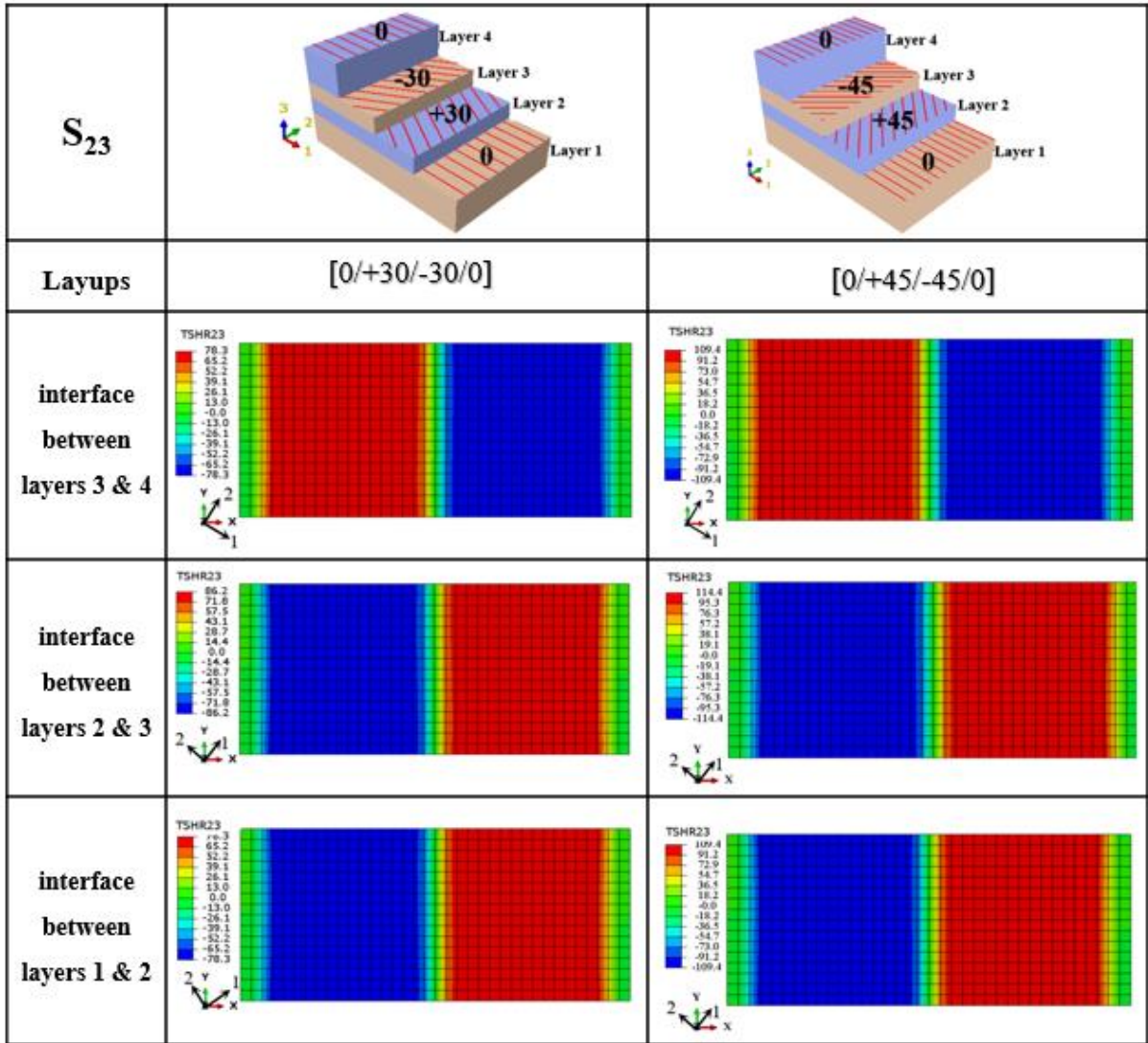


Figure 5.13: Contour plots of the rolling shear in the principal material directions ( $S_{23}$ ) for asymmetric four-layer CLT panel

## CONCLUSION

The goal of this research was to evaluate the rolling shear properties of Eastern Hemlock with respect to fiber orientation for use in CLT panels. The results of 75 planar shear tests and 16 short-span CLT consisting of four-different fiber orientations of 30°, 45°, 60° and 90° in mid-layers indicate that (1) the shear strength and effective shear modulus of Eastern Hemlock used as lam stock in CLT is sufficient to meet requirements of ANSI/APA PRG-320 for grade E3 and (2) the rolling shear properties of CLT panels will be improved significantly by using laminates with different fiber orientation in the cross layers. Based on the planar shear test, it is possible to draw the following specific conclusions:

- A gradual ductile failure mode was detected in the perpendicular-to-the grain specimens (90°), while a brittle failure mechanism with larger ultimate loads and lower shear deformation was observed in the parallel-to-the grain specimens (0°). For the specimens with fiber angles between these two orientations, the failure load increased nonlinearly from 90° to 0° due to the effect of the interaction between horizontal shear and rolling shear strength.
- Hankinson formula appears to provide an acceptable prediction for off-axis shear strength and modulus of wood.
- The average shear strength and modulus of Eastern Hemlock varies considerably with respect to the orientation of fibers. Two upper and lower values of 398 and 45 MPa obtained for shear modulus parallel- and perpendicular-to-grain direction, respectively, were 23% and 13% less than if, compared with the suggested values in the ANSI/APA PRG-320 which have been estimated based on the fraction of the

modulus of elasticity. However, the effective shear modulus of CLT panel ( $GA_{eff}$ ) for all layups of Eastern Hemlock is further than the standard requirement for CLT grade E3.

- The characteristic shear strength (5th percentile with 75% confidence) exceeded the required characteristic values from the standard. These values were about 4.5 and 0.89 MPa for parallel-and perpendicular-to-grain specimens, which are 89% and 12% higher than the specified values in the CLT standard, respectively.
- The characteristic shear strength for the specimens with the fiber orientation of 30°, and 45° were 59% and 98% higher than rolling shear strength, respectively, which could be an alternative candidate for using in the layups of the CLT panels in order to improve the rolling shear properties of the panels.
- A finite element model showed that shear distribution in the two-plate test is uniform and stresses perpendicular to the shear plane are low indicating that the two-plate test method is an appropriate test method for determining the shear properties for CLT.

According to the three-point bending tests, for both symmetric and asymmetric layups the 30° CLT panels were the stiffest and strongest, followed by the 45°, 60°, and 90° panels. The 30° panels had a mean shear strength at failure 48% greater than the 90° panels; the effective shear modulus was also 8.3 times greater than 90°. The inclusion of angle-ply laminate in the mid-layer shifted the failure mode from rolling shear to a mixture of flexural tension and rolling shear failure. These results support the hypothesis that reorientation of fibers would improve the mechanical properties of CLT panel, and especially the rolling shear modulus and strength. The results also indicate that angled CLT

panels may have a structural advantage over regular CLT (90° panels), allowing for increased span lengths or load-carrying capacity for a given panel span-to-depth ratio or using angled low-value of wood species in CLT where the standard has not been met with 90° CLT layups. The key findings of three-point bending test can be summarized as below:

- For symmetric layups of the three layers of CLT, the average effective shear modulus ( $GA_{\text{eff}}$ ) of angled specimens for 60°, 45° and 30° improved to 209%, 367%, and 828% than of the 90° specimens, respectively.
- The contribution of shear deformation in 90° CLT panels was 73%, which is common for 90° panels with the short span-to-depth ratio of 6. However, the shear deformation contribution is decreased in the angled panel by 56%, 42% and 25% for 60°, 45°, and 30° three layers CLT panels, respectively, which is attributed to the improvement of the effective shear modulus of angled CLT panels.
- For 90° CLT, a reasonable agreement was achieved, between the experimental data and the FE model generally showing a slight increase in deformation prediction compared to the shear analogy method. However, for angled CLT panels, both the FE model and the shear analogy method estimated higher values of deformation over the experimental data. This difference between the FE and experimental results was increased by changing the fiber orientation from 90° to 30°, which is due perhaps to the biaxial shear stresses from off-axis loading and bending-twisting coupling effect. In fact, the assumption of plane strain state of deformation made in the analysis is not valid, and further 3D finite element analysis is required.
- First rolling shear crack occurred in the mid-layer region between the support and loading area, which, according to the shear stress distribution of the FE along the

length of the CLT, is in the high shear stress zone where there are no noticeable secondary stresses. However, the shear analogy method predicted higher and uniform values along the length of the CLT. The model further elucidates the shear stresses distribution in the cross-section by evaluating the higher values than the shear analogy method in the top and lower layers. However, for mid-layer, FE estimated the lower shear stress values than the shear analogy method.

- The results of the FE model for four-layers asymmetric layups under three-point bending test indicate that there is a bending-shearing coupling in the angle-ply layers which are estimated 18% of the bending stress of the layers. It is well recognized, due to low bending stress in the mid-layers of the panels, the shear in-plane stress are lower than the bi-axial shear stress components in the principal material directions.

## APPENDIX A

### SAMPLE CALCULATION FOR SHEAR PROPERTIES

This appendix describes sample calculations of effective shear modulus, apparent bending modulus and shear strength for short-span panel using shear analogy method (specimen S1-90°)

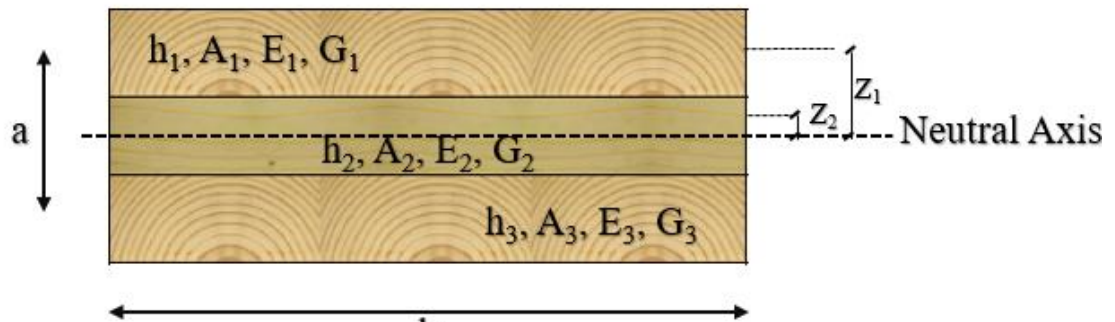


Figure A.1: Cross Section of Three-Layers Short-Span Specimen

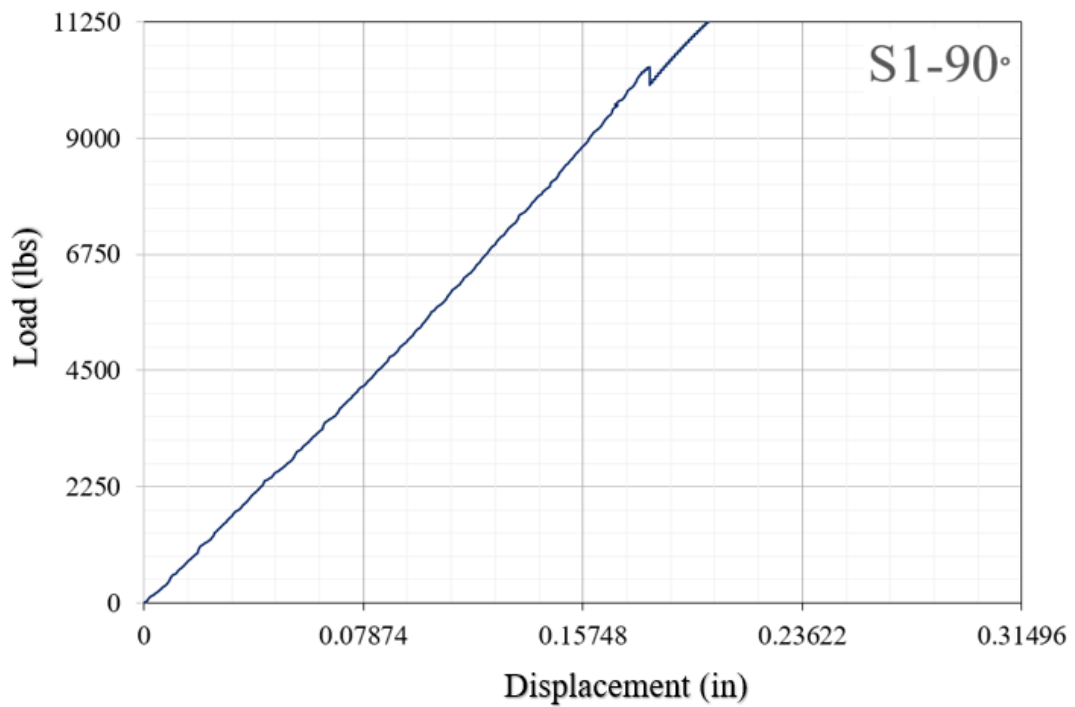


Figure A.2: Short-span bending load-displacement graph for Specimen S1-90°

Parameter and material properties:

$$h_1=1.3 \text{ in} \quad b_1=12 \text{ in} \quad A_1=15.6 \text{ in}^2 \quad E_0=1.2 \times 10^6 \text{ Psi} \quad G_0=57700 \text{ Psi}$$

$$h_2=1.3 \text{ in} \quad b_2=12 \text{ in} \quad A_2=15.6 \text{ in}^2 \quad E_{90}=40000 \text{ Psi} \quad G_{90}=6560 \text{ Psi}$$

$$h_3=1.3 \text{ in} \quad b_3=12 \text{ in} \quad A_3=15.6 \text{ in}^2 \quad E_0=1.2 \times 10^6 \text{ Psi} \quad G_0=57700 \text{ Psi}$$

$$\Delta_{max}=0.164 \text{ in} \quad \text{from experiment of specimen S1-90}^\circ$$

$$P=10000 \text{ lbf in the elastic range, } L=24 \text{ in}$$

$$P_{Max}=20010 \text{ lbf}$$

Effective bending modulus:

$$(EI)_{eff} = \sum_{i=1}^n E_i b_i \frac{h_i^3}{12} + \sum_{i=1}^n E_i A_i z_i^2$$

$$(EI)_{eff} = 2 \times [1.2 \times 10^6 \times ((12 \times 1.3^3)/12) + (15.6 \times 1.3^2)] + (4.66 \times 10^4$$

$$\times (12 \times 1.3^3)/12) = 68.6 \times 10^6 \text{ lbf-in}^2/\text{ft}$$

$$(EI)_{eff} = 645 \times 10^9 \text{ N-mm}^2/\text{m}$$

Apparent bending modulus:

$$EI_{app} = \frac{1}{48} \times \frac{Pl^3}{\Delta_{max}}$$

$$EI_{app} = \frac{1}{48} \times \frac{10000 \times 24^3}{0.164} = 17.56 \times 10^6 \text{ lbf-in}^2/\text{ft}$$

$$(EI)_{app} = 165.3 \times 10^9 \text{ N-mm}^2/\text{m}$$

Effective shear modulus:

$$GA_{eff} = \frac{Pl}{4k \times \left( \Delta_{max} - \frac{1}{48} \times \frac{Pl^3}{EI_{eff}} \right)}$$

$$GA_{eff} = \frac{10000 \times 24}{4 \left( \frac{5}{6} \right) \times \left( 0.1437 - \frac{1}{48} \times \frac{10000 \times 24^3}{6.86 \times 10^7} \right)} = 0.59 \times 10^6 \text{ lbf/ft}$$

$$GA_{eff} = 8.61 \times 10^6 \text{ N/m}$$

### Evaluation of Shear Strength:

$$(B)_A = \sum_{i=1}^n E_i \cdot I_i = \sum_{i=1}^n E_i \cdot b_i \cdot \frac{h_i^3}{12} = 2 \times [1.2 \times 10^6 \times (12 \times 1.3^3)/12] + (4 \times 10^4 \times (12 \times 0.65^3)/12) = 5.29 \times 10^6 \text{ lbf-in}^2/\text{ft}$$

$$(B)_B = \sum_{i=1}^n E_i \cdot A_i \cdot z_i^2 = 2 \times [1.2 \times 10^6 \times (15.6 \times 1.3^2) + 4.0 \times 10^4 \times (15.6 \times 0.325^2)] = 6.33 \times 10^7 \text{ lbf-in}^2/\text{ft}$$

$$P_A = \frac{B_A}{B_A + B_B} \times P_{Max} = 20010 \times (5.29 \times 10^6 / (5.29 \times 10^6 + 6.33 \times 10^7)) = 1543 \text{ lbf /ft}$$

$$P_B = \frac{B_B}{B_A + B_B} \times P_{Max} = 20010 \times (6.33 \times 10^7 / (5.29 \times 10^6 + 6.33 \times 10^7)) = 18470 \text{ lbf /ft}$$

$$V_A = \frac{P_A}{2} = 1543/2 = 772 \text{ lbf /ft}$$

$$V_B = \frac{P_B}{2} = 18470/2 = 9235 \text{ lbf /ft}$$

Shear forces of each individual layer of beam A can be obtained by:

$$V_{A,i} = \frac{E_i I_i}{B_A} \times V_A$$

$$V_{A,1} = ((1.2 \times 10^6 \times 2.197) / (5.29 \times 10^6)) \times 772 = 384 \text{ lbf /ft}$$

$$V_{A,2} = ((4 \times 10^4 \times 0.274) / (5.29 \times 10^6)) \times 772 = 1.6 \text{ lbf /ft}$$

Shear stress of each individual layer of beam A can be obtained by:

$$\tau_{A.i} = 1.5 \times \frac{V_{A.i}}{b \times h_i}$$

$$\tau_{A.1} = (384 \times 1.5) / (12 \times 1.3) = 37 \text{ Psi/ft}$$

$$\tau_{A.2} = (1.6 \times 1.5) / (12 \times 0.65) = 0.31 \text{ Psi/ft}$$

Shear stresses at the interface of two layers of beam B can be obtained by:

$$\tau_{B.i.i+1} = \frac{V_B}{B_B} \cdot \sum_{j=i+1}^n E_j \cdot A_j \cdot Z_j$$

$$\tau_{B_{1.2}} = (9235 \times (1.2 \times 10^6 \times 15.6 \times 1.3)) / (12 \times 6.33 \times 10^7) = 296 \text{ Psi/ft}$$

$$\tau_{B_{2.3}} = (9235 \times ((1.2 \times 10^6 \times 15.6 \times 1.3) + (4 \times 10^4 \times 15.6 \times 0.325))) / (12 \times 6.33 \times 10^7) = 298 \text{ Psi/ft}$$

$$\tau_{B_{1.2}} = \tau_{B_{1.2}} + \tau_{A.2} = 298 + 0.31 = 298.3 \text{ Psi/ft}$$

$$\tau_{Max} = \tau_{B_{1.2}} = 2.05 \text{ Mpa}$$

## APPENDIX B

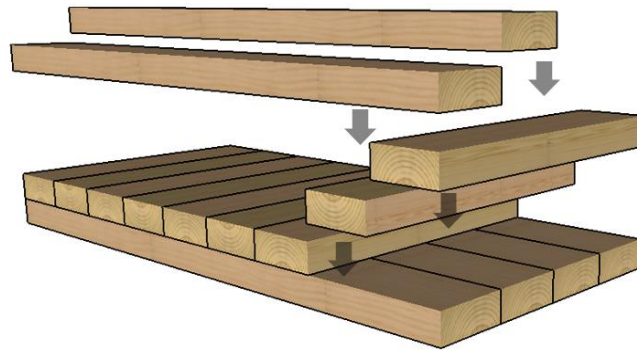
### PLANAR SHEAR PROPERTIES OF EASTERN HEMLOCK FOR DIFFERENT FIBER ORIENTATIONS

#### ABSTRACT

Planar shear properties are an essential design consideration in cross-laminated timber (CLT) assemblies, especially for low-valued species employed in floors with short span-to-depth ratios. Understanding how these properties vary with respect to grain orientation - from perpendicular-to-grain to parallel-to-grain - can lead to new and innovative panel layups with improved panel performance. In this study, two-plate shear specimens were fabricated using locally grown Eastern Hemlock 2x4 lumber. Fiber orientations of 0°, 30°, 45°, 60°, and 90° with respect to the load direction were considered. The planar shear method test was employed according to ASTM D2718 to measure the shear modulus and strength as a function of fiber orientation. The influence of fiber orientation and interaction of resisting components on the shear properties are discussed concerning observations of the types of failure modes. Results revealed that the effective shear stiffness ( $GA_{\text{eff}}$ ) and the characteristic shear strength ( $F_s$ ) for both parallel and perpendicular-to-grain satisfies the requirement of ANSI/APA PRG-320 for CLT grade E3. However, the mean shear modulus is less than that estimated using values in the standard. Angled cross layers with 30° and 45° fiber orientation with respect to the major axis were found to significantly improve shear properties of CLT .

## INTRODUCTION

Cross-laminated timber (CLT) is a newly engineered wood panel product. It is composed of layers of lumber stacked and laminated in alternating orthogonal directions (Fig. 1). Used worldwide in walls, roofs, floors, and bridge decking systems, it is found in both residential and non-residential structures. Using CLT, specifically in floor systems, is a growing trend that has structural benefits over traditional light-frame wood-joisted floors, such as bidirectional strength and stiffness allowing for open floor plans and other attractive architectural features (John W. Olver Design Building at the University of Massachusetts Amherst). Although a concrete slab has an adequate capacity to meet the demand in the construction industry, there is a considerable opportunity for CLT capacity to meet the growing demand for future construction. However, currently CLT market is in an early stage of development both in Europe and in North of America.



**Fig. 1.** Typical assembly of cross-laminated timber

One issue associated with CLT floors is that planar shear properties of wood in the perpendicular to the grain direction, (i.e. rolling shear), are low compared to shear properties in the parallel to grain direction (i.e. horizontal or longitudinal shear). Owing to

the orientation of the cross-layers, this leads to relatively large shear deformation, and corresponding vertical deflection, in CLT floors when subjected to transverse loading (Fellmoser and Blab 2004). This issue is more prominent when the lumber in the cross-layers are not edge-glued or if low-grade species are used. In these cases, low effective shear stiffness and strength of CLT can govern the design and performance of CLT floor.

Rolling shear properties depend on multiple factors relating to the cross-layer, including: specific density, growth ring orientation, species, moisture content, shrinkage rate, thickness, geometry of cross section, and relating to the overall panel, span-to-depth ratio (Brandner 2013, Gagnon and Pirvu 2011, Yawalata and Lam 2011, Flores et al. 2015). Moreover, CLT floors with span-to-depth ratios below 30 are particularly vulnerable to large shear deformation (Fellmoser and Blaß 2004, Aicher et.al (2016)).

Many studies have been conducted to establish wood shear property relationships. For example, some experimental and numerical research studies have found that, in general terms, shear modulus to elastic modulus ratio for wood varies from 1/12 to 1/20 (Fellmoser and Blaß 2004, Holzbrettern et al. 2000, Zhou et al. 2014). Similarly, product standards (ANSI/APA PRG320) have suggested that the rolling shear modulus is approximately 10% of the longitudinal shear modulus ( $G_r = G_0/10$ ). Munthe and Ethington (1968) found that, for Sitka spruce specifically, rolling shear strength was 20% of the longitudinal shear strength. Along the same lines, Aicher and Dill (2016) calculated the rolling shear modulus of European Beech and Spruce to be 370 MPa and 53 MPa, respectively, which is 2/9ths and 1/24th of the tensile modulus of elasticity ( $G/E_t$ ). In 2000, the same authors found that the rolling shear modulus depends highly on the growth ring orientation of the laminate, is

at a maximum value when the growth ring of the cross-layer is 45 degrees, and that the modulus of 3-layer Norway spruce was between 50 MPa and 200 MPa.

Blass and Görlacher (2000) estimated the characteristic values of rolling shear strength and stiffness of European spruce to be 1 MPa and 50 MPa, respectively, independent of the strength class of timber. It was noted, however, that these values may have differed slightly depending on density and annual ring orientation (Fellmoser & Blass, 2004).

Zhou et al. (2014) observed that cross layers cut in rift-sawn orientation, in comparison to flat-sawn or quarter-sawn orientation, could increase rolling shear modulus. In another study, they used bending tests and two-plate shear tests to compare rolling shear modulus and strength of the cross-layer in CLT. Their finding showed that the results of the two-plate shear test could accurately estimate the deflection of CLT specimens (Zhou et al., 2014). Moreover, Li (2015), in his PhD thesis, found that the mean rolling shear strength for Beetle-Kill Pine varies from 1.4 MPa to 1.76 MPa and confirmed to previous claims that the rolling shear strength relies on specimen size, loading type, and loading protocol. In another research, Saavedra Flores et al. (2015) studied the influence of edge-gluing, wood density and span-to-depth ratio on rolling shear capacity. They developed a numerical model to predict the rolling shear capacity of CLT panels. Their numerical model predicted a 40% reduction in failure load if the cross-layers are not edge glued. In addition, their model predicted 21% increase in failure load when wood density increases by 37.5%.

Pirvu (2011) studied the effects of edge gluing and larger sectional size (using cross-sectional sizes of 38×38 mm, 38×89 mm and 38×140 mm) on the rolling shear

modulus of laminates using planar shear tests on lodge pole pine specimens. According to his finding, using a larger size of the specimen is more effective for increasing shear modulus than the edge-gluing specimen. Additionally, he found that increasing the specimen's width had no noticeable effect on rolling shear modulus.

Lam et al. (2016) measured rolling shear properties of Beetle-Kill Pine through torque loading tests on small wood blocks. The rolling shear strength values for three- and five-layer CLT tube specimens were 3.8 and 4.8 MPa, respectively, which are much higher compared to a previous study, (Li, 2015) likely due to size effect and pure shear. Yawalata and Lam (2011) studied the effects of manufacturing process variables on the rolling shear strength of three-layer spruce-pine-fir (SPF) and hem-fir CLT panels. Their findings revealed that the rolling shear strength of three-layer SPF panels produced under 0.4 MPa of pressure was 2.22 MPa, which was higher than the 1.85 MPa result achieved under 0.1 MPa of pressure, suggesting that higher manufacturing pressure produces stronger panels, resulting in higher shear strength. More recently, researchers have developed a modified method with reference to ASTM D2718 (ASTM 2011) to measure rolling shear properties of cross-layers by using the three-layer CLT specimens (Gong et al. 2015, Wang et al. 2017).

Eastern Hemlock (*Tsuga Canadensis*) is a low-value species native to the northeastern United States. The species generally has favorable strength properties but is considered low value partly because it is prone to ring shake, a lengthwise separation that occurs between and parallel to growth rings (Gardner and Diebel 1995). According to the Northeastern Lumber Manufacturers Association lumber grading rules (NELMA 2017), ring shake is not allowed in the better and more valuable grades of boards. In the absence

of a strong market for these trees, the cost of thinning exceeds the value of the timber produced, resulting in minimal to no forest management. The infestation of a small insect - the Hemlock Woolly Adelgid (*Adelges tsugae*) - further worsens these conditions by causing tree death within 4 to 10 years (Webb et.al 2003, US Forest Service 2014). It would be possible to reduce these concerns by using low-grade species solely or in conjunction with high-grade species in CLT products.

The goal of this study is to evaluate the planar shear properties of Eastern Hemlock for different fiber orientations in order to increase its potential for use in CLT products. To this end, a planar shear test (also called two-plate shear test) was conducted according to ASTM 2718 (ASTM 2011).

## **MATERIALS AND METHODS**

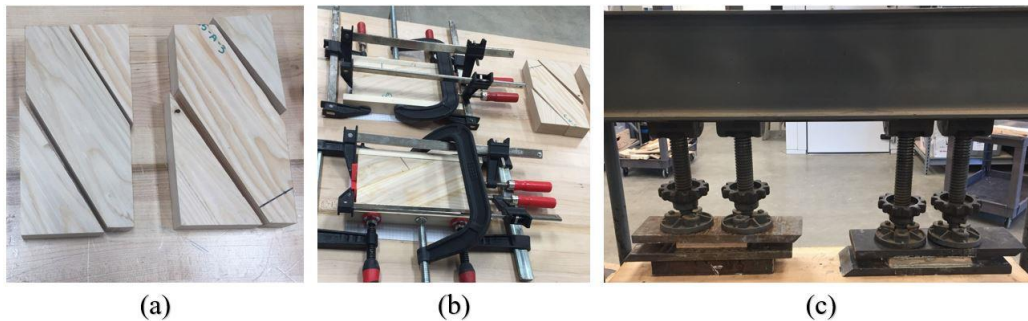
### **Specimen Preparation**

A total of 20 kiln dried Eastern Hemlock 2x4s of lengths between 2 to 3.5 m were purchased from a local mill in Massachusetts. The boards arrived planed and joined to dimensions of 33mm x 84mm. The first author graded the boards according to NELMA (Northeastern Lumber Manufacturers Association) grading rules and found all boards to be flat-sawn, and either No.1 and No.2 grade. The specific gravity was measured in accordance with ASTM D 2395 (ASTM 2014), and ranged from 0.37 to 0.5 with a mean value of 0.42. The boards were placed in an environmental conditioning chamber set at a temperature of  $20\pm 3^{\circ}\text{C}$  and relative humidity of  $65\pm 2\%$  to maintain equilibrium moisture content of about 12%.

The required sample size for each fiber orientation was determined to be 12 replications using the two-stage method (ASTM D2915-2010) assuming a coefficient of

variation of 14% for Eastern Hemlock (Ross 2010) and a 75% confidence interval. Accordingly, a total of 75 specimens were prepared consisting of five groups of 15 specimens for each fiber orientation.




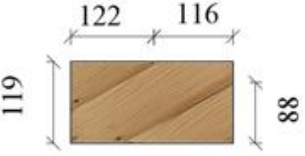

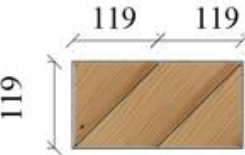

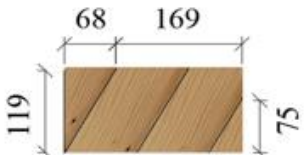

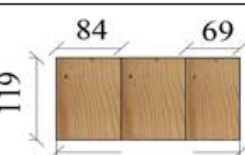
Figure 2 depicts the basic process used to fabricate the two-plate assembly: cutting the wood pieces to size, edge gluing the pieces together, preparing the steel plates (not shown), and then pressing the assembly in a mechanical press. The following sections describe the process in detail.



**Fig. 2.** Fabrication process for two-plate shear test assembly: (a) Wood cutting, (b) edge gluing and surface preparation, (c) specimen pressing, curing

The dimensions of the wood pieces used in making the specimens for each fiber orientation is given in Fig. 3. Although each orientation is made up of different size pieces, the overall volume of wood used is consistent for each orientation (33mm thick  $\times$  119 mm wide  $\times$  237mm long). Specimen lengths and widths were measured to the nearest 0.25 mm, and thickness was measured to the nearest 0.025 mm. Due to limitations of the testing machine, the width and length dimensions were slightly less than suggested by ASTM D2718 (ASTM 2011), which is either (a) 150mm width  $\times$  450 mm length, or (b) smaller dimensions, if the width and length are more than four and twelve times, respectively, the

thickness of the wood. The growth ring orientations of the adjacent pieces were alternated and edge bonded to optimize shear strength performance.

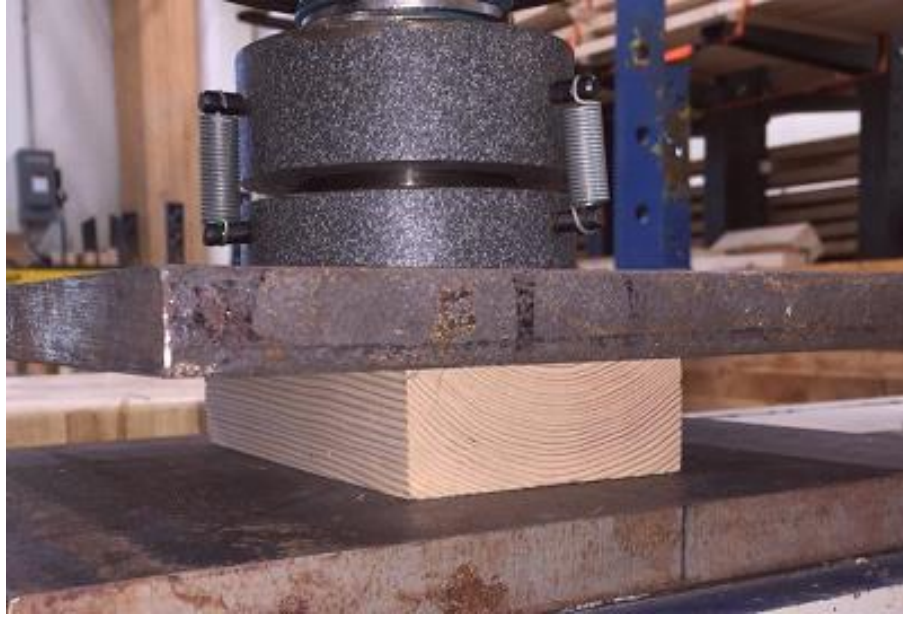
Fiber Orientation (degrees)	Sketch of wood pieces glued to steel plates	Wood dimensions (in mm)
0		
30		
45		
60		
90		

**Fig. 3.** Size of the pieces for different fiber orientation in two-plate shear test

Preliminary compression perpendicular to grain tests (ASTM D143-2000) were conducted to assess the capacity of the Eastern Hemlock prior to gluing the specimens. This was done to ensure no damage would occur to the wood from pressure needed to cure the glue. In total, 15 specimens were milled to 33×84×203 mm and load was applied through bearing plates to the tangential surface of the specimen (Fig. 4). The mean compressive strength perpendicular to the grain was 4.1 MPa with extreme values ranging from 2.6 to 5.8 MPa.

The steel plates were prepared by first scrubbing them with a clean bristle brush under cold running tap water to remove residue from any previous test. The steel plates were then heated in an oven at 150°C for 1 hour to dry completely and to avoid any oxidation of the metal surfaces. Three types of adhesives were assessed for bonding the wood to the steel: 1) Loctite PL Premium Fast Grab Polyurethane, (LOCTITE®) 2) System Three G-2 epoxy, and 3) System Three T-88 epoxy (SYSTEMTHREE). In the end, Loctite PL Premium adhesive, with the spread rate of 1500 g/m<sup>2</sup> and an assembly time 20 min, was used for bonding the specimens to avoid glue failure during the shear tests.

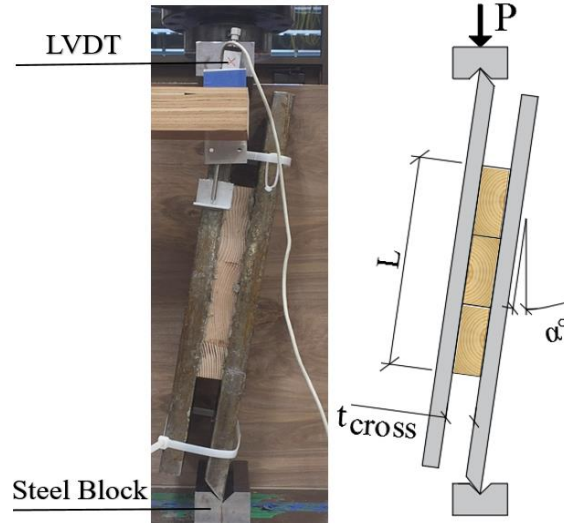
The two-plates shear test assembly was finally formed by applying a uniform pressure of 1.0 MPa through a mechanical press for 48h at 25°C. Specimen thickness was measured before and after pressing to be sure that the thickness of the specimen did not change.



**Fig. 4.** Test setup for compression perpendicular to grain test

### **Test Method**

Figure 5 shows the test setup whereby the compressive load is applied through steel blocks with grooves which concentrically load the knife edges of the steel plates. The knife-edge of the plates provides pin support during loading of the specimen. The angle of specimen inclination ( $\alpha$ ), between the direction of the applied shear force ( $V$ ) and the bond line of the specimen, is a function of the steel plate size and the specimen size. In our case, the angle of inclination was 8 degrees.



**Fig. 5.** Experimental setup for two-plate shear test

In accordance with ASTM D2718 (ASTM 2011), failure should occur in the range of 3 to 12 minutes elapsed time from start of loading. The shear force should be continuously applied to the steel plate at a constant rate as follows:

$$N = 0.0075 \times R \times \sum t \quad (1)$$

where N is the crosshead speed, R is a ratio of the shear modulus of the parallel plies to the shear modulus of the perpendicular plies and t is the total thickness of laminates. In our case, the crosshead speed of 0.508 mm/min lead to specimen failures within 5 to 9 minutes depending on the fiber orientation of specimens.

Shear modulus (G) was calculated based on the equation provided in ASTM D2718 (ASTM 2011) adjusted to account for the angle of specimen inclination ( $\alpha$ ) as follows:

$$G = \frac{P \times \cos \alpha}{\Delta} \left[ \frac{t}{L \times w} \right] \quad (2)$$

Where  $t$  is the thickness of the specimen,  $L$  and  $W$  are the specimen length and width respectively, and  $P/\Delta$  is the slope of the linear range of the load-deformation curve below the proportional limit (i.e. within a load range of 10% to 40% of the maximum load). Linear Variable Differential Transformers (LVDTs) were employed to measure the relative displacement of the movable steel plate (on the left in Fig. 4) to the supported one during the test to the nearest 0.002 mm.

The shear strength ( $F_v$ ) of the specimens was calculated based on the maximum load as follows:

$$F_v = \frac{P_{max} \times \cos \alpha}{L \times W} \quad (3)$$

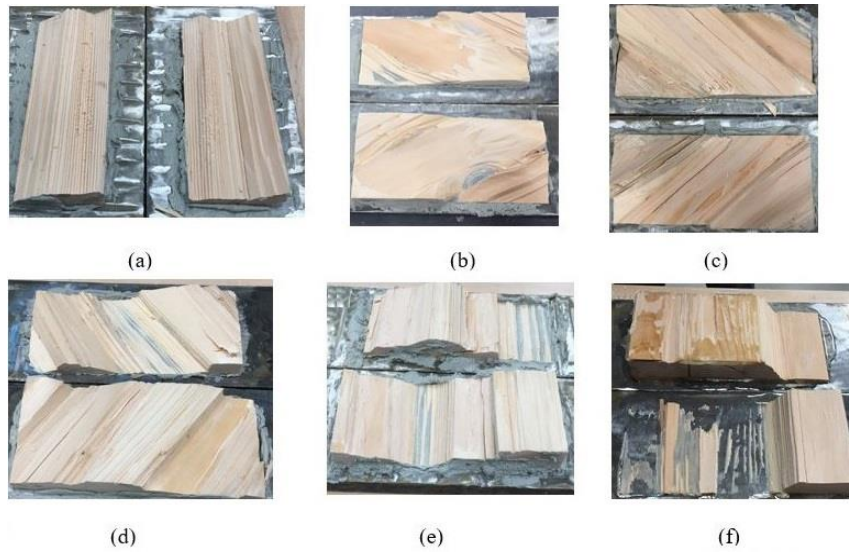
where  $P_{max}$  is the peak load.

## RESULTS & DISCUSSION

### Failure modes

Figure 6 displays typical failure surfaces of specimens for each fiber angle tested. Not surprisingly, the predominant failure mode for the parallel to grain ( $0^\circ$ ) specimens (in horizontal shear) was distinctly different than that of the angled specimens (in combined horizontal and rolling shear) or the  $90^\circ$  specimens (in rolling shear). The  $0^\circ$  specimens (Fig. 6a) failed in a brittle manner along the fiber direction without any obvious pre-cracking developing in the specimens during the test. However, for specimens with fiber angles from  $30^\circ$  to  $90^\circ$  (Figs. 6b, 6c, 6d, 6e), an initial inclined shear crack generally appeared at approximately 50% to 60% of the peak load (Fig. 7a). The crack propagated along the growth ring with increasing load until the entire specimen fractured (Fig. 7b) precipitating a nonlinear maximum loading range.

No glue failure was observed for the 30° to 60° specimens. Glue failure did occur, however, for two 0° specimens and three 90° specimens (Fig. 6F). In total, 80 specimens were tested and five of them were excluded from the data analysis due to glue failure.



**Fig. 6.** Typical failure appearances of specimens tested in 2 plate shear: (a) 0°, (b) 30°, (c) 45°, (d) 60°, (e) 90°, (f) glue failure

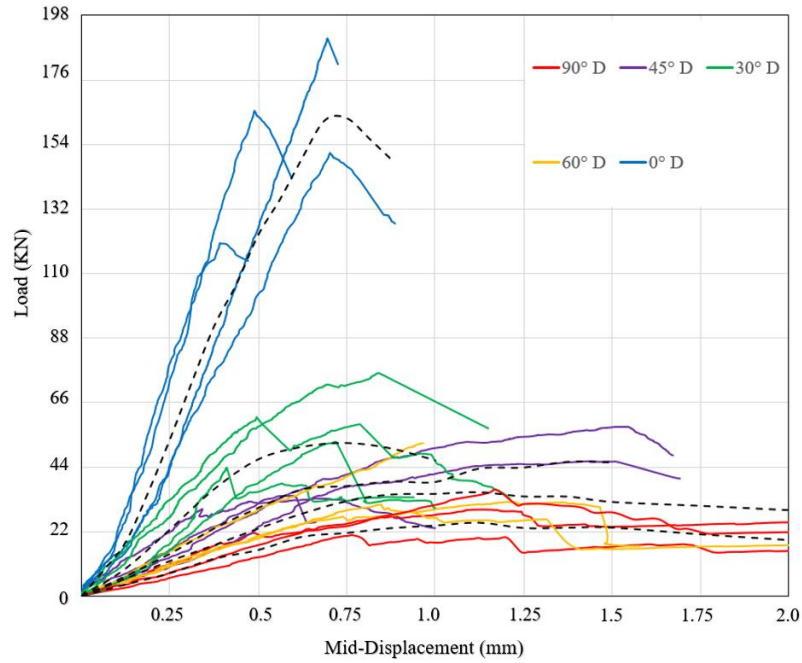


**Fig. 7.** Failure mode I: (a) formation of the first crack (b) propagation of cracks along growth rings at final failure

### **Load-displacement curves**

Fig. 8 presents the full range of the load-displacement curves of the specimens. The mechanical behavior of the five data sets is clearly different. Most obvious is that the pure rolling shear failure of the  $90^\circ$  specimens is much weaker than the pure horizontal shear failure of the  $0^\circ$  specimens; moreover, the  $90^\circ$  specimens are far more ductile with large deformation after peak load than the  $0^\circ$  specimens which fail consistently in an abrupt, brittle manner with the yield load and ultimate load being consistently coincident. For the mixed mode specimens, with fiber angles of  $30^\circ$ ,  $45^\circ$ , and  $60^\circ$ , it can generally be seen that with increasing fiber angle, there is decreasing initial stiffness and strength. A common behavior observed for these specimens was a type of sequential fiber failure and

corresponding load peaks and drops evident in their curves. After the formation of the first failure crack, the shear stress was redistributed until the next crack initiated. This pattern repeated several times before the ultimate peak load and the slope of curves progressively decreased, gradually reducing the stiffness of the specimens, with increased displacement.



**Fig. 8.** Load-displacement curves of specimens under two-plate shear test for different fiber orientations

### Planar Shear Properties

Descriptive statistics for planar shear properties of Eastern Hemlock, for all fiber orientations tested, are provided in table 1. The shear moduli ( $G$ ) were evaluated in accordance with Equation 2 and the shear strength ( $F_v$ ) were evaluated at peak load per Equation 3. Figures 9 and 10 present the data visually for moduli and strength respectively, as cumulative frequencies with fitted Burr cumulative distribution curves. The Burr distribution has been used to fit a wide variety of experimental data, including failure data.

A one-way analysis of variance (ANOVA) was performed at the 5 percent significance level between the five fiber orientations for both stiffness and strength. The results confirmed that there were highly significant differences among the means of these groups (p-values < 0.001), indicating that fiber orientation had a statistically highly significant effect on both stiffness and strength.

The mean rolling shear modulus  $G_{90}$  (45 MPa) was 11% of the mean longitudinal shear modulus  $G_0$  (398 MPa) which is consistent with the ratio suggested in ANSI/APA PRG-320 for rolling shear to longitudinal shear moduli ( $G_{90}=0.10G_0$ ). Meanwhile, the mean  $G$  values of the specimens with  $60^\circ$ ,  $45^\circ$ , and  $30^\circ$  fiber orientation were approximately 35%, 95% and 244% higher values, respectively, than  $G$  perpendicular-to-grain, demonstrating a progressive increase in shear modulus when fiber orientation decreases with respect to load direction.

The findings are similar for shear strength: the mean longitudinal shear strength  $F_{v0}$ , is 5.5 times more than the rolling shear strength  $F_{v90}$  and for the angles in between the mean strengths were 33%, 50%, and 100% more. Referencing figure 10, one can compare the characteristic design strength values of each angle (i.e. the 5<sup>th</sup> percentile with 75% confidence). The characteristic rolling shear strength  $F_{vr,05}$  (0.89 MPa), is approximately 20% of the characteristic longitudinal shear strength  $F_{v,05}$  (4.5 MPa ). This ratio is in agreement with Bendtsen (1976), who studied five western and four eastern softwood species and found rolling shear strength is about 20-25% of longitudinal shear strength. Also, it is within the range of 18% to 28% which is given in the Wood Handbook (Ross 2010). For reference, ANSI/APA PRG-320 suggests the rolling shear strength to be one-third (33%) of the longitudinal shear strength. The characteristic shear strength for

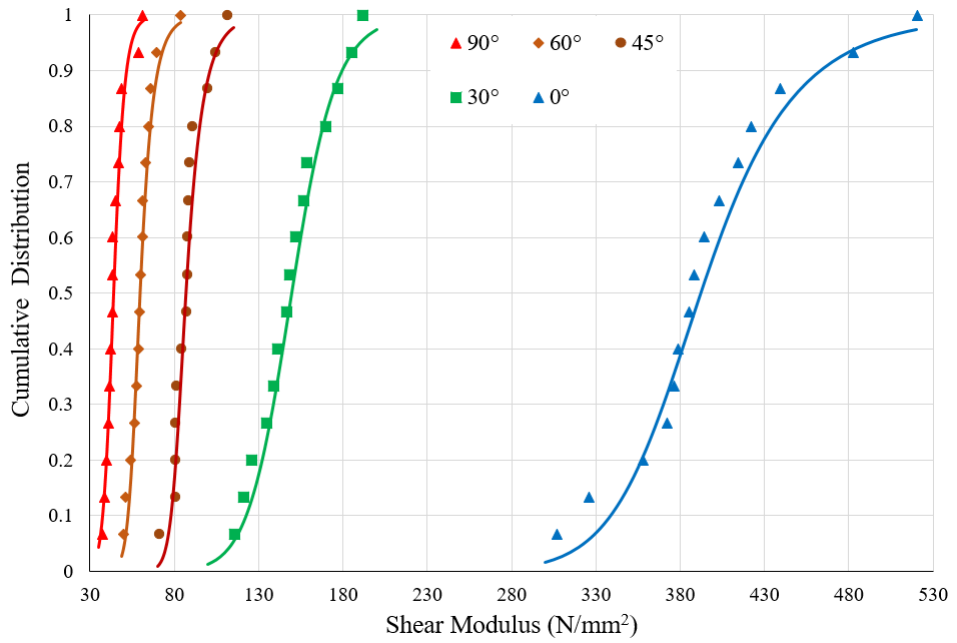
perpendicular and parallel direction is 12% and 89% higher than characteristic shear strength requirement for CLT grade E3.

The characteristic shear strength for 60°, 45°, and 30° fiber orientation is 1.17, 1.42, and 1.77 MPa respectively, which is 26%, 31% and 39% of the longitudinal shear strength value.

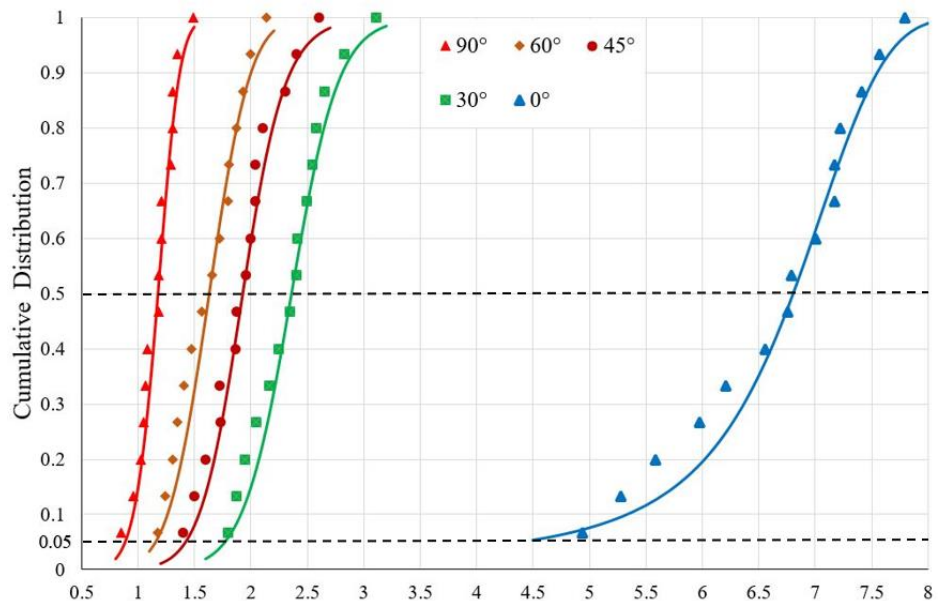
**Table 1.** Planar shear properties for different fiber orientations

Fiber Orientation	0°		30°		45°		60°		90°	
Mechanical Property	F <sub>v</sub> (MPa)	G (MPa)	F <sub>v</sub> (MPa)	G (MPa)	F <sub>v</sub> (MPa)	G (MPa)	F <sub>v</sub> (MPa)	G (MPa)	F <sub>v</sub> (MPa)	G (MPa)
Mean	6.6	398	2.4	151	1.8	88	1.6	61	1.2	45
COV (%)	12.9	13.7	15.3	15.1	16.6	11.7	18.1	13.4	14.2	15.1
Min	4.9	307	1.9	121	1.2	71	1.2	50	0.9	37
Max	7.8	521	3.1	192	2.1	104	2.1	83	1.5	61

Note: COV = coefficient of variation.



**Fig. 9.** Cumulative frequency and fitted Burr distribution for shear modulus from 0° to 90° fiber orientation



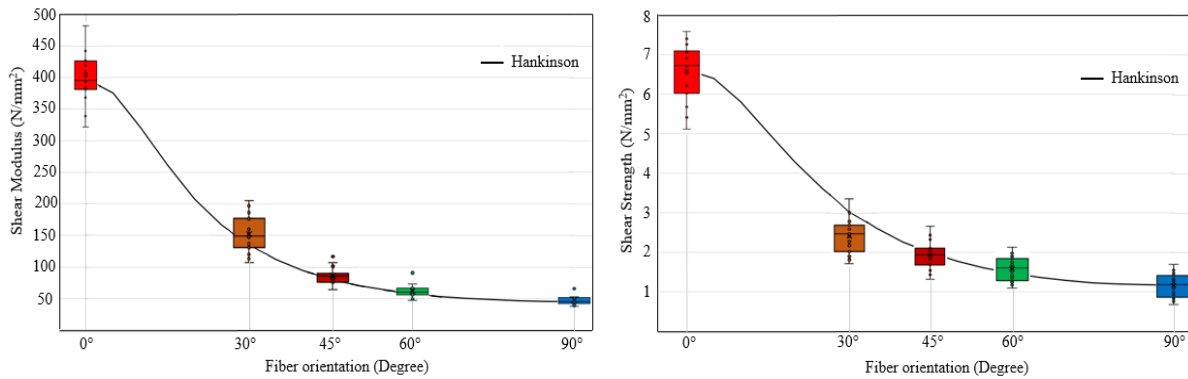
**Fig. 10.** Cumulative frequency and fitted Burr distribution for shear strength from 0° to 90° fiber orientation

## Effect of Fiber Orientation on Planar Shear Properties

Figure 11 visually depicts the relationship between fiber orientation and shear modulus (left) and between fiber orientation and shear strength (right). Also plotted on these graphs is Hankinson formula to gauge its effectiveness in predicting moduli and strength based on fiber orientation. The Hankinson formula was developed by the U.S. Army in 1921, and is widely used for estimating the off-axis uniaxial compressive strength of wood (Kim, 1986). When determining shear stresses values at an angle to grain, Hankinson formula takes the following form:

$$F_{V\theta} = \frac{F_{V0} \times F_{V90}}{F_{V0} \times \sin^2 \theta + F_{V90} \times \cos^2 \theta} \quad (4)$$

where  $F_{V\theta}$  is the shear stresses at angle  $\theta$ , and  $F_{V0}$  and  $F_{V90}$ , are stresses parallel and perpendicular to the grain, respectively. The formula appears to fit the data fairly well, particularly for shear modulus. The largest difference from the mean is for the 30° specimens in both cases: for shear modulus, the predicted value is 135MPa (10% lower than experimental mean) and for shear strength, the predicted value is 3.05 MPa (27% higher than experimental mean).



**Fig. 11.** A comparison of Hankinson Formula with planar test for shear properties of Eastern Hemlock in different fiber orientation: (left) modulus, (right) strength

It is well understood that the 0° specimens are stiffest and strongest owing to wood’s natural resistance to fibers sliding past each other in the longitudinal direction; and in contrast, the 90° specimens are the least stiff and least strong due to the wood’s natural low resistance to the fibers rolling over each other. What happens in between these two ‘pure’ shear stress states, in the angled specimens, is a mixed stress state that is part longitudinal shear and part rolling shear.

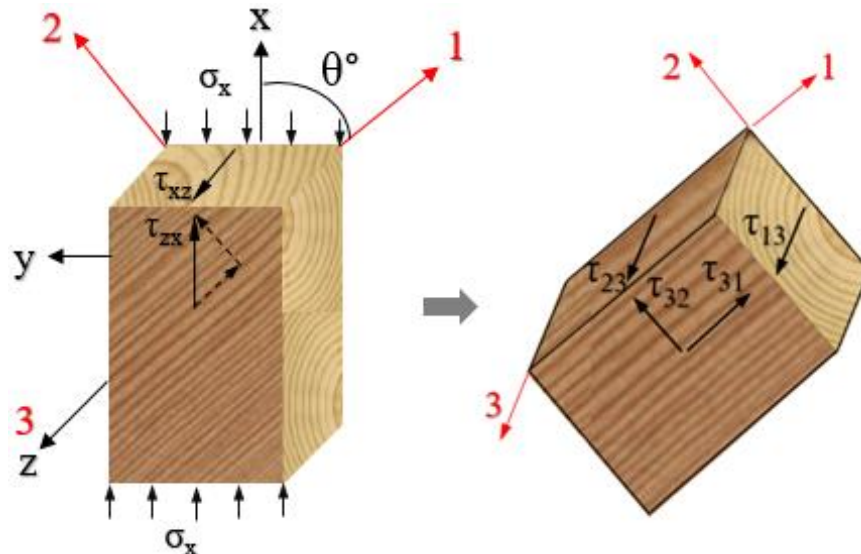
Referring to Figure 12, an applied shear force at an angle to grain produces the theoretical components of stress along the principal material directions. The off-axis shear stress ( $\tau_{zx}$ ) at  $\theta^\circ$  to the fibers can be broken down into bi-axial shear stress components in

$$\tau_{13}=\tau_{31}=\tau_{zx}.\text{Cos}\theta$$

$$\tau_{23}=\tau_{32}=\tau_{zx}.\text{Sin}\theta$$

the principal material directions according to equations 5, as follows:

Table 2 summarizes these components for different fiber orientations. For the perpendicular-to-grain specimen ( $\theta=90^\circ$ ), the stress state is pure rolling shear so  $\tau_{13}=\tau_{31}=0$ ,  $\tau_{23}=\tau_{zx}=F_{v90}=1.2$  MPa. For the parallel-to-grain specimen ( $\theta=0^\circ$ ), the stress state is pure longitudinal shear so  $\tau_{23}=\tau_{32}=0$ ,  $\tau_{13}=\tau_{zx}=F_{v0}=6.6$  MPa. For the angled specimens ( $\theta=30^\circ$ ,  $45^\circ$ , and  $60^\circ$ ), both stresses  $\tau_{13}$  and  $\tau_{23}$  are present in the coordinates of the material, and a failure criteria should be considered for evaluation of the shear capacity. Because the shear strength perpendicular-to-grain is much lower than shear parallel-to-grain, it is expected the shear strength of the angled specimens are significantly influenced by the rolling shear strength ( $F_{v90}$ ). For example, considering angled specimens with  $\theta=60^\circ$ , the estimation of shear strength based on the rolling shear strength is calculated to be 1.38 MPa, which is close to the mean shear strength value obtained from the planar test ( $F_{v60}=1.6$  MPa).



**Fig. 12.** Biaxial stresses from off-axis loading

**Table 2.** Breakdown of the off-axis loading in the principal material coordinate

Stress	Fiber Orientation (Degree)				
	0°	30°	45°	60°	90°
$\tau_{13}$	$\tau_{zx}$	$0.87\tau_{zx}$	$0.71\tau_{zx}$	$0.5\tau_{zx}$	0
$\tau_{23}$	0	$0.5\tau_{zx}$	$0.71\tau_{zx}$	$0.87\tau_{zx}$	$\tau_{zx}$

**Evaluation of CLT Panel Effective Shear Stiffness  $GA_{eff}$** 

To assess the rolling shear moduli ( $G_{90}$ ) and determine the potential for Eastern Hemlock use in ANSI/APA PRG-320 grades, we can estimate the effective shear stiffness ( $GA$ )<sub>eff</sub> for different CLT layups using equation (6):

$$(GA)_{eff} = \frac{a^2}{\frac{h_1}{2 \cdot G_1 \cdot b} + \sum_{i=2}^{n-1} \frac{h_i}{G_i \cdot b} + \frac{h_n}{2 \cdot G_n \cdot b}} \quad (6)$$

where  $b$  is a width of the layers,  $a$  is the distance from centroid of top layer to the centroid of bottom layer,  $h_i$  and  $G_i$  are thickness and shear modulus of each layer, respectively.

The results for three, five and seven layers of CLT panel using Eastern Hemlock are given in Table 3. As shown, these values for all layups just exceed the standard requirement for CLT grade E3. The mean values of both longitudinal and rolling shear modulus from the two-plate shear tests were used for calculation of the effective shear stiffness ( $GA$ )<sub>eff</sub>. Although the effective shear modulus of different panel layups using Eastern Hemlock meet the requirement of the standard, the superior results of the angled

specimens show there is potential for significantly improved shear performance by using angled layers in CLT panels.

These values are less than that estimated from the relations suggested in the ANSI/APA PRG-320. As can be seen in table 4, while the CLT standard estimates the longitudinal and rolling shear Moduli to be 517 and 51.7 MPa, respectively, the mean values of 398 and 45 MPa are obtained from the planar tests which slightly differ from the 50 percentile of the Burr distribution curves. The other mechanical properties presented in table 4, including compressive perpendicular to the grain, modulus of elasticity, parallel and rolling shear strength are the average of small clear specimens per the Wood Handbook (Ross 2010).

**Table 3.** Comparison between effective shear stiffness of experimental test and CLT standard

CLT Grade	CLT thickness (mm)	Number of Layers	GA <sub>eff</sub>	
			(106 N/m)	
			ANSI/APA PRG- 320	Two-Plate Shear Test
E3	105	3	5.3	5.54
	175	5	11	11.07
	245	7	16	16.6

### Finite Element Analysis of 2 plate rolling shear properties

In order to provide insight into the complex stress distribution in the specimen of the two-plate shear test, a numerical Finite Element (FE) analysis was developed using

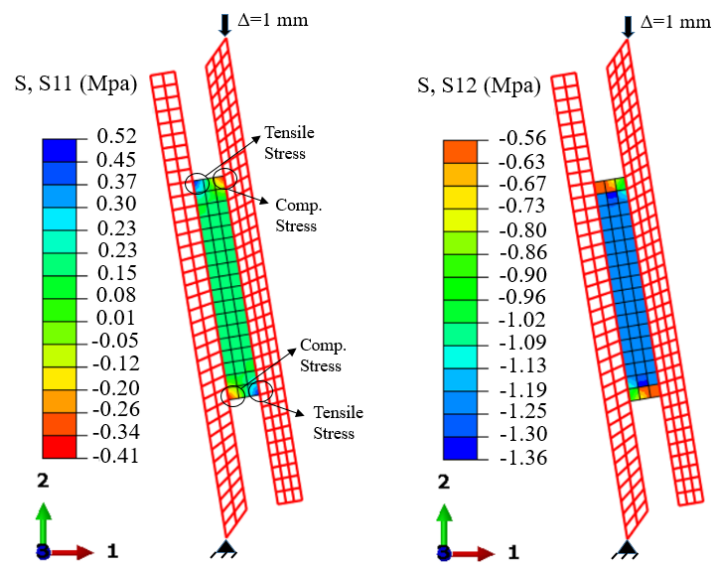
ABAQUS finite element software. The model geometry was built following the test setup dimensions of the study. While the boundary conditions of the knife-edge for one steel plate was assumed pinned, the other knife-edge of the steel plate was subjected to the compressive load in the form of displacement. The shear specimen was modeled as linear elastic, orthotropic material with the constitutive rolling shear property values taken from Table 4. A 2D plane strain model was developed using 8-node biquadratic plane strain quadrilateral (CPE8R) elements. This 2D simulation is only valid for modeling the longitudinal and rolling shear specimens. The state of the plane strain assumption is not valid for angled specimens due to the interaction of mixed mode and out-of-plane deformation.

**Table 4.** Mechanical properties of Eastern Hemlock

Species	Mechanical Properties(MPa)					
	MOE	Compression Strength Perpendicular to Grain ( $F_{C\perp}$ )	Shear Strength Parallel to Grain ( $F_v$ )	Rolling Shear Strength ( $F_v$ )	Parallel Shear Modulus ( $G_0$ )	Rolling Shear Modulus ( $G_{90}$ )
Eastern Hemlock	8300	4.5	7.3	1.31	517	51.7

Figure 13, shows 2D rolling shear modeling of planar test subjected to the 1-mm displacement. As can be seen in the right figure, the shear stresses are distributed nearly uniformly in most part of the shear plane ( $\tau_{12} = 1.25$  MPa). Moreover, the stresses perpendicular to the shear plane are relatively low (Fig. 13, left). The normal stresses in the plane are around 0.1 MPa which are 8% of the uniform shear stresses; however, local

stress concentration zones were observed in the corner area close to free edges. Therefore, it can be concluded that the effect of the secondary stresses is minimum on the determination of the specimen's shear properties, although this test setup does not create pure shear.



**Fig. 13.** Finite element model of the two-plate shear test: normal stresses (left) and shear stresses (right)

## Conclusion

The goal of this research was to evaluate the variation of shear properties of Eastern Hemlock with respect to fiber orientation for use in CLT panels. The results of 75 planar shear tests indicate that (1) the shear strength and effective shear modulus of Eastern Hemlock used as lam stock in CLT is sufficient to meet requirements of ANSI/APA PRG-320 for grade E3 and (2) the rolling shear properties of CLT panels will be improved by

using laminates with different fiber orientation in the inner layer of panels. Based on the above results and discussion, it is possible to draw the following specific conclusions:

- A gradual ductile failure mode was detected in the perpendicular-to-the grain specimens ( $90^\circ$ ), while a brittle failure mechanism with larger ultimate loads and lower shear deformation was observed in the parallel-to-the grain specimens ( $0^\circ$ ). For the specimens with fiber angles between these two orientations, the failure load increased nonlinearly from  $90^\circ$  to  $0^\circ$  due to the effect of the interaction between horizontal shear and rolling shear strength.
- Hankinson formula appears to provide an acceptable prediction for off-axis shear strength and modulus of wood.
- The average shear strength and modulus of Eastern Hemlock varies considerably with respect to the orientation of fibers. Two upper and lower values of 398 and 45 MPa obtained for shear modulus parallel- and perpendicular-to-grain direction, respectively, were 23% and 13% less than if, compared with the suggested values in the ANSI/APA PRG-320 which have been estimated based on the fraction of the modulus of elasticity. However, the effective shear modulus of CLT panel ( $G_{A_{eff}}$ ) for all layups of Eastern Hemlock is further than the standard requirement for CLT grade E3.
- The characteristic shear strength (5th percentile with 75% confidence) exceeded the required characteristic values from the standard. These values were about 4.5 and 0.89 MPa for parallel-and perpendicular-to-grain specimens, which are 89% and 12% higher than the specified values in the CLT standard, respectively.
- The characteristic shear strength for the specimens with the fiber orientation of  $30^\circ$ , and  $45^\circ$  were 59% and 98% higher than rolling shear strength, respectively, which could be an alternative candidate for using in the layups of the CLT panels in order to improve the rolling shear properties of the panels.
- A finite element model showed that shear distribution in the two-plate test is uniform and stresses perpendicular to the shear plane are low indicating that the two-plate test method is an appropriate test method for determining the shear properties for CLT.

## APPENDIX C

### IMPROVING THE ROLLING SHEAR PROPERTIES OF CROSS-LAMINATED TIMBER (CLT) PANELS BY OPTIMIZING LAMINATE FIBER ORIENTATION

#### ABSTRACT

The development of cross-laminated timber (CLT) technology has provided new possibilities for low-valued softwood species, which traditionally have not been used as structural engineering applications. As CLT gains industry acceptance, low-value softwood species, not specified in current ANSI standards, need to be investigated for use in CLT panels. One possible issue in using softwood species is that they have low rolling shear properties in the plane perpendicular to the fiber direction, which may affect the mechanical properties of CLT. To improve the shear properties of laminates, this study examines the effect of the fiber orientation on the mechanical properties of CLT. For this purpose, several numbers of three layers of short-span CLT specimens were fabricated from locally grown Eastern Hemlock species into four groups. The mid-layer of each group was oriented 30°, 45°, 60°, and 90° with respect to the major direction. To measure the deformation and shear strength of the panels, the three-point bending test was used according to ASTM D198. The influence of fiber orientation on the effective shear modulus and other mechanical properties are discussed. To determine the shear stress distribution and estimate the deformation of panels under the three-point bending test, further numerical Finite Element (FE) analysis in the elastic range was conducted using ABAQUS software. The results of the experimental test were compared with the finite element modeling as well as shear analogy method.

Based on the results, there was a general tendency for both bending properties and rolling shear capacities to increase by changing the fiber orientation of the mid-layer from 90° to 30°. The values of effective shear stiffness ( $G_{Aeff}$ ) and shear strength ( $F_v$ ) obtained from the CLT panel with 30° fiber orientation were 828% and 48% higher than those for regular CLT, respectively. Additionally, it was revealed that the results of the FE simulation were in good agreement with the experiments for 90° CLT. However, for angled CLT specimens, the FE model and shear analogy method were predicted to have higher deformation due to the biaxial shear stresses from off-axis loading and bending-twisting coupling in the mid-layer, which is not taken into account by the FE model and shear analogy method.

## **INTRODUCTION**

Cross-Laminated Timber (CLT) is a multilayer wood board produced by gluing orthogonally oriented layers of laminated wood boards together. CLT panel usage in construction has increased considerably during the last decade. Because of the obvious advantages of CLT products, hundreds of structures have been built, competing with steel and concrete materials in mid-rise and even high-rise buildings. Typical construction applications include wall panels, roof slabs and flooring elements in buildings, as well as bridge decking. The key advantages of CLT panels, which make possible fast project completion, especially in mid-rise buildings, are easy handling and accurate prefabrication (Karacabeyli & Douglas, 2013). CLT can also be cost-competitive with composite structural lumber (LSL, LVL, and PSL) and light framing in mid-rise construction where wood is not traditionally used (Pöyry, 2017). Prices for CLT, still in its growth phase, are expected to settle close to other lightweight engineered wood products.

In the last decade, the use of CLT has moved from residential low-rise buildings to mid-rise and even high-rise commercial buildings. In recent years, standards and a design handbook have been published (ANSI/APA PRG-320-2012; Schickhofer et al. 2009; Gagnon and Pirvu 2013), although there is still room for improving and modifying CLT standards.

The cross-layers of CLT produce uniform swelling and shrinkage properties, generating a monolithic structural member that can distribute the load in the minor direction. However, due to low shear properties, cross layers cause large shear deformation and deflection in CLT panels, which is critical for CLT with low-grade wood species and short span-to-depth ratios.

Several recent studies have investigated the rolling shear effects in wood and CLT (Zhou et al. 2014; Mestek 2011; Blass and Fellmoser 2004b; Aicher and Dill-Langer 2000). These studies focused on the method of measuring the rolling shear properties and analyzing CLT panel bending properties, which led to model predictions of the rolling shear properties. Other studies conclude that many variables influence the wood's rolling shear properties, such as specific density of cross-layer, growth ring orientation, species, moisture content, size, layer thickness, span-to-depth ratio, shrinkage, and the geometry of the laminate's cross-section (Brandner 2013, Gagnon and Pirvu 2011, Yawalata and Lam 2011, Flores et al. 2015, Franzoni et al. 2016).

Using a planar shear test to measure the rolling shear modulus of black spruce lumber for different growth ring orientation, Zhou et al. (2014) observed that cross layers with growth ring orientation in rift-sawn lumber could increase the rolling shear modulus in comparison to flat-sawn or quarter-sawn. In another study, the authors used two methods

bending tests and a two-plate shear test to compare the rolling shear modulus and strength of the cross-layer in CLT. Their findings show that the results of the two-plate shear test can accurately estimate deflection of CLT specimens. The authors also found that the width of the specimen has no obvious effect on the apparent modulus of elasticity and shear modulus of CLT panels (Zhou et al., 2014).

Recent studies have determined the variables that influence rolling shear. Using lodge-pole pine specimens, Pirvu (2011) performed the two-plate shear test to examine the influence of edge gluing and sectional size on the rolling shear properties of laminates. Pirvu found that average rolling shear modulus of the larger cross-sectional specimens are higher than the edge-gluing specimens, indicating the appropriateness of using the larger specimen size than the smaller edge-gluing one.

Flores et al. (2015) examined the effect of edge-gluing, wood density, and span-to-depth ratio on the rolling shear properties, predicting that cross edge-gluing of laminates could increase the failure load by 40%. Furthermore, by using 37.5% denser wood species, the critical load would increase by 21%; and increasing the span-to-depth ratio would decrease the failure load proportionally (Flores et al. 2015). In another study, Pirvu (2011) found that, although edge gluing the specimen is effective in rolling shear modulus, using a larger specimen size is more influential for increasing shear modulus. Additionally, he found that increasing the specimen's width had no notable effect on the rolling shear modulus.

In still another study, Yawalata and Lam (2011), investigating the effects of manufacturing process variables on the rolling shear strength of three-layer CLT panels, found that higher vertical clamping pressure creates stronger panels and increases the

rolling shear strength of panels. For their part, Buck et al. (2016) tested a CLT panel with  $\pm 45^\circ$  alternating layers against a regular panel of  $90^\circ$  orientation, using 40 5-layer panels fabricated in two configurations with dimensions of 95 mm thickness, 1200 mm width and 4136 mm length. The results of the four-point-bending test exhibited a 35% and 15% increase in bending strength and modulus of elasticity, respectively, compared to the CLT panel with  $90^\circ$  orientation.

The need to research alternative uses for low-value species lies in the abundance of typically nonstructural grade softwood species and the desirability of an economic and sustainable market. Eastern Hemlock in the northeast region of United States is an example of locally grown softwood identified as a low-value species, because of its tendency for ring shake, a lengthwise separation that occurs between and parallel to annual rings (Gardner and Diebel 1995). The Hemlock Woolly Adelgid (*Adelges tsugae*), a small insect lately infesting this species, can cause tree death within 4 to 10 years (Webb et al. 2003, USDA FS 2013), so a value-added use for lumber species can create market and forest management improvements in the forest industry.

While few researchers have studied locally grown species to use in CLT products, such species have shown considerable potential for creating an economically viable and sustainable market for low-value timber to produce high-performance and cost-effective CLT products (Fortune and Quenneville, 2010, Hindman and Bouldin, 2015, Kramer et al. 2014).

In this study, the primary objective is to examine the effect of the fiber orientation on the shear properties of short-span CLT panels made from local Eastern Hemlock and to determine the potential load-bearing capacity, thus improving the rolling shear properties

of CLT panels. This alignment has not been evaluated on industrially manufactured CLT products to date. The mechanical properties of angled CLT panels were compared with the regular CLT regarding effective shear modulus, rolling shear strength and apparent bending modulus. A finite element analysis was developed in ABAQUS to simulate the three-point bending test and to compare it with the results of the shear analogy method and experimental test.

## **MATERIALS AND METHODS**

### *Manufacturing CLT*

Eastern Hemlock was obtained from a local supplier in Massachusetts, which included No.1 and No.2 grade 2x4 lumber, sawn flatwise, planed and joined to the 84 mm × 33 mm. To target equilibrium moisture content of about 12%, all wood was placed in a standard room set at a temperature of 20±3°C and relative humidity of 65±2% prior to CLT manufacturing. After conditioning, the measured moisture content of the lumbers was in the range of 9.1%-12.4%, then lumbers cut into clearly specified sizes.

All of the CLT panels in these tests were three-layered, each 33 mm in thickness, with each panel having a three lumber thickness totaling a panel thickness of approximately 99 mm. The width of each lumber was approximately 84 mm, with each panel having four boards in width with an average full panel width of 336 mm after pressing. The adhesive used between the layers was LOCTITE HB X452 PURBOND single-component polyurethane adhesive. The glue spread rate for each panel was 180 g/m<sup>2</sup>, which was within the recommended rate of 120 to 195 g/m<sup>2</sup>. This adhesive system is recommended for wet-use or dry-use exposure and meets the requirements of AITC 405-2008 (Standard for Adhesives for Use in Structural Glued Laminated Timber). Prior to adhesive

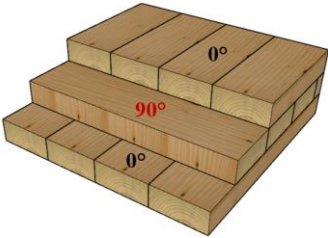
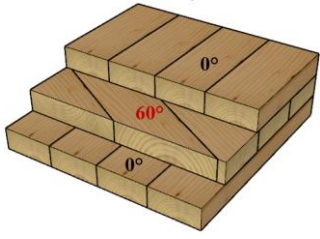
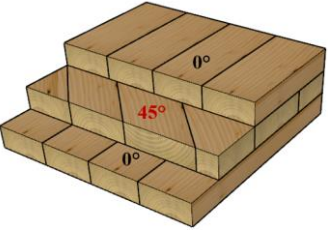
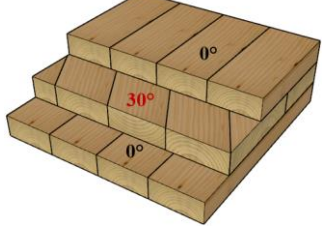
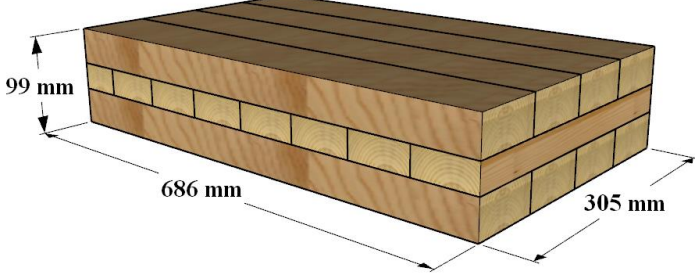
application, a surfactant primer was sprayed with a ratio of 5% concentration to 95% water, and approximately 20 g/m<sup>2</sup> (light spray) on the surface of the lumber. The wood was dried for 15 minutes before gluing. The adhesive was applied with a paint roller and the total assembly time of each test specimen was less than 45 minutes, measured from the start of the adhesive application to the time of the total pressure being applied to the panel.

To achieve higher shear strength and prevent a possible movement of cross-layers, the growth ring orientations of adjacent lumber were arranged alternatively and edge-bonded. Three-layer CLT panels were laid up for each of four configurations as described in Table 1. As shown in this table, all top and lower layers of the CLT panel were parallel to the major direction, but the mid-layers were oriented in 0°, 30°, 45°, and 60° with respect to the major direction.

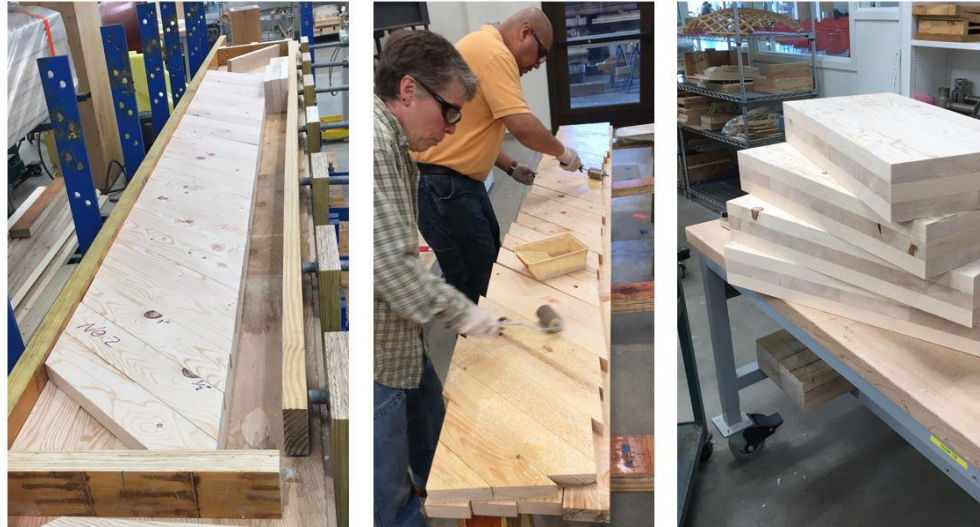
Following the application of adhesive, vertical pressure of 0.69 MPa was applied by the hydraulic press for 24 hours. The required pressing time for the adhesive was approximately 135 min, which was always met or exceeded. To squeeze the panels in the transverse direction and avoid gaps between the boards, the side pressure was applied by clamps.

Fig. 1 shows the fabrication process of short-span CLT panels. ANSI/APA PRG-320 suggests using the specimen's width of not less than 305 mm and a span-to-depth ratio of 5 to 6 could produce a high percentage of shear failures. To meet the requirement of the short span-to-depth ratio of 6 and obtain straight edges, the 3048 mm long continuous CLT panels were cut to 686 x 305 mm short-span panels using a large band saw. In total, 16 short-span CLT panels were prepared into four groups according to fiber orientation in

mid-layer. Specimen lengths and widths were measured to the nearest 0.25 mm and thickness to the nearest 0.025 mm.

Treatment	Layups	Fibers Orientation
1	[0/90/0]	
2	[0/60/0]	
3	[0/45/0]	
4	[0/30/0]	
		

**Fig. 1.** The size of the three layers short-span CLT panel for different lumber orientation

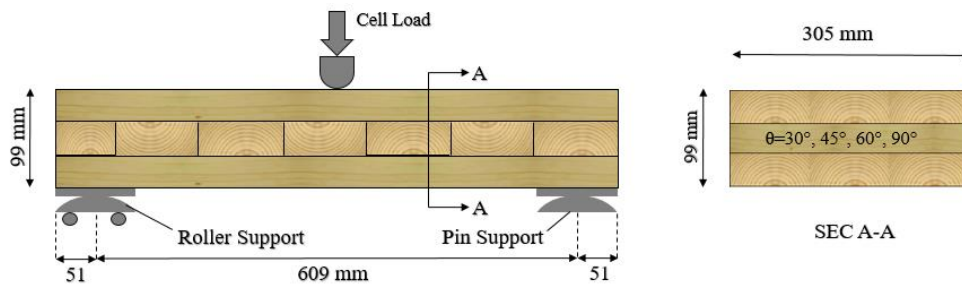


**Fig. 2.** The detailed fabrication process for short-span CLT panels

#### *Three Point Bending Test Method*

The shear tests were performed according to the ANSI/APA PRG 320 (ANSI/APA 2012), which refers back to the three-point bending test illustrated in the ASTM D198. These tests were used to determine the shear properties of short-span CLT panels. As shown in Figs. 3 and 4, the load was applied to the middle of the 0.619 m span with a single 200 mm radius wooden load head. The specimen span was 610 mm, measured between the centerline of the supports. Each support had a steel top plate that rested on a roller allowing free rotation. To minimize the support effect and avoid bearing failure, the bearing length was 76 mm, which was less than the specimen depth suggested in the ANSI/APA PRG 320. Two yokes, one on each side, were supported at the neutral axis over the supports. To measure the neutral axis mid-span deflection using two linear variable differential transformers LVDTs ( $\pm 25.4$  mm range,  $\pm 0.25\%$  sensitivity), the mean value of two

readings from LVDTs was recorded as the beam deflection. Testing was conducted in two phases. Initially, to determine the shear and bending stiffness, the center point loading was applied up to 60% of estimated maximum load using an MTS universal testing machine with a load rate of 5 mm/min, ensuring specimen failure within 6–20 min as specified by ASTM D198. In the second phase, both LVDTs were removed to prevent damage. The point loading was then applied to failure at a constant rate of displacement and the peak load of the shear test recorded.



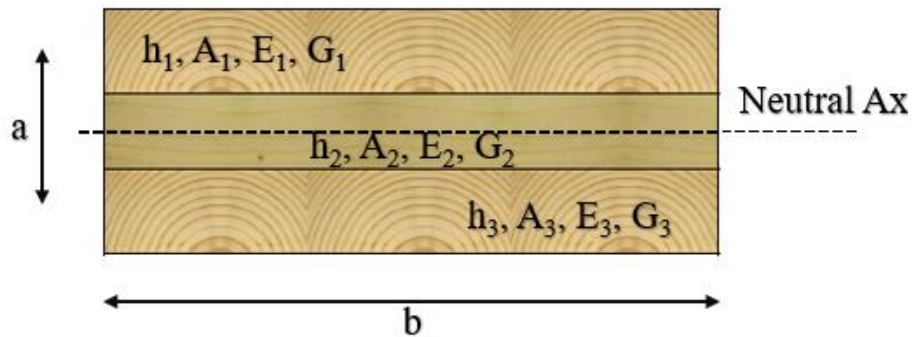
**Fig. 3.** Longitudinal and cross-section of CLT floor panel



**Fig. 4.** Typical test setup for short-span CLT test

*Estimation of the deflection using shear analogy method*

As shown in Table 1, for each group of CLT panels, the material properties of laminates, including modulus of elasticity and shear modulus, were used to predict the deflection of the panels under the three-point bending test, using the shear analogy method. The shear modulus values in different orientation were obtained from the two-plate shear test (Bahmanzad et al. 2019). The mid-span deflection value can be estimated in accordance with Equation (1) from ASTM D198 (ASTM 2015). Fig. 5 shows the schematic of a cross-section of 3-layer CLT.



**Fig. 5.** Cross-section of 3-layer CLT

**Table 1.** Modulus of Elasticity and Shear Modulus of Eastern Hemlock for Different Fiber Orientation

Species	Elastic Properties(MPa)						
	$E_L$	$E_T$	$G_{0^\circ}$	$G_{30^\circ}$	$G_{45^\circ}$	$G_{60^\circ}$	$G_{90^\circ}$
Eastern Hemlock	8300	276	520.56	191.68	104.11	83.43	61.36

$$\Delta_{\text{Mid}} = \frac{1}{48} \times \frac{Pl^3}{EI_{\text{eff}}} + \frac{1}{4K} \times \frac{Pl}{GA_{\text{eff}}} = \frac{1}{48} \times \frac{Pl^3}{EI_{\text{app}}} \quad (1)$$

where P is the load applied, L is the CLT span, and K is equal to 5/6 for the rectangular section.

The effective bending stiffness ( $EI_{\text{eff}}$ ) and effective shear stiffness ( $GA_{\text{eff}}$ ) can also be obtained from Equations (2) and (3), respectively from shear analogy method explained in CLT Handbook (2013)

$$(EI)_{\text{eff}} = \sum_{i=1}^n E_i b_i \frac{h_i^3}{12} + \sum_{i=1}^n E_i A_i Z_i^2 \quad (2)$$

$$(GA)_{\text{eff}} = \frac{a^2}{\frac{h_1}{2 \cdot G_1 \cdot b} + \sum_{i=2}^{n-1} \frac{h_i}{G_i \cdot b} + \frac{h_n}{2 \cdot G_n \cdot b}} \quad (3)$$

where  $E_i$  and  $G_i$  are the modulus of elasticity and shear modulus of layer  $i$ , respectively,  $A_i$  is the area of cross-section of layer  $i$  and  $Z_i$  is the distance between the center axis of layer  $i$  and the neutral axis of the entire cross-section,  $a$  is the distance between the centroid of the top and lower layers of cross-section, and  $h_i$  is the thickness of layer  $i$ .

#### *Evaluation of the effective shear modulus using the Three-point Bending Test*

The mid-span deflection was calculated in the elastic range of the load-displacement curves following Equation (4).

$$\delta_e = \frac{P}{K_e} \quad (4)$$

where P is a load in the elastic range, and Ke is the slope of the force-deformation curve below the proportional limit load obtained from the linear regression of data.

The effective shear modulus (GA<sub>eff</sub>) and apparent bending modulus (EI<sub>app</sub>) of short-span CLT panel were computed from the mid-span deflection of the three-point bending test, using Equations (5) and (6) explained in the ASTM D198 (ASTM 2015).

$$EI_{app} = \frac{1}{48} \times \frac{PL^3}{\delta_e} \quad (5)$$

$$GA_{eff} = \frac{PL}{4K \times \left( \delta_e - \frac{1}{48} \times \frac{PL^3}{EI_{eff}} \right)} \quad (6)$$

#### *Evaluation of shear stresses at peak load from test results*

To determine shear stress at the peak load of the short-span CLT panels, the shear analogy method, developed by Kreuzinger (1999), was used; it is the most accurate method since it takes into account the shear deformations of the CLT. The method is based on the combination of two virtual beams, A and B, which are constrained to have the same vertical deflection at any point along their length. Beam A considers flexural stiffness of individual layers about their neutral axes while their shear rigidity is assumed to be infinite. Beam B considers bending stiffness and shear stiffness of individual layers about their “Steiner” points. The two beams are coupled so that they have equal deflections under the loads.

Using this method, under the transverse shear load  $V$ , the rolling shear stress in cross-layer  $i$  is calculated by adding together the shear stresses  $f_{vA,i}$  in Beam A and  $f_{vB,i}$  in Beam B.

$$f_{vAi} = \frac{E_i I_i}{B_A} \times 1.5 \times \frac{V_A}{b \times h_i} \quad (7)$$

$$f_{vB_{i,i+1}} = \frac{V_B}{B_B} \times \sum_{j=i+1}^n E_j A_j z_j \quad (8)$$

where  $B_A$  and  $B_B$ , are the bending stiffness of Beam A and Beam B, calculated by

$$(B)_A = \sum_{i=1}^n E_i I_i \quad (9)$$

$$(B)_B = \sum_{i=1}^n E_i I_i z_i^2 \quad (10)$$

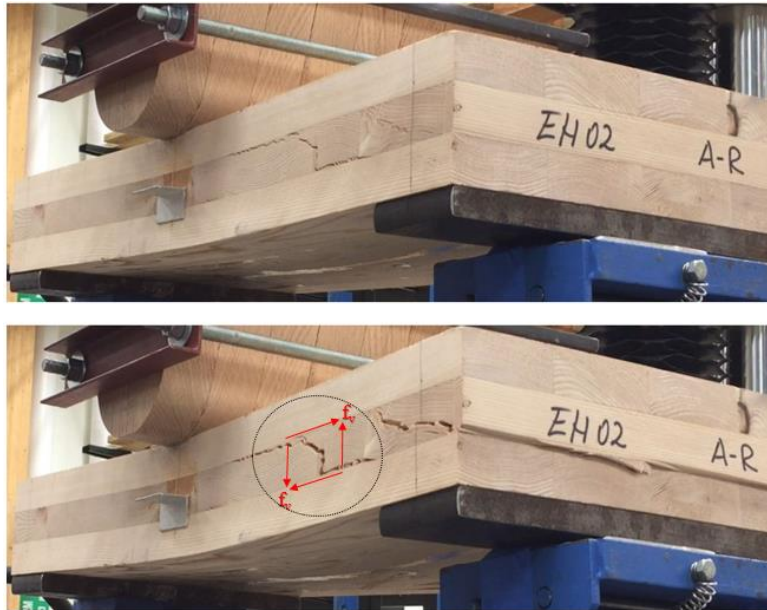
## TEST RESULTS AND DATA ANALYSIS

There were two failure modes in the bending tests. As expected, the main type of failure mode was rolling shear failure that occurred in 90° CLT panels. In this type of failure, the first rolling shear crack with 30° to 45° inclined angle started between the supports and loading area and, as the load increased, it propagated along the length of the panel toward the support areas, where the final fracture occurred following the nonlinear maximum loading range (Fig. 6).

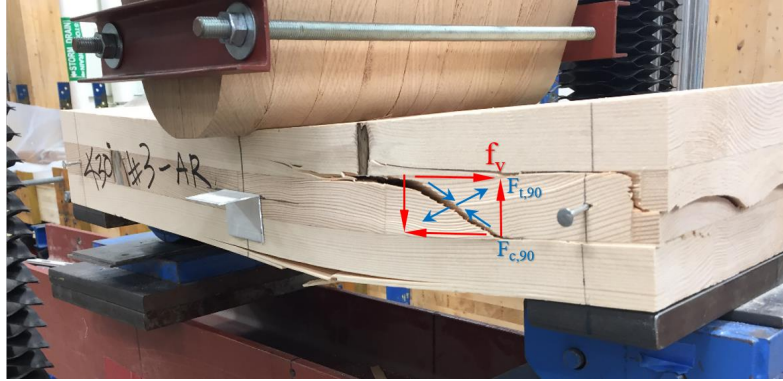
The failure type of the angled panels was similar to the regular panels, except that the out-of-plane shear deformation along the angle-fibers occurred in the mid-layer of the CLT due to the biaxial shear stresses from off-axis loading. Fig. 7 shows typical mixed failure mode (a) along the angle-fibers, and (b) rolling shear of the mid-layer in the angled panels. Due to symmetric layups of the laminates, there is a bending-twisting coupling in the mid-layer. In this type of the deformation, the panel twisting about the spanwise axis,

in addition to the CLT's major flexure (Jones 2014, Gibson 2016) . The authors will in the following paper discuss more about this type of deformation.

At the last stage of the failure, the mixed mode of the bending and rolling shear failure were observed, especially for 30° CLT, indicating greater shear strength resistance than in other samples.



**Fig. 6.** Typical failure of 90° CLT panels: formation of first crack (top) and its propagation of crack along the length of the panel at the final failure step (bottom)

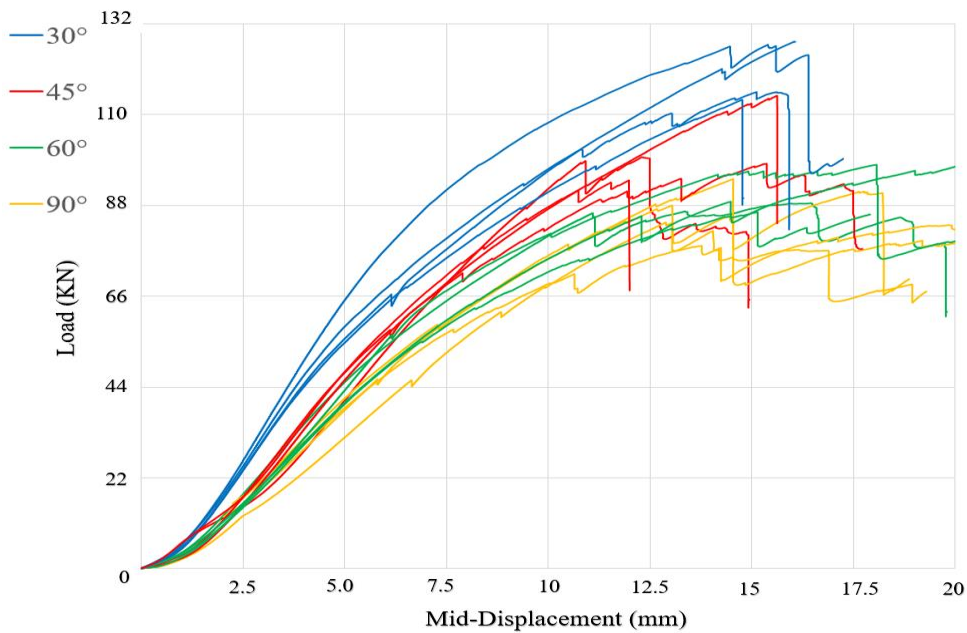


**Fig. 7.** Typical failure of angled CLT panels

Fig.8 presents the load-deflection curve of the short-span CLT panels for four data sets under the three-point bending test. Data mapping was only performed for the 90° specimens to display all curves in a single figure. The mean peak load of angled CLTs is clearly higher than regular CLT (90°), having the lowest mean value of 88.3kN for 90° and 122.2kN for 30° which indicates the higher strength of the angled CLT panels. Also, it can be seen that the slope of the curves increase as the fiber orientation of the mid-layer changes from 90° to 30°, indicating that the mechanical properties are enhanced by reorientation of the fibers.

As can be seen from the load-displacement curves, there is a minor load drop around 60-70% of peak load showing the formation of the first crack for most of the specimens. Increasing the load, the slope of curves, which represents the apparent bending stiffness of the specimens, progressively decreases. For the 90° CLT, several load peaks and drops occurred before the major drop, indicating that shear stress was redistributed. However, fewer sequential load drops and fiber failure occurred by changing the fiber orientation toward 30°. In other words, for 90° CLT, the shear stress was better redistributed along the length of the panel. This behavior is in agreement with the two-pla

shear test finding, which has shown that angled specimens have a higher failure load with the brittle failure mechanism compared to the shear perpendicular-to-grain specimens with the large deformation and lower failure loads (Bahmanzad et al. 2019).



**Fig. 8.** Load-deflection response for short-span CLT panels

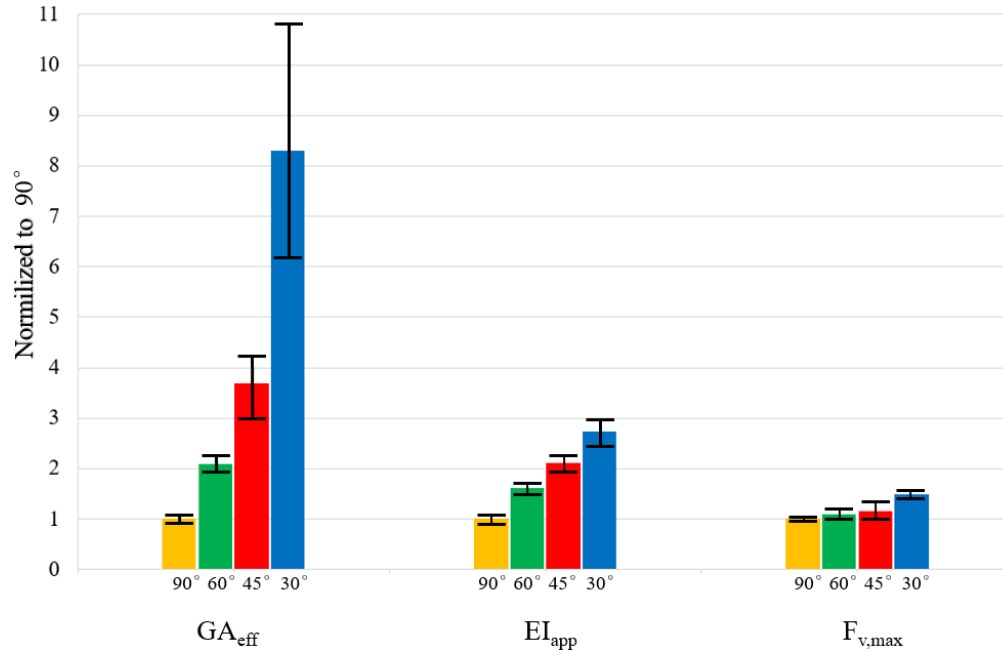
#### *Effective Shear Modulus and Rolling Shear Strength*

Summary test results for the bending tests are shown in Table 2. These include the apparent bending modulus, effective shear modulus, and peak load for each specimen, which were evaluated using Equations (5) and (6). The comparison of these properties for different fiber orientation which are normalized to 90° are presented in Fig.9. As can be seen, the specimens generally exhibited the lowest degree of variability in both strength and stiffness, which may be attributed to their being made entirely from No.1 flat sawn lumbers in CLT panel. The 90° CLT panels generally exhibited the lowest stiffness in both bending and shear modulus. For this type of panel, the mean apparent bending modulus

and effective shear modulus were  $177.3 \times 10^9$  N-mm<sup>2</sup>/m and  $9.49 \times 10^6$  N/m, respectively. The mean values for 60° CLT panels were 61% and 209% greater than for 90° CLT. Comparing 45° with 90° CLT, the values grow by 212% and 368%, respectively, and the highest values were calculated from 30° CLT, with a 274% and 829% growth rate compared to the 90° CLT.

Table 2 and Fig.9 also give the average rolling shear strength at peak load for the short-span specimens calculated from the shear analogy method using Equations (7) and (8). As shown in the table an figure, the mean rolling shear strength value of 3-layer 30°, 45°, and 60° CLT specimens is 2.83, 2.36 and 2.2 MPa, respectively; they are 39%, 16%, and 8% higher than the 90° CLT panel.

It is well recognized that as the fiber orientation of the mid-layer varies from 90° to 30°, the mean effective shear modulus and shear strength values per unit width increase. The highest values in the investigated specimens were recorded for the 30° CLT panels with the  $78.7 \times 10^6$  N/m effective shear modulus and 3 MPa shear strength. What happens in the angled specimens, is a mixed stress state that is part longitudinal shear and part rolling shear. In this case, the contribution of longitudinal shear stress increase as fiber orientation decrease. For the 90° specimens, these properties are the lowest, due to the wood's natural low resistance to the fibers rolling over each other.



**Fig. 9.** Comparison of effective shear Modulus ( $GA_{\text{eff}}$ ), apparent bending modulus ( $EI_{\text{app}}$ ), and shear stress ( $f_v$ ) for fiber orientation of  $30^\circ, 45^\circ, 60^\circ, 90^\circ$

**Table 2.** Summary mean results of short-span shear test for fiber orientation of  $30^\circ, 45^\circ, 60^\circ, 90^\circ$

Mid-layer Angle	Peak Load (kN)	$EI_{\text{app}}$ ( $10^9$ N-mm <sup>2</sup> /m)	$GA_{\text{eff}}$ ( $10^6$ N/m)	$f_{v,\text{max}}$ (MPa)
90°	88.3 (5.8%)	177.3(6.7%)	9.5 (9.3%)	2.03 (5.8%)
60°	95.9 (10%)	286.3 (2.6%)	19.9 (4.6%)	2.2 (10%)
45°	102.7 (8.8%)	375.9 (6.1%)	34.9 (13.8%)	2.36 (8.8%)
30°	129.1 (2.1%)	486.3 (7.6%)	78.68 (33.3%)	3.00 (2.1%)

(CoV in parentheses;  $EI_{\text{app}}$  = apparent bending modulus;  $GA_{\text{eff}}$  = effective shear Modulus; shear stress<sup>max</sup>=maximum shear stress).

#### *Finite Element model of short span shear CLT panel*

To investigate the shear stress distribution in the short-span shear CLT panel and predict the behavior of the panel in the elastic range, further numerical finite element (FE) analysis was developed on the 686 mm short-span CLT and subjected to three-point bending using ABAQUS finite element software. The model geometry, consisting of three

layers of orthotropic plies illustrated in Fig. 10, was modeled as a linear elastic. A 2D plane strain model was developed with an 8-node biquadratic plane strain quadrilateral (CPE8R) elements with side lengths of 12.7 mm. As shown in Fig. 11, because the geometry is symmetric about the mid-span, half of the CLT panel was modeled considering the boundary condition of zero displacement component perpendicular to the centerline and rotational component parallel to centerline, however the displacement along the centerline is free to move ( $U_x = 0$ ;  $U_y = \text{free}$ ;  $R_z = 0$ )

### *Material property assumptions*

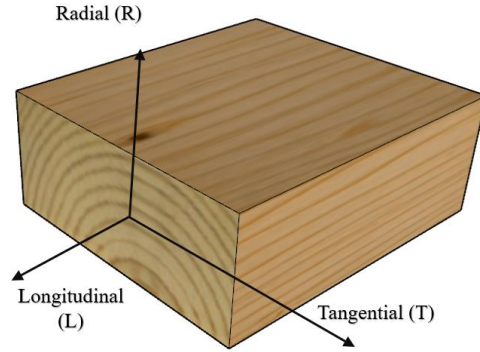
For 2D plane strain conditions, such as in a shell element, the values of  $E_L$ ,  $E_R$ ,  $E_T$ ,  $\nu_{LR}$ ,  $\nu_{LT}$ ,  $\nu_{TR}$  and  $G_{LR}$  are required to define an orthotropic material. For plane-strain problem we have:

$$\begin{bmatrix} \epsilon_L \\ \epsilon_R \\ \epsilon_T = 0 \\ \gamma_{LR} \end{bmatrix} = \begin{bmatrix} \frac{1}{E_L} & -\frac{\nu_{LR}}{E_R} & -\frac{\nu_{LT}}{E_3} & 0 \\ -\frac{\nu_{RL}}{E_L} & \frac{1}{E_R} & -\frac{\nu_{RT}}{E_T} & 0 \\ -\frac{\nu_{TL}}{E_L} & -\frac{\nu_{TR}}{E_R} & \frac{1}{E_T} & 0 \\ 0 & 0 & 0 & \frac{1}{G_{LR}} \end{bmatrix} \begin{bmatrix} \sigma_L \\ \sigma_R \\ \sigma_T \\ \sigma_{LR} \end{bmatrix} \quad (11)$$

$\epsilon_T$  is the strain in direction T due to uniaxial stress  $\sigma_L$

Each layer was modeled as a linear elastic, orthotropic material with constitutive properties collected for Eastern Hemlock from two-plate shear test results and wood handbook which are displayed in table 3 (Ross 2010). For angled short-span CLT, shear modulus of mid-layer obtained from angled specimens under two-plate shear test

(Bahmanzad et al. 2019). A supporting plate was modeled as isotropic steel plate (modulus of elasticity and Poisson's ratio were set to 200 GPa and 0.25, respectively)



**Fig. 10.** Three Axes of Wood with Respect to Grain Direction

**Table 3.** Mechanical Properties input in FE Model

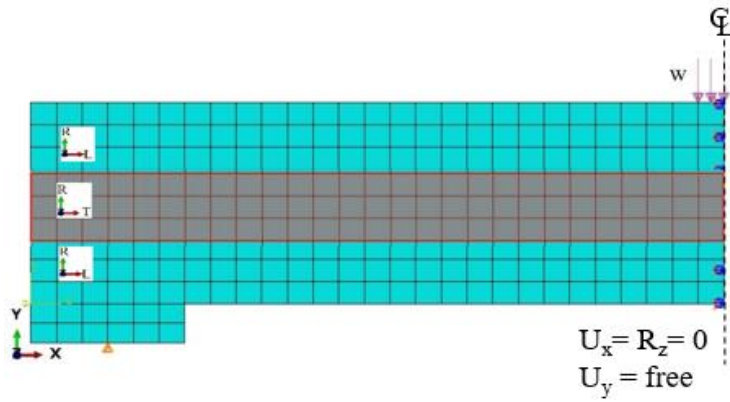
Specie	$E_L$ (MPa)	$E_R$ (MPa)	$E_T$ (MPa)	$\nu_{LR}$	$\nu_{LT}$	$\nu_{TR}$	$G_{LR}$ (MPa)	$G_{LT}$ (MPa)	$G_{TR}$ (MPa)
Eastern Hemlock	8300	276	276	0.485	0.423	0.442	520.56	61.36	61.36

The Poisson's ratio  $\nu_{RL}$  is implicitly given as  $\nu_{RL}=(E_L/E_R) \nu_{LR}$ .

In orthotropic materials, both stiffness and compliance must be positive definite to reach the solution (Jones, 1999). ABAQUS checks all these restrictions by using input values (ABAQUS, 2016).

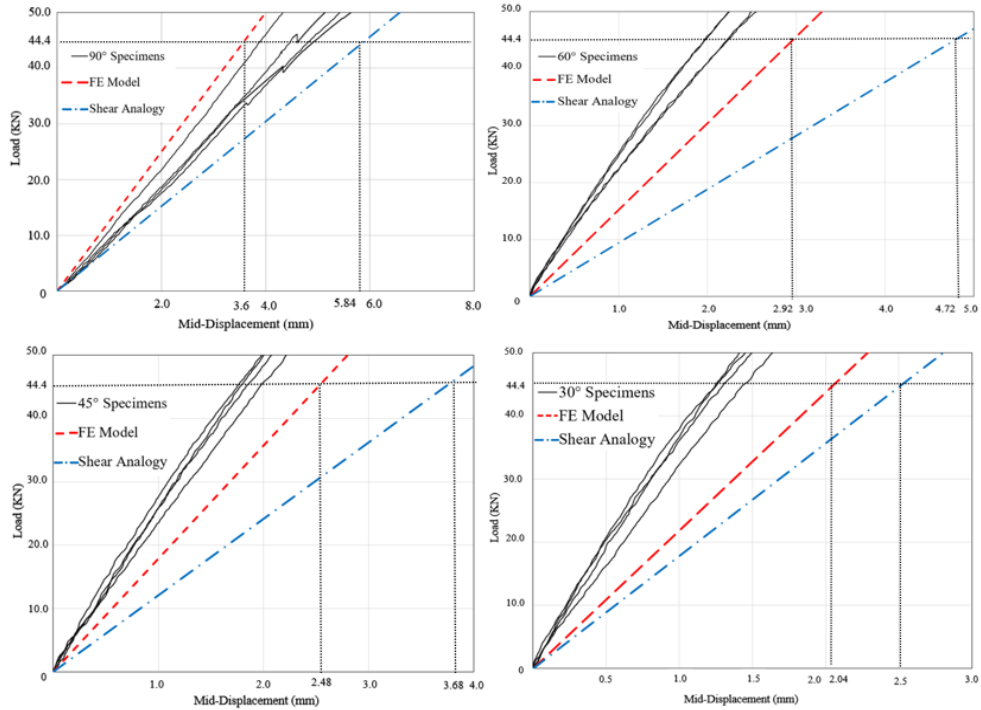
$$E_L, E_R, E_T, \nu_{LR}, \nu_{RT}, \nu_{LT}, G_{LR}, G_{LT}, G_{TR} > 0, \quad (12)$$

$$|\nu_{RL}| < (E_L/E_R)^{1/2}$$



**Fig. 11.** FEM Element Global Coordinates and Mesh

In Fig. 12, the results of the load-displacement curves for all CLT panels obtained from experiments are compared with the finite element analysis results. As can be seen, in the elastic range, the finite element model predicts deformation better than the shear analogy method.



**Fig. 12.** Comparison of the load-displacement curves of experiments with FE modeling and shear analogy method for 90°, 60°, 45°, 30° CLT

The results of the FE model for mid-span deflection of short span panels and maximum shear stress are compared in table 4 and Fig.13 to the experimental test and shear analogy method. In the table 4, the maximum shear stresses are calculated based on peak load, but mid-span deflections of numerical analysis are calculated in the range of 0 to 44.5 KN. For the experiments, the slope of the curves between 15 KN and 44.5 KN (where the load-displacement curves are linear) were used to calculate the panels' mid-span deflection. As can be seen in Fig.13, for 90° CLT specimens the discrepancy between the average deflection of mid-span calculated from the experimental test and FE simulation is the lowest (around 8%), and in contrast, for the 30° specimens this discrepancy are the highest (44%). As can be seen, this discrepancy proportionally increases with changing the mid-layer fiber orientation from 90° to 30°.

Comparing shear analogy method with FE model and experimental test, it generally predicts higher deflection values. For example, shear analogy method predicts the 49%, 96%, 100%, and 93% higher deflection for 90°, 60°, 45°, 30° than the experiments, respectively.

According to these analyses, for 90° CLT, the prediction of the FE model is in fair agreement with the experimental results. However, for angled CLT, the prediction accuracy of stiffness proportionally decreases with changing the mid-layer fiber orientation from 90° to 30°. This proportional difference can be attributed to the biaxial shear stresses from the off-axis loading and bending-twisting coupling which are typically present in the symmetric angle-ply laminates. In the bending-twisting coupling deformation, the CLT not only bends along the direction of the span but also twists about the neutral axis of the CLT, causing the out-of-plane deformation (XZ-plane in Fig. 11). Neither the 2D finite element

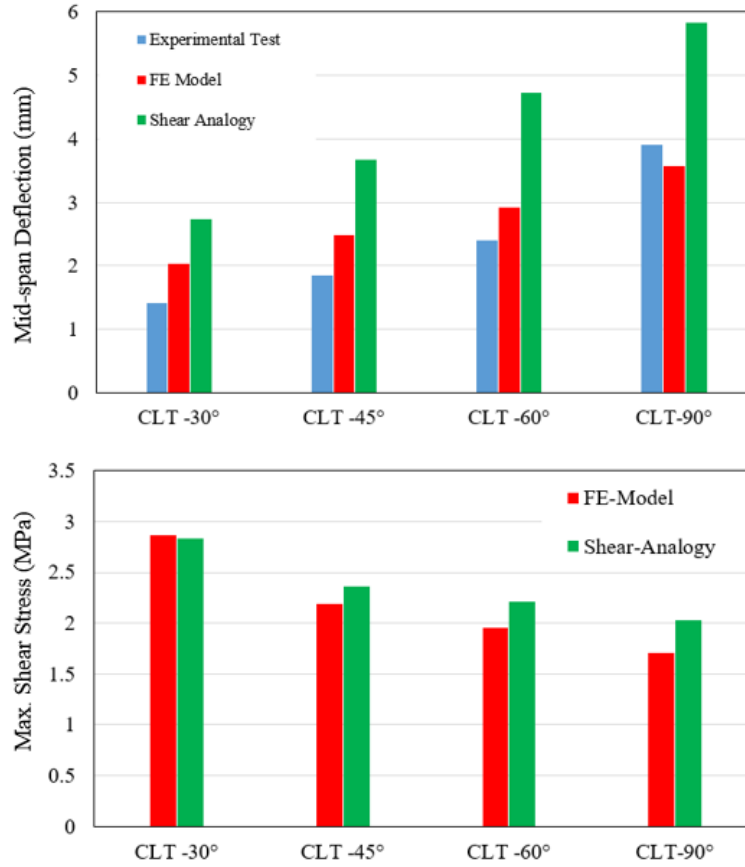
model nor the shear analogy method considered this deformation, causing conservative prediction in stiffness of angled specimens. In the three layers angled specimens, due to the low bending stresses in the mid-layer, the bending-twisting coupling is minimal for practical purpose, but for five layers and more, this type of deformation needs to be investigated. Considering a portion of deformation occurring in the minor axis of specimens, the assumption of plane strain condition is not valid for data analysis and for more accurate prediction, the behavior of angled specimens needs to be investigated in 3D model.

Fig. 14 shows the ratios of shear and bending deformation for a short-span panel in different fiber orientations. Due to the low rolling shear modulus of 90° specimens, the proportion of shear deformation is 73% of the total deformation. In contrast, for the 30° specimens the contribution of shear deformation is 25% of the total deformation, indicating the effective shear modulus increasing as the fiber orientation of the mid-layer varies from 90° to 30°.

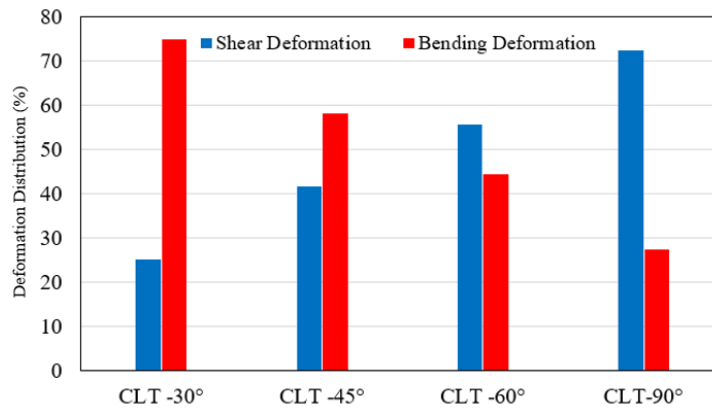
**Table 4.** Comparison of FE Modeling with Experimental Test and Shear Analogy Method for Short-Span CLT Panel with 90° Specimens

Specimen	Experimental Test		FE Model		Shear Analogy Method	
	Mid-span Deflection (mm)	Peak Load (KN)	Mid-span Deflection (mm)	$f_v^{\max}$ (MPa)	Mid-span Deflection (mm)	$f_v^{\max}$ (MPa)
CLT-90°	3.9	88.3	3.58 (8%)	1.71	5.84 (49%)	2.03
CLT -60°	2.4	96.0	2.92 (22%)	1.95	4.72 (96%)	2.21
CLT -45°	1.84	102.7	2.48 (35%)	2.19	3.68 (100%)	2.36
CLT -30°	1.42	122.2	2.04 (44%)	2.87	2.74 (93%)	2.83

Note: numbers in percentage represent the deflection difference of analysis with the experimental test



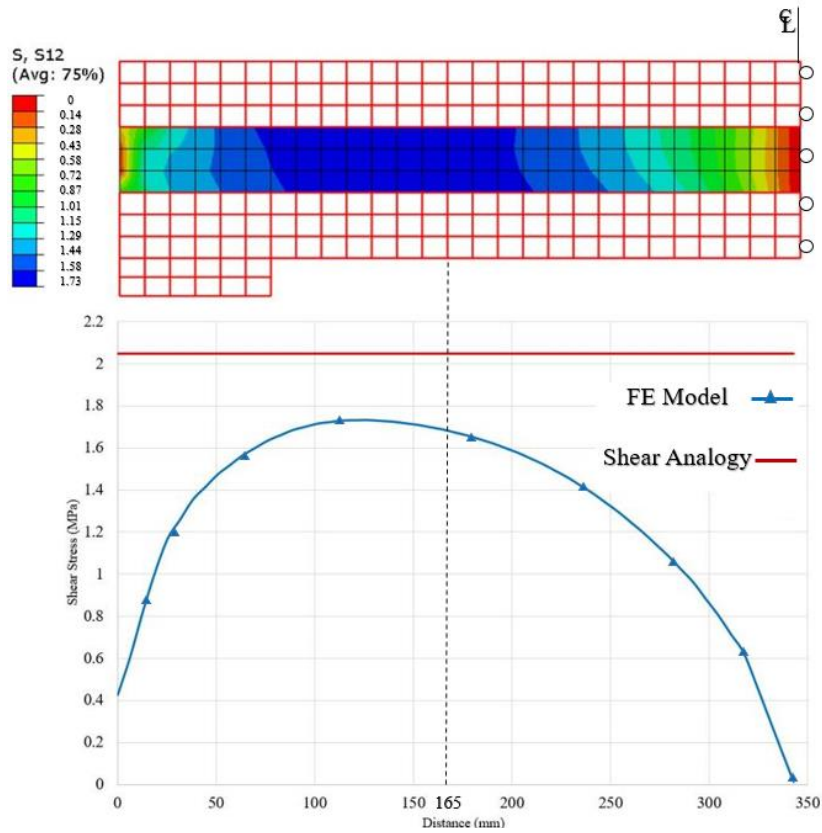
**Fig. 13.** Comparison of FE Modeling with Experimental Test and Shear Analogy Method



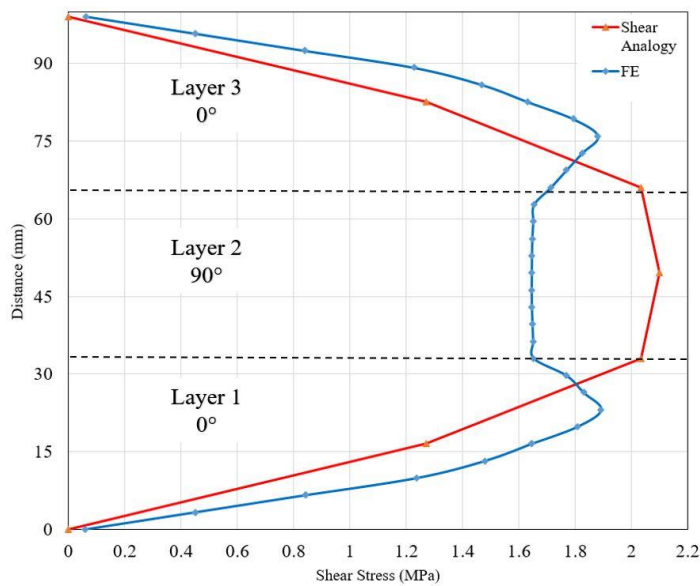
**Fig. 14.** Proportion of shear and bending deformation versus CLT with different fiber orientation in mid-layer for the short-span panel

Table 4 and Fig. 13 also give the average maximum shear stress calculated from the shear analogy method and FE model at peak load. As can be seen, the shear analogy method estimated higher values than the FE model. Since the FE model predicted the experimental deflection more accurately, we can consider that the stress distribution from the FE model is more realistic than the shear analogy method, especially for 90° CLT.

Accordingly, the shear stresses distribution from the FE model for one of the 90° specimen (with a peak load of 89 KN) in both cross-section and longitudinal directions are compared to the shear analogy analysis. Fig. 15 and 16 depict the shear stress distribution in both longitudinal and cross section of CLT panel using shear analogy method and FE model. As shown in Fig. 15, for FE analysis, the shear stress distribution along the length of the CLT panel, ranging from 0.05 to 1.83 MPa, is not uniform. However, the shear analogy method is estimated higher than the constant shear stress values ( $f_{Max}=2.05$  MPa).



**Fig. 15.** Distribution of shear stress along the length of the CLT panel (dashed line indicates the location of the line profiles of distribution for Figure 13).



**Fig. 16.** Distribution of shear stresses in cross-section of the CLT panel.

Clearly, in Fig. 15, the shear stress is maximum in the region between the support and loading area where the first rolling shear crack formed. This is the region, where the secondary stresses are low and as the load increase, the rolling shear crack propagates along the length of the panel toward the support areas, where eventually the interaction of shear and secondary stresses cause the final fracture.

For shear stress distribution in the cross-section (Fig. 16), the stresses of FE model in the top and lower layers are estimated higher values than in shear analogy method. However, the FE model's prediction for mid-layer is lower than in the shear analogy method. Although the shear stress is maximum at the top and lower layers, due to the higher longitudinal shear strength, the rolling shear cracks form only in the mid-layer of the specimens.

## **CONCLUSION**

This study investigated the shear performance of three-layer short-span CLT consisting of four-different fiber orientations of 90°, 60°, 45° and 30° in mid-layers. According to the three-point bending tests, the 30° CLT panels were the stiffest and strongest, followed by the 45°, 60°, and 90° panels. The 30° panels had a mean shear strength at failure 48% greater than the 90° panels; the effective shear modulus was also 8.3 times greater than 90°. The inclusion of angle-ply laminate in the mid-layer shifted the failure mode from rolling shear to a mixture of flexural tension and rolling shear failure. These results support the hypothesis that reorientation of fibers would improve the mechanical properties of CLT panel, and especially the rolling shear modulus and strength. The results also indicate that angled CLT panels may have a structural advantage over regular CLT (90° panels), allowing for increased span lengths or load-carrying capacity for

a given panel span-to-depth ratio or using angled low-value of wood species in CLT where the standard has not been met with 90° CLT layups. Based on the above results and discussion, it is possible to draw the following conclusions:

The average effective shear modulus ( $G_{Aeff}$ ) of angled specimens for 60°, 45° and 30° raised to 209%, 367%, and 828% compared to 90° specimens, respectively.

The contribution of shear deformation in 90° CLT panels was 73%, which is common for 90° panels with the short span-to-depth ratio of 6. However, the shear deformation contribution is decreased in the angled panel by 56%, 42% and 25% for 60°, 45°, and 30° CLT panels, respectively, which is attributed to the improvement of the effective shear modulus of angled CLT panels.

For 90° CLT, a reasonable agreement was achieved, with the experimental data generally showing a slight increase deformation over the FE model prediction compared to the shear analogy method. However, for angled CLT panels, both the FE model and the shear analog method estimated higher values of deformation over the experimental data. This difference between the FE and experimental results was increased by changing the fiber orientation from 90° to 30°, which is due perhaps to the biaxial shear stresses from off-axis loading and bending-twisting coupling effect. In fact, the assumption of plane strain state of deformation made in the analysis is not quite valid, and further 3D finite element analysis is required.

First rolling shear crack occurred in the mid-layer region between the support and loading area, which, according to the shear stress distribution of the FE along the length of

the CLT, is in the high shear stress zone where there are no noticeable secondary stresses. However, the shear analogy method predicted higher and uniform values along the length of the CLT. The model further elucidates the shear stresses distribution in the cross-section by evaluating the higher values than the shear analogy method in the top and lower layers. However, for mid-layer, FE estimated the lower shear stress values than the shear analogy method.

## BIBLIOGRAPHY

Aicher, S., Christian, Z., & Hirsch, M. (2016). Rolling shear modulus and strength of beech wood laminations. *Holzforschung*, 70(8), 773-781.

American Wood Council. (2015). National design specification (NDS) supplement: Design values for wood construction.

APA–The Engineered Wood Association. (2012). Standard for performance-rated cross laminated timber. *Ansi/apa Prg*, 320

Arwade, S. R., Clouston, P. L., & Winans, R. (2009). Measurement and stochastic computational modeling of the elastic properties of parallel strand lumber. *Journal of Engineering Mechanics*, 135(9), 897-905.

ASTM D143-14 Standard Test Methods for Small Clear Specimens of Timber

ASTM D198-15 Standard Test Methods of Static Tests of Lumber in Structural Sizes, ASTM International, West Conshohocken, PA, 2015

ASTM D2915-10 Practice for Sampling and Data-Analysis for Structural Wood and Wood-Based Products, ASTM International, West Conshohocken, PA, 2010,

ASTM D2718-00(2016) Standard Test Methods for Structural Panels in Planar Shear (Rolling Shear), ASTM International, West Conshohocken

ASTM, D.4761 “Standard test method for mechanical properties of lumber and wood-base structural material,” D4761-05. *Annual Book of ASTM Standards*, 4, 523-532.

Babuska, P., Wiebe, R., & Motley, M. R. (2018). A beam finite element for analysis of composite beams with the inclusion of bend-twist coupling. *Composite Structures*, 189, 707-717.

Bahmanzad, A., Clouston, PL., Arwade, SR., & Schreyer, (2019). Improving the Shear Properties of Cross-Laminated Timber (CLT) Panels by Optimizing Laminate Fiber Orientation. *Elsevier journal Engineering Structures*. In Press

Bahmanzad, A., Clouston, PL., Arwade, SR., & Schreyer, A. Measurement of Shear Properties of Eastern Hemlock Using Two-Plate Shear Test. In: Proceedings of the 72nd forest product society international conference, Madison, WI, United States, June 11 - 14, 2018

Bahmanzad, A., Clouston, PL., Arwade, SR., & Schreyer, (2019). Planar Shear Properties of Eastern hemlock for Different Fiber Orientation. ASCE Journal of Materials in Civil Engineering. In Press

Berg, S., Turesson, J., Ekevad, M., & Huber, J. A. (2019). Finite element analysis of bending stiffness for cross-laminated timber with varying board width. Wood Material Science & Engineering, 1-12.

Bejtka, I., & Lam, F. (2008). Cross laminated timber as innovative building material. Proceedings of the Canadian Society for Civil Engineering (CSCE) 2008 Annual Conference, Quebec City, Canada,

Bendtsen, B. A. (1976). Rolling shear characteristics of nine structural softwoods. Forest Products Journal.

Blass, H. J., & Fellmoser, P. (2004). Design of solid wood panels with cross layers. 8th World Conference on Timber Engineering, , 14(17.6) 2004.

Blaß, H. J., & Görlacher, R. (2000). Rolling shear in structural bonded timber elements. Paper presented at the Annales GC Bois, , 5 1-5.

Brandner, R. (2013). Production and technology of cross laminated timber (CLT): A state-of-the-art report. Focus Solid Timber solutions—European Conference on Cross Laminated Timber (CLT). the University of Bath, Bath,

Bucher, C. (2009). Computational analysis of randomness in structural mechanics: Structures and infrastructures book series CRC Press.

Buck, D., Hagman, O., Wang, A., & Gustafsson, A. (2016). Further development of cross-laminated timber (clt)—mechanical tests on 45° alternating layers. Wcte2016,

Canadian Standard Association. (2009). Engineering design of wood. CSA O86. Canadian Standard Association, Mississauga, Ontario,

Clouston, P. L. (2001). Computational Modeling of Strand-Based Wood Composites in Bending,

Choi, C., Kojima, E., Kim, K. J., Yamasaki, M., Sasaki, Y., & Kang, S. G. (2018). Analysis of Mechanical Properties of Cross-laminated Timber (CLT) with Plywood using Korean Larch. *BioResources*, 13(2), 2715-2726.

de Normalisation, C. E. (2003). Eurocode 5–Design of Timber structures–Part 1-1: General Rules and Rules for Buildings,

Ehrhart, T., & Brandner, R. (2018). Rolling shear: Test configurations and properties of some European soft-and hardwood species. *Engineering Structures*, 172, 554-572.

EN, C. (1991). 26891–Timber structures. joints made with mechanical fasteners general principles for the determination of strength and deformation characteristics. Iso En, 26891

EN standard (2012) 408 Timber structures – Structural timber and glued laminated timber – Determination of some physical and mechanical properties. European Committee for Standardisation, Brussels, Belgium

Fellmoser, P., & Blaß, H. (2004). Influence of rolling shear modulus on strength and stiffness of structural bonded timber elements. *CIB-W18 Meeting*, , 37

Fink, G., Kohler, J., & Brandner, R. (2018). Application of european design principles to cross laminated timber. *Engineering Structures*, 171, 934-943.

Flores, E. S., Saavedra, K., Hinojosa, J., Chandra, Y., & Das, R. (2016). Multi-scale modelling of rolling shear failure in cross-laminated timber structures by homogenisation and cohesive zone models. *International Journal of Solids and Structures*, 81, 219-232.

- Fortune, A., & Quenneville, P. (2010). Feasibility study of new zealan radiata pine crosslam. Incorporating sustainable practise in mechanics and structures of materials CRC Press.
- Fragiacomo, M., & Lukaszewska, E. (2011). Development of prefabricated timber–concrete composite floor systems. *Proceedings of the Institution of Civil Engineers-Structures and Buildings*, 164(2), 117-129.
- Frangi, A., Fontana, M., Hugi, E., & Jübstl, R. (2009). Experimental analysis of cross-laminated timber panels in fire. *Fire Safety Journal*, 44(8), 1078-1087.
- Gagnon, S., & Pirvu, C. (2011). *Cross laminated timber (CLT) handbook*. FPInnovations, Vancouver, Canada,
- Gardner, D. J., and J. F. Diebel. "Eastern hemlock (*Tsuga canadensis*) uses and properties." *Proceedings, hemlock ecology and management conference*. Madison, Wisconsin: University of Wisconsin. 1995.
- Gere, J., Gere, J. M., & Goodno, B. J. (2012). *Mechanics of materials* Nelson Education.
- Gibson, R. F. (2016). *Principles of composite material mechanics* CRC press.
- Gsell, D., Feltrin, G., Schubert, S., Steiger, R., & Motavalli, M. (2007). Cross-laminated timber plates: Evaluation and verification of homogenized elastic properties. *Journal of Structural Engineering*, 133(1), 132-138.
- Hankinson, R. (1921). Investigation of crushing strength of spruce at varying angles of grain. *Air service information circular*, 3(259), 130.
- He, M., Sun, X., & Li, Z. (2018). Bending and compressive properties of cross-laminated timber (CLT) panels made from Canadian hemlock. *Construction and Building Materials*, 185, 175-183.
- Hindman, D. P., & Bouldin, J. C. (2014). Mechanical properties of southern pine cross-laminated timber. *Journal of Materials in Civil Engineering*, 27(9), 04014251.

HOLZBRETTERN, M. I., LE MODULE, ÉLÉMENTS DE BASE SUR, DE CISAILLEMENT, D., & BOIS, P. E. (2000). Basic considerations to rolling shear modulus in wooden boards. *Otto-Graf-Journal*, 11, 157.

Ibach, R., & Handbook, W. (1999). Wood as an engineering material. Gen.Tech.Rep.FPL-GTR-113. Madison, WI: Department of Agriculture, Forest Service, Forest Products Laboratory, *Wood and Fiber Science*, 46(2), 259-269.

International Code Council, Building Officials, Code Administrators International, International Conference of Building Officials, & Southern Building Code Congress International. (2015). *International building code* International Code Council.

Jones, R. M. (2014). *Mechanics of composite materials*. CRC press.

Karacabeyli, E., & Douglas, B. (2013). *CLT handbook: Cross-laminated timber* FPIInnovations.

Kim, K. (2007). A note on the hankinson formula. *Wood and Fiber Science*, 18(2), 345-348.

Lam, F., Li, Y., & Li, M. (2016). Torque loading tests on the rolling shear strength of cross-laminated timber. *Journal of Wood Science*, 62(5), 407-415.

Liu, J. Y. (2007). Effects of shear coupling on shear properties of wood. *Wood and Fiber Science*, 32(4), 458-465.

Li, Y. (2015). *Duration-of-Load and Size Effects on the Rolling Shear Strength of Cross Laminated Timber*,

Mahamid, M., & Torra-Bilal, I. (2018). Analysis and Design of Cross-Laminated Timber Mats. *Practice Periodical on Structural Design and Construction*, 24(1), 04018031.

Masoudnia, R., Hashemi, A., & Quenneville, P. (2018). Predicting the Effective Flange Width of a CLT Slab in Timber Composite Beams. *Journal of Structural Engineering*, 144(7), 04018084.

- Mestek, P., Kreuzinger, H., & Winter, S. (2008). Design of cross laminated timber (CLT). Proceedings of the 10th World Conference on Timber Engineering,
- M. Gong, D.Y. Tu, L. Li, Y.H. Chui, Planar shear properties of hardwood cross layer in hybrid cross laminated timber, in: Proceeding of the 5th International scientific conference on hardwood processing, Quebec City, Canada, Sept. 15-17, 2015.
- Mohammad, M., Gagnon, S., Douglas, B., & Podesto, L. (2012). Introduction to cross laminated timber. *Wood Design Focus*, 22(2), 3-12.
- Munthe, B., & Ethington, R. L. (1968). Method for evaluating shear properties of wood US Department of Agriculture, Forest Service, Forest Products Laboratory.
- Negrão, J., Maia, d. O., Leitão, d. O., & Cachim, P. (2010). Glued composite timber-concrete beams.II: Analysis and tests of beam specimens. *Journal of Structural Engineering*, 136(10), 1246-1254. doi:10.1061/(ASCE)ST.1943-541X.0000251
- NELMA 2017: <https://www.nelma.org/library/2013-standard-grading-rules-for-northeastern-lumber/>
- Park, H., Fushitani, M., Sato, K., Kubo, T., & Byeon, H. (2006). Bending creep performances of three-ply cross-laminated woods made with five species. *Journal of Wood Science*, 52(3), 220-229.
- Ross, Robert J. "Wood handbook: Wood as an engineering material." (2010).
- Schickhofer, G. (2010). Cross laminated timber (CLT) in Europe—from conception to implementation. Presentation, University of British Columbia, Department of Wood Science, Vancouver, Canada,
- Steiger, R., Gülzow, A., & Gsell, D. (2008). Non-destructive evaluation of elastic material properties of cross-laminated timber (CLT). *Conference COST E*, , 53 29-30.

Stürzenbecher, R., Hofstetter, K., & Eberhardsteiner, J. (2010). Structural design of cross laminated timber (CLT) by advanced plate theories. *Composites Science and Technology*, 70(9), 1368-1379.

Tadikamalla, Pandu R. "A look at the Burr and related distributions." *International Statistical Review*, Vol. 48, Number 3, 1980, pp. 337–344.

Van de Kuilen, J., Ceccotti, A., Xia, Z., & He, M. (2011). Very tall wooden buildings with cross laminated timber. *Procedia Engineering*, 14, 1621-1628.

Version, A. (2008). 6.8. User's manual. ABAQUS. Inc., RI,

Wang, Z., Fu, H., Gong, M., Luo, J., Dong, W., Wang, T., & Chui, Y. H. (2017). Planar shear and bending properties of hybrid CLT fabricated with lumber and LVL. *Construction and Building Materials*, 151, 172-177.

Wegener, G. (1997). Increasing public awareness of the contribution of forestry and wood utilization to ecology. *Restoration of forests* (pp. 77-96) Springer.

Winn, M. F., & Araman, P. A. (2005). (2005). Study of the utilization options for dead and dying eastern hemlock in the southern appalachians. Paper presented at the Proceedings, Third Symposium on Hemlock Woolly Adelgid in the Eastern United States, 360-363.

Yawalata, D., & Lam, F. (2011). Development of technology for cross laminated timber building systems. Res Rep Submitted to Forestry Innovation Investment Ltd., FPInnovation, Vancouver. Google Scholar,

Yeoh, D., Fragiaco, M., De Franceschi, M., & Heng Boon, K. (2011). State of the art on timber-concrete composite structures: Literature review. *Journal of Structural Engineering*, 137(10), 1085-1095.

Zhou, Q., Gong, M., Chui, Y. H., & Mohammad, M. (2014). Measurement of rolling shear modulus and strength of cross laminated timber fabricated with black spruce. *Construction and Building Materials*, 64, 379-386.

Zhou, Q., Gong, M., Chui, Y., & Mohammad, M. (2014). Measurement of rolling shear modulus and strength of cross-laminated timber using bending and two-plate shear tests. *Wood and Fiber Science*, 46(2), 259-269.